

Dissertation
submitted to the
Combined Faculties for the Natural Sciences and for
Mathematics
of the Ruperto-Carola University of Heidelberg, Germany
for the degree of
Doctor of Natural Sciences

presented by
Dipl.-Biol. Ruth Merkle
born in Munich, Germany
oral examination: 14.04.2015

Impact of growth factors, therapeutic inhibitors and cytostatic compounds on the response of non-small-cell lung carcinoma cell lines

Referees:

Prof. Dr. Ursula Klingmüller

Prof. Dr. Martina Muckenthaler

To my parents

Acknowledgements

This work would not have been possible without the support of many people.

First of all, I would like to thank my supervisor Prof. Dr. Ursula Klingmüller for her advice and guidance and for giving me the opportunity to work on this exciting interdisciplinary project.

I thank Prof. Dr. Martina Muckenthaler for being the second referee for this thesis.

Many thanks to all current and former lab members for their support and the nice working atmosphere. In particular I would like to thank the LungSys team leader Dr. Sofia Depner for her support and advice, Dr. Marcel Schilling for sharing his modeling expertise and his support, Dr. Agus Rodriguez for his inspiring enthusiasm and extensive discussions about lung cancer, Marvin Wäsch for providing such great help, Tibor Szekeres and Xiaoyun Huang for their advice in microscopy, Philippe Lucarelli for supporting me with his knowledge about TGF- β and many inspiring discussions, the Western Blot expert Florian Salopiata, Markus Stepath for the technical and mental support and Sandra Bonefas, Susen Lattermann, Katharina Waldow, Nao Iwamoto, Dr. Lorenza D'Alessandro, Lorenz Adlung, Frédérique Kok and Dr. Marie Wagner for all the motivation and the good times we had. Thank you all for being awesome colleagues and friends inside and outside the lab!

I would also like to acknowledge all my collaboration partners, including Bernhard Steiert and Prof. Jens Timmer for their work on the EpoR model, Dr. Hauke Busch, Dr. Melanie Börries and Prof. Dr. Norbert Gretz for the work on the microarray data, Prof. Dr. Heimo Mairbörl for providing AECII, Dr. Sebastian Marwitz and Prof. Dr. Torsten Goldmann for the nice cooperation in the BAMBI project and Dr. Naveed Ishaque, Stephen Krämer and Prof. Dr. Benedikt Brors for their genome and and Dr. Carsten Maus, Dr. Erika Kuchen and Prof. Dr. Thomas Höfer .

I acknowledge funding by LungSys initiative of the BMBF.

Finally, I want to thank my family for their love and support. Special thanks to Kati, Sinan and my sister Katrin and last but not least my parents, to whom I dedicate this work.

1. Table of Contents

1.1	Table of Contents	1
2.	Summary	5
3.	Zusammenfassung	6
4.	Introduction	7
4.1	Lung cancer	7
4.1.1	Genetic alterations in lung cancer	7
4.1.2	Dysregulated cell cycle in lung cancer	8
4.2	MEK inhibitor treatments in lung cancer	8
4.3	Chemotherapeutic treatments in lung cancer	10
4.3.1	Cisplatin-induced apoptosis	11
4.3.2	Resistance to chemotherapeutic treatments	13
4.4	EpoR signaling in lung cancer	13
4.4.1	EpoR signaling in the erythroid system	13
4.4.2	EpoR signaling and its role in tumorigenesis	15
4.5	TGF- β signaling in lung cancer	16
4.5.1	TGF- β signaling	16
4.5.2	TGF- β and its role in metastasis by inducing EMT	18
4.6	Systems Biology approach	19
4.7	Objectives	21
5.	Results	23
5.1	Establishment of Standard Operating Procedures (SOPs)	23
5.1.1	Identification of cell lines as model system for NSCLC	23
5.1.2	Establishment of optimized confluency conditions for long-term and short-term experiments	25
5.2	Cisplatin-induced apoptosis in NSCLC cell lines	27
5.2.1	Time- and dose-dependent effect of cisplatin on NSCLC cell lines	27
5.2.2	Rescue of cisplatin-induced apoptosis by MEK inhibition	28
5.2.2.1	Influence of signaling pathway inhibitors on cisplatin-induced apoptosis	28
5.2.2.2	Influence of MEKi on protein levels of ERK	31
5.2.2.3	Influence of MEKi on the cell cycle	33
5.2.2.4	Influence of MEKi on gene expression	37

5.2.2.5	Time- and dose-dependent effect of different clinically relevant MEK inhibitors (MEKi) on cisplatin-induced apoptosis.....	40
5.3	Role of Epo in NSCLC	44
5.3.1	Rescue of cisplatin-induced apoptosis by Epo treatment	44
5.3.2	EpoR signaling in NSCLC and primary erythroid progenitor cells.....	48
5.3.2.1	Establishment of a mathematical model for the Epo-induced signaling in lung cancer cells and primary erythroid progenitor cells	48
5.3.2.2	Generation of quantitative time-resolved data.....	51
5.3.2.3	Model selection and calibration.....	52
5.3.2.4	Identification of differences in Epo-induced signaling.....	53
5.3.2.5	Experimental validation of the predicted cell type-specific SOCS3 mRNA turnover rate.....	56
5.4	TGF- β signaling in NSCLC cell lines	59
5.4.1	TGF- β is able to induce TGF- β signaling in NSCLC cell lines	59
5.4.2	Expression analysis of TGF- β -dependent genes in the NSCLC cell line H1975...61	
5.4.3	Validation of selected target genes induced by TGF- β in NSCLC cell lines.....	65
5.4.4	The TGF- β pseudoreceptor BAMBI is downregulated in NSCLC	67
5.4.5	BAMBI reconstitution decreases the expression of TGF- β -dependent genes in the NSCLC cell line H1975	69
6.	Discussion	72
6.1	Effect of MEKi on cisplatin-induced apoptosis in NSCLC cell lines.....	72
6.1.1	Cisplatin activates the RAS–RAF–MEK–ERK cascade and induces apoptosis in NSCLC cells	72
6.1.2	Pre-incubation with MEKi decreases the cisplatin sensitivity of NSCLC cells.....	73
6.2	Role of Epo-induced signaling in NSCLC cell lines	75
6.2.1	Epo treatment decreases the cisplatin sensitivity of the EpoR-expressing cell line H838	75
6.2.2	A mathematical model of the Epo-induced signaling pathway predicts differences between NSCLC cell line H838 and erythroid progenitor cells.....	77
6.3	Role of TGF- β signaling in NSCLC cell lines.....	79
6.3.1	TGF- β treatment induces EMT in NSCLC cell lines	79
6.3.2	Role of BAMBI as a potential tumor suppressor.....	81
6.4	Conclusions and outlook.....	83
7.	Materials and methods.....	85
7.1	Software and general equipment	85

7.2	Cell culture chemicals, solutions and media for NSCLC cell lines	85
7.3	Cell culture plastic ware and volumes for the amplification and experiments with NSCLC cell lines	86
7.4	Inhibitors	86
7.5	Treatments	87
7.6	Antibodies	87
7.7	Cell culture SOPs and cell-based techniques.....	88
7.7.1	NSCLC cell lines	88
7.7.2	Detaching and amplification of NSCLC cells	88
7.7.3	Freezing and thawing of NSCLC cells.....	89
7.7.4	Seeding NSCLC cells for experiments	89
7.7.5	AECII cells	90
7.7.6	Tumor samples adenocarcinoma	90
7.7.7	Preparation of murine fetal liver cells (CFU-Es)	90
7.7.8	CellTiter-Blue cell viability assay	91
7.8	Molecular biology: RNA	91
7.8.1	RNA extraction.....	91
7.8.2	Quantitative Real Time PCR (qRT-PCR)	92
7.8.3	Gene expression arrays.....	94
7.8.4	RNA sequencing (RNAseq)	94
7.9	Molecular biology: DNA	94
7.9.1	DNA extraction.....	94
7.9.2	WGS and MCIp.....	95
7.10	Molecular biology: proteins	95
7.10.1	Preparation of total cell lysates (TCL)	95
7.10.2	Protein quantification	96
7.10.3	Immunoprecipitation of EpoR.....	96
7.10.4	SDS-PAGE	96
7.10.5	Immunoblotting	97
7.11	Microscopy	97
7.11.1	Caspase-3 assay	97
7.11.2	Volume measurements with GFP and Hoechst staining.....	98
7.11.3	Cell cycle analysis with the FUCCI sensor	98

7.12	Dynamic pathway modeling	99
8.	Abbreviations	100
9.	References	104
10.	Erklärung.....	117

2. Summary

Lung cancer with its most prevalent form non-small-cell lung carcinoma (NSCLC) is one of the leading causes of cancer-related deaths worldwide and is characterized by early metastatic spread. TGF- β is one of the growth factors that can be involved in the regulation of this process. Lung cancer is generally treated with chemotherapeutic drugs, e.g. with cisplatin, often in combination with different inhibitors, such as MEK inhibitors (MEKi). An important obstacle for lung cancer patients is the chemotherapy-induced anemia that can be treated with erythropoietin (Epo). Unfortunately, Epo was found to have tumor-stimulating effects.

To establish reliable and reproducible experimental conditions, standard operating procedures for the NSCLC cell lines H1975 and H838 were developed. Cisplatin was shown to induce apoptosis in a dose-dependent manner in H838 cells. The MEKi U0126 was found to rescue H838 cells of cisplatin-induced apoptosis by arresting the cells in the cell cycle phase G1 and this effect could be reproduced with clinically relevant MEK inhibitors. Epo treatment of the cell line H838 resulted in decreased cisplatin sensitivity. To identify the differences in Epo-induced signaling in erythroid progenitor cells and the cell line H838, a dynamic pathway model was established that was able to describe the Epo-induced dynamics of the activation of the JAK2/STAT5 pathway in both cell types. The mathematical model predicted 8 cell type-specific parameters. Among these, the SOCS3 mRNA turnover rate was predicted to be slower in CFU-Es which was experimentally validated by qRT-PCR. Moreover, it was shown by genome wide expression profiling, that TGF- β treatment of NSCLC cells led to the upregulation of EMT genes and the downregulation of cell cycle genes. The TGF- β pseudoreceptor BAMBI was found to be downregulated in NSCLC. Its reconstitution resulted in a decreased TGF- β signaling in the cell line H1975.

In conclusion, the study shows that MEKi treatment in combination with cisplatin-based chemotherapy poses a potential risk for lung cancer patients. Furthermore, the presence of EpoR in NSCLC cell lines results in response to Epo stimulation in a decreased sensitivity to cisplatin. Finally, TGF- β was verified to induce EMT in NSCLC and BAMBI was identified as a potential tumor suppressor in lung cancer. These studies show that molecular alterations can define responsiveness to therapeutic agents.

3. Zusammenfassung

Lungenkrebs mit seiner am weitesten verbreitete Form des nicht-kleinzelligen Lungenkarzinoms (NSCLC) ist weltweit eine der häufigsten Ursachen für Krebstodesfälle und ist durch eine frühe Metastasierung charakterisiert. Diese kann durch TGF- β reguliert sein. NSCLC wird im Allgemeinen mit dem Chemotherapeutikum Cisplatin behandelt, oft auch in Kombination mit einem MEK Signalweginhibitor (MEKi). Ein großes Problem für Lungenkrebspatienten ist die Chemotherapie induzierte Anämie, die aber mit Erythropoietin (Epo) behandelt werden kann. Leider wurde festgestellt, dass Epo auch eine stimulierende Wirkung auf den Tumor haben kann.

Um zuverlässige und reproduzierbare Bedingungen zu ermöglichen, wurden Standardvorgehensweisen für die NSCLC Zelllinien H1975 und H838 etabliert. Es wurde gezeigt, dass Cisplatin Apoptose in H838 Zellen induziert. Bei der zusätzlichen Gabe von MEKi U0126 oder anderen klinisch relevanten MEKi wurde festgestellt, dass H838 Zellen durch einen Arrest in der Zellzyklusphase G1 vor der Apoptose gerettet werden können. Auch die Gabe von Epo konnte der Apoptose entgegen wirken. Um Unterschiede in der Epo induzierten Aktivierung des JAK2/STAT5 Signalweges von erythroiden Vorläuferzellen und H838 Zellen zu identifizieren, wurde ein mathematisches Modell etabliert. Von den 8 vorhergesagten zelltypspezifischen Parametern, wurde die SOCS3 mRNA Degradationsrate durch qRT-PCR experimentell validiert. Darüber hinaus wurde durch genomweite Expressionsanalyse gezeigt, dass TGF- β zur Hochregulierung von EMT Genen und der Herunterregulierung von Zellzyklusgenen in H1975 Zellen führte. Außerdem konnte gezeigt werden, dass der TGF- β Pseudorezeptor BAMBI in NSCLC herunter reguliert war und eine Rekonstitution in H1975 Zellen zu verminderter TGF- β Signalwegaktivierung führte.

Zusammenfassend wurde die Behandlung mit MEKi parallel zu Cisplatin als potenzielles Risiko für Lungenkrebspatienten identifiziert. Ferner wurde gezeigt, dass die EpoR Expression in NSCLC Zelllinien bei Epo Gabe zu einer verringerten Sensitivität gegenüber Cisplatin führt. Darüber hinaus wurde TGF- β als ein EMT induzierender Faktor in NSCLC bestätigt und BAMBI als ein potenzieller Tumorsuppressor in Lungenkrebs identifiziert. Diese Studien zeigen, dass molekulare Veränderungen die Wirkung von Therapeutika bestimmen können.

4. Introduction

4.1 Lung cancer

Lung carcinoma is one of the leading causes of cancer-related deaths worldwide. The main types of lung cancer are small-cell lung carcinoma (SCLC) and non-small-cell lung carcinoma (NSCLC). The most frequent form with around 85% is NSCLC and can be classified into squamous-cell carcinoma, large-cell carcinoma and with 40% the most prevalent subgroup adenocarcinoma [1]. The origin of NSCLC is believed to be lung alveolar epithelial cells type II (AECII) [2-5].

4.1.1 Genetic alterations in lung cancer

Lung cancer is known for a high metastasis rate independent of tumor size. This key medical problem is often combined with a high mutation rate in the genome, especially for genes that are involved in processes like cell growth, proliferation and migration indicating a direct correlation. Most prevalent mutations in oncogenes were observed for *EGFR* (epidermal growth factor receptor), *KRAS*, *ALK* (anaplastic lymphoma kinase), *BRAF*, *MET*, *TP53* (p53), *PIK3CA* and *ERBB2*, *MAP2K1* and *NRAS* [6, 7] (**Figure 1**). Therefore, specific targeted therapies by small molecule inhibitors or therapeutic antibodies based on the mutation profile of the tumor are applied for selected cases.

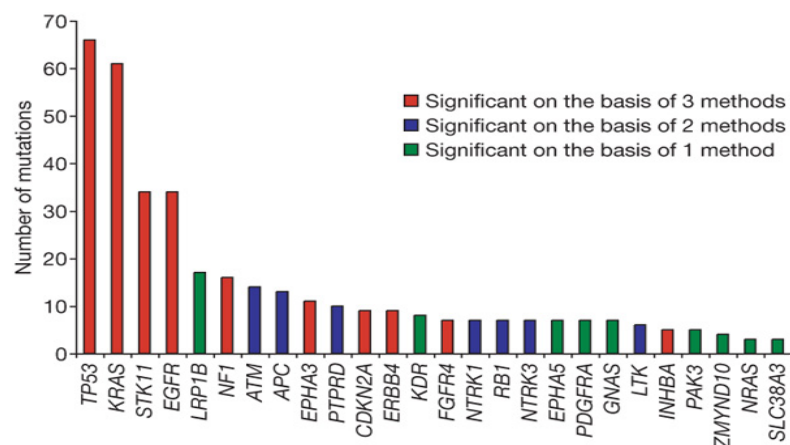


Figure 1: Significantly mutated genes in lung adenocarcinomas. The bars indicate the number of somatic mutations in each indicated gene in 188 tumor and normal tissue pairs analyzed by PCR-based methods [7].

4.1.2 Dysregulated cell cycle in lung cancer

The formation of lung tumors is often induced by uncontrolled proliferation that might have its origin in a dysregulated cell cycle. The cell cycle starts with the interphase that consists of G1 (gap1), S (synthesis) and G2 (gap2) phase in which the cell grows, duplicates the DNA and prepares for the cell division in the M (mitotic) phase, in which the cell splits into two daughter cells. The cell can rest in the G0 (quiescent) phase or directly start a new cycle with G1 phase. The two main regulatory classes of the cell cycle phases are cyclins and cyclin-dependent kinases (CDKs). They are conserved among all eukaryotes and form an active heterodimer where different cyclin-CDK combinations determine the target proteins that are phosphorylated. Arrest of the cell cycle can be achieved by expression of p21 (*CDKN1A*, cyclin-dependent kinase inhibitor 1) or p27 (*CDKN1B*) that regulate G1/S cell cycle transition by inhibiting cyclin-CDK complexes and is controlled either in a p53-dependent or –independent manner [8-10]. One possibility how the cell can react to extracellular or intracellular influences to either initiate cell cycle arrest or progression is via the MAPK (mitogen-activated protein kinase) pathway. Activation of the MAP kinase ERK (extracellular signal-regulated kinase) is also required to enter the S phase [11-13] and inhibition of ERK results in cell cycle arrest [14]. As many components that are involved in the regulation of the cell cycle, e.g. p53 or MAPK pathway components, are often mutated in lung cancer cells, uncontrolled cell division is an issue that needs to be understood in more detail to enable the development of strategies for effective medical treatments.

4.2 MEK inhibitor treatments in lung cancer

To overcome uncontrolled cell proliferation caused by mutations that increase or constantly activate MAP kinase signaling, MAPK inhibitors are currently tested in clinical trials. The RAS–RAF–MEK1/2–ERK1/2 pathway is the best characterized MAPK pathway and one of the most frequently dysregulated signaling cascades [15]. *KRAS*, for instance, is with 17% one of the most frequent mutated genes in lung cancer [16]. The mitogen-activated protein kinase kinase MEK is synthesized in the two isoforms MEK1 and MEK2 that share a high homology and are thus an applicable drug target

[15]. MEK inhibitors (MEKi) are small molecules that inhibit one or both isoforms and can be subdivided into ATP non-competitive and ATP competitive inhibitors. Most of the inhibitors do not directly compete but rather bind to an allosteric site adjacent to the ATP binding site and thus preventing ATP binding [17]. Available MEK inhibitors are U0126, CI-1040 (PD184352), and in currently running clinical trials AZD8330 (ARRY-424704), refametinib (BAY 86-9766, RDEA119), cobimetinib (GDC-0973, XL-518, RG7421), E6201, MEK162 (ARRY-438162), pimasertib (AS703026, MSC1936369B), RO4987655 (CH4987655), RO5126766 (CH5126766), TAK-733, GDC-0623, WX-554, selumetinib (AZD6244, ARRY-142,886), PD0325901 and trametinib (GSK1120212) with the last three tested for NSCLC (**Table 1**).

EK1/2 inhibitors	Company	Current stage of clinical development
AZD8330 (ARRY-424704)	AstraZeneca, UK and Array Biopharma, USA	Phase I
Refametinib (BAY 86-9766, RDEA119)	Bayer, Germany and Ardea Bioscience, USA	Phase II (in HCC)
Cobimetinib (GDC-0973, XL-518, RG7421)	Exelixis, USA and Hoffmann-La Roche, Switzerland	Phase III (in melanoma)
E6201	Eisai, USA	Phase I
MEK162 (ARRY-438162)	Array Biopharma, USA and Novartis, Switzerland	Phase III (in melanoma, low-grade serous ovarian, fallopian tube, or peritoneal cancer)
PD0325901	Pfizer, USA	Phase II (in NSCLC, CRC, and pancreatic cancer)
Pimasertib (AS703026, MSC1936369B)	EMD Serono, USA	Phase II (in melanoma, CRC, pancreatic cancer, and ovarian cancer)
RO4987655 (CH4987655)	Hoffmann-La Roche, Switzerland	Phase I
RO5126766 (CH5126766)	Hoffmann-La Roche, Switzerland	Phase I
Selumetinib (AZD6244, ARRY-142,886)	AstraZeneca, UK and Array Biopharma, USA	Phase III (in NSCLC)
TAK-733	Takeda, Japan	Phase I
Trametinib (GSK1120212)	GlaxoSmithKline, UK	Phase III (in melanoma)
GDC-0623	Genentech, USA	Phase I
WX-554	Wilex, Germany	Phase I/II

Table 1: MEK inhibitors in clinical trials, adapted from Zhao *et al.* [15]; Abbreviations: HCC: hepatocellular carcinoma; CRC: colorectal cancer; NSCLC: non-small-cell lung carcinoma;

Trametinib was the first MEK inhibitor and is so far the only one that was approved for the treatment of patients with BRAF V600E/K-mutant melanoma by the U.S. Food and Drug Administration (FDA) in 2013 [18]. For the treatment of lung cancer, promising results could be observed with selumetinib in combination with docetaxel as it prolonged progression-free survival and increased response rates in patients with *KRAS*-mutated NSCLC in a randomized phase II trial [19]. Despite these achievements, also toxic effects were caused by some MEK inhibitors leading to termination, e.g. of a phase II study in NSCLC patients with PD0325901 due to ocular and neurological toxicity (ClinicalTrials.gov Identifier: NCT00174369) [20]. This development points out the importance and need of a better understanding of how MEK inhibition works in detail.

4.3 Chemotherapeutic treatments in lung cancer

Depending on the stage of the tumor and the patient's state of health, NSCLC can be treated with surgery, radiotherapy and/or chemotherapy. Due to the fact that lung cancer metastasizes already at early stages, widely spread metastases can often be found already at the time of the first diagnose [21]. As standard of care, lung cancer patients are treated with platinum-based chemotherapeutic drugs [22], such as cisplatin or *cis*-diamminedichloroplatinum(II). It was the first FDA-approved platinum compound for cancer treatment in 1978 and although several analogues were synthesized and 13 even tested in clinical trials, just carboplatin and oxaliplatin have additionally been FDA-approved so far [23, 24] (**Figure 2**).

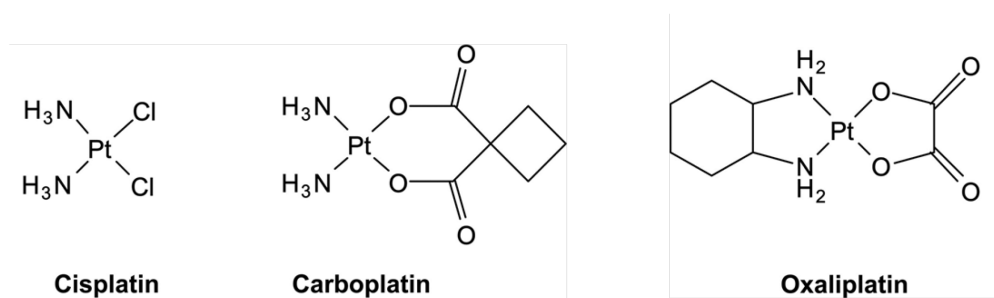


Figure 2: Platinum-based FDA-approved drugs used for chemotherapy (taken from Yonezawa *et al.* [25]).

Cisplatin is given to the patient as an intravenous infusion with a dose of 80 mg/m² at day 1 of a therapy cycle. This is repeated every three weeks for 4 cycles [26]. With an average body surface area of 1.73 m² [27], around 140 mg cisplatin is given per one treatment. As the human body contains between 5 and 6 liters blood, the concentration in the human body is approximately 20-30 mg/l cisplatin or less if degradation processes are taken into account. Clearance of platinum compounds is triphasic in nature, with a distribution half-life of 13 minutes, elimination half-life of 43 minutes, and terminal half-life of 5.4 days for total cisplatin [28, 29].

4.3.1 Cisplatin-induced apoptosis

Cisplatin-induced apoptosis is well described in literature (**Figure 3**). The drug is a small molecule that can enter the cell by diffusion, but also some transporters are suggested to play a role like CTR1 (copper transporter 1) [30]. After reaching the nucleus, cisplatin binds to purine bases of the DNA and thus cross-links the DNA strands (inter- and intra-strand cross-links). This leads to the initiation of the repair mechanisms NER (nuclear excision repair) and MMR (mismatch repair) that are linked to cell cycle arrest [30].

The key player of these repair mechanisms but also of cisplatin-induced apoptosis that takes place if the DNA damage failed to be repaired is p53. This p53-involved process is rather complex and includes many signaling components which allow the cell to fine tune the process. If the damage is irreparable, p53 levels are strongly increasing and the cells start to undergo the apoptotic program. This includes activation of the AKT and MAPK (JNK, p38 and ERK) pathways [31-44]. These pathways are connected to several Bcl-2-family members (anti-apoptotic: Bcl-2, Bcl-xL; pro-apoptotic: Bad, Bax, Bak, Bcl-xS, Bik, Bim, Bid) that among others regulate the cytochrom c release from the mitochondria that takes place, e.g. in renal tubule cells after about 9 hours upon treatment [45]. In the next step the apoptosome is formed which results in the final part of apoptosis, the cleavage of caspases (caspase-9, caspase-3 and caspase-8) [45, 46]. Besides anti-apoptotic Bcl2-family members, some other players can also negatively regulate p53-induced apoptosis, including IAPs (Inhibitor of apoptosis proteins, e.g. XIAP) [35, 47, 48] and Mcl1 that are mainly activated by the AKT pathway. Mdm2 that

inhibits p53 is expressed as a negative feedback loop by the binding of p53 to the DNA [30]. Moreover, p53 also induces its own expression besides other target genes like *PUMA*, *CDKN1A* (p21), *Bcl-xL*, *BAX*, *CCND1* (cyclin-D1), *CCNG* (cyclin-G), *GADD45* and *NOXA* [37, 49, 50], that are responsible for regulation of cell cycle and apoptosis. For instance, *GADD45* regulates the cell cycle arrest at G2 phase and is involved in DNA repair mechanisms [51, 52].

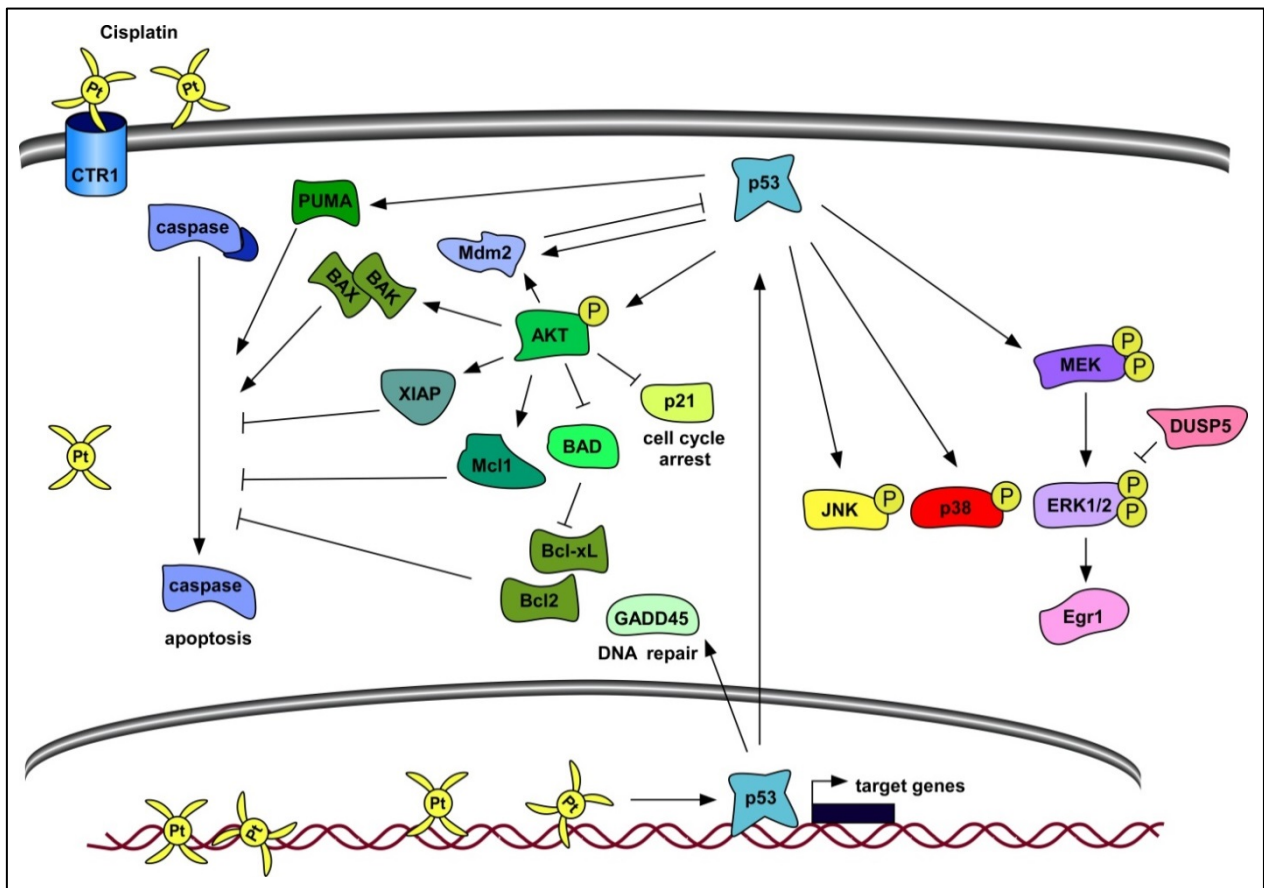


Figure 3: Cisplatin-induced apoptosis. Cisplatin intercalates in DNA and thus activates p53. The start of DNA repair mechanisms is coupled to cell cycle arrest. Increasing amounts of p53 lead to the induction of the apoptotic program with the key pathways MAPK and AKT that regulate the Bcl-2 members which are amongst others key players for the cleavage of caspases.

4.3.2 Resistance to chemotherapeutic treatments

A complication that many lung cancer patients are suffering from is the resistance to chemotherapeutic drugs like cisplatin. Even if the treatment is quite effective at the beginning, many cancer patients relapse with a cisplatin-resistant disease [23, 53].

Although the exact mechanism is not known, some possibilities are suggested in the literature. Resistance to cisplatin that is based on genetic alterations can be found for instance in human lung and cervical cancer cell lines that over-express HSP27, IAPs or AKT, or have constitutive activated AKT levels [54, 55]. AKT seems to play a key role in resistance mechanism as it was shown that inhibition of PI3K or knock out of AKT with siRNA leads to an increased apoptosis rate upon cisplatin treatment [33, 34]. AKT is further suggested to be an upstream key factor in resistance via its targets XIAP, BAD and HSP27 [32-35, 48, 54, 56, 57]. Moreover, the microRNA miR-214 was shown to target PTEN and thus inducing resistance to cisplatin [58]. Another protein that can be involved in the mechanisms of resistance and is highly mutated in 55% of NSCLC tumors [59] is the key mediator of apoptosis p53 that also regulates DNA repair and cell cycle. Additionally, *TP53* is connected to severely reduced tumor suppression and poor prognosis in lung cancer [7, 60]. Re-expression of hematopoietic receptors like EpoR is discussed in the literature and activation of its downstream components STAT5 and Mcl1 result in cell survival in the erythroid system and lymphoblastic leukemia [61, 62]. Although cisplatin can be used in combination with other drugs, e.g. paclitaxel [24, 63] or MEK inhibitors (Clinical Trial Identifiers: NCT01192165 and NCT02151084, [20]), resistance mechanisms are still not fully understood in lung cancer and thus need to be further investigated.

4.4 EpoR signaling in lung cancer

4.4.1 EpoR signaling in the erythroid system

Chemotherapy-induced anemia can be treated by blood transfusion or by the erythropoiesis stimulating agents (ESAs), such as erythropoietin α (Epo- α , Amgen) or Epo- β (Roche) which have comparable properties. The Epo receptor (EpoR) and its signaling pathway are well characterized in erythroid progenitor cells (CFU-Es, colony

forming unit-erythroid) (**Figure 4**) as it is the key regulator of red blood cell production that ensures growth, differentiation and survival of erythroid progenitors in the fetal liver, bone marrow and spleen. The biosynthesis of Epo in the kidney is stimulated by reduced blood oxygen level [64]. EpoR is a member of the cytokine receptor superfamily and is present on the cell surface as a homodimer, which self-interacts at its transmembrane domain [65]. After Epo binding, the erythropoietin receptor undergoes a conformational change that leads to the phosphorylation of the pre-bound, cytoplasmic, tyrosine kinase Janus kinase 2 (JAK2) [66]. The activated JAK2 auto-phosphorylates tyrosine residues on the EpoR cytoplasmic domain that serve as docking sites for interaction with proteins containing a SH2 domain. EpoR phosphorylation activates the phosphoinositide 3-kinase (PI3K) pathway and the MAP kinase cascade of the extracellular signal-regulated kinase (ERK1/2) [67]. The latent transcription factor STAT5 (Signal Transducers and Activators of Transcription) binds to two tyrosine residues of EpoR, is phosphorylated by JAK2 and translocates as a dimer to the nucleus where it starts the expression of target genes like *CISH* (CIS protein, Cytokine-inducible SH2-containing protein) and *SOCS3* (suppressor of cytokine signaling 3), which are translated and serve as negative regulators of JAK2/STAT5 signaling back in the cytoplasm [68]. CIS inhibits STAT5 activation by binding to EpoR, whereas SOCS3 directly binds to the kinase domain of JAK2 and EpoR, thereby inhibiting tyrosine-kinase activity [62, 69-71]. There are three major classes of proteins involved in the negative regulation of EpoR signaling: the protein tyrosine phosphatases SHPs (SH2 domain-containing protein-tyrosine phosphatase), the protein inhibitors of activated STATs (PIAS) and the suppressor of cytokine signaling (SOCS) proteins [71].

Furthermore, the JAK/STAT pathway is able to activate the MAP kinase p38 leading to the stabilization of *SOCS3* mRNA [72-74]. On the contrary, miR-203 can negatively regulate the *SOCS3* mRNA level [75, 76]. Additionally, it has been suggested that Epo binding promotes degradation and endocytosis of the Epo receptor [77, 78] and Epo [79] (**Figure 4**). Moreover, EpoR is expressed in several non-hematopoietic tissues including myocytes, cortical neurons, and prostatic, breast and ovarian epithelia [80-82]. Besides controlling erythropoiesis, Epo is therefore known to have other biological functions

such as involvement in the wound healing process [83], rescue of cells from apoptosis [84-87] and it plays an important role in the brain's response to neuronal injury [82, 88].

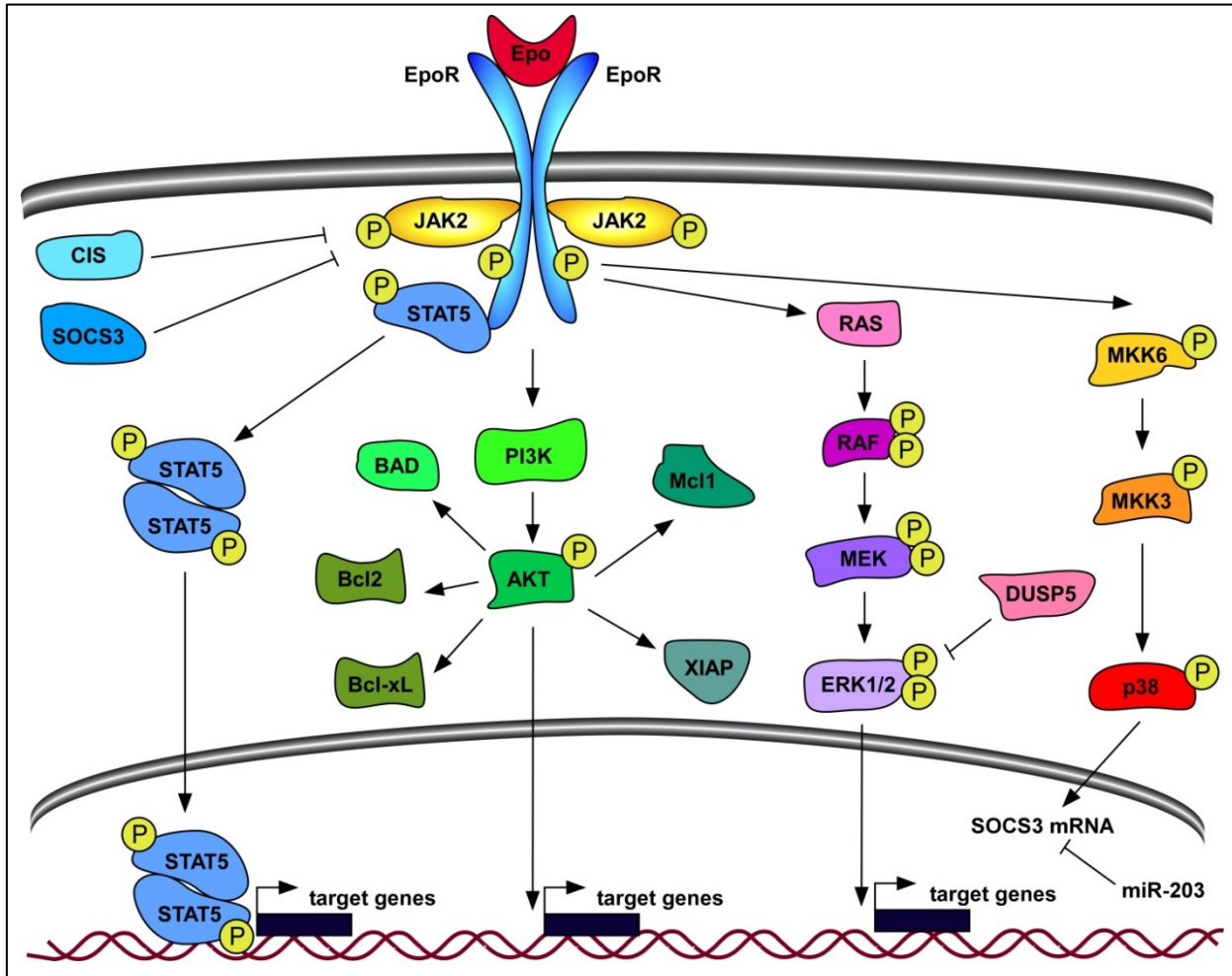


Figure 4: EpoR signaling. Binding of the ligand erythropoietin (Epo) to its receptor EpoR leads to the activation of JAK2 that phosphorylates EpoR and thus activates the three main signaling pathways: JAK2/STAT5, PI3K/AKT and MAPK. Phosphorylated STAT5 dimerizes, translocates into the nucleus and starts the expression of the negative feedback components *CISH* and *SOCS3*.

4.4.2 EpoR signaling and its role in tumorigenesis

Erythropoietin treatment is the standard of care for patients suffering from a chemotherapy-induced anemia. Unfortunately, recent studies have shown that Epo can have tumor stimulating effects [89] and Epo and EpoR co-expression is shown to be associated with poor survival of non-small cell lung cancer patients, even at stage I [90].

The Epo receptor was shown to be present in some cancer cell lines. Protein levels of the phosphorylated and unphosphorylated EpoR signaling compounds ERK, AKT and STAT5 could be detected in the NSCLC cell line H838 [91]. In H838 cells the SOCS3 promoter is suggested to be hyper-methylated resulting in reduced expression of SOCS3, which leads to constitutively phosphorylated STAT5 and JAK2 [92]. Moreover, other NSCLC cell lines, like A549, H661 and H1650, also express EpoR [93-95]. For this reason, the treatment of patients with Epo is discussed controversially [91, 96-98].

4.5 TGF- β signaling in lung cancer

4.5.1 TGF- β signaling

Epithelial-to-mesenchymal transition (EMT) plays a crucial role in the tumor progression by increasing the invasive capacity of cells. Transforming growth factor beta (TGF- β) is a key regulator of EMT. TGF- β signaling (**Figure 5**) is mediated by the TGF- β serine/threonine kinase receptors type I and type II (TGFBR1/2). By binding of the ligand, a complex of two receptor homo-dimers is formed, activated and stabilized. This active tetrameric receptor complex phosphorylates receptor-regulated SMAD proteins (R-SMADs, e.g. SMAD2, SMAD3), which then bind co-SMADs (e.g. SMAD4). The SMAD complexes are transported into the nucleus and act as transcription factors for multiple target genes [99-102]. Besides the most prominent downstream signaling cascade of SMADs, also other pathways can be activated. For instance, the MAP kinase pathway is activated via RAS which leads to the phosphorylation of MEK, ERK1 and ERK2 [103]. Moreover, the ubiquitin ligase TRAF6 binds to TGFBR1 and activates Jun/p38 via MAPKKK TAK1 [104, 105]. Additionally, the MAPK pathway is able to target R-SMADs including SMAD2 and SMAD3 [106, 107]. Another protein that can be activated upon TGF- β stimulation is PI3K which leads to phosphorylation of AKT at Ser-473 [108, 109]. By inducing the expression of p21, TGF- β also plays a role in regulation of cell cycle [110].

Two TGF- β target genes are *SMAD6* and *SMAD7* that are classified as inhibitory SMADs (I-SMADs). *SMAD7* negatively feeds back to the SMAD complexes and TGFBR1 [111], whereas *SMAD6* negatively regulates *SMAD4*. The E3 ubiquitin ligase

SMURF1 (SMAD ubiquitination regulatory factor-1) ubiquitinates and thus induces proteosomal degradation of SMAD1 and SMAD5 and SMURF2 targets SMAD1, SMAD2, SMAD3, SMAD6 and SMAD7. Other co-repressors such as SKI, SnoN and TGIF attenuate SMAD-mediated transactivation [112].

Moreover, BAMBI (BMP and activin membrane-bound inhibitor homolog), a TGF- β pseudoreceptor lacking an intracellular serine/threonine kinase domain required for signaling, also negatively regulates TGF- β signaling [113] and if over-expressed is able to increase proliferation and migration rate in vitro in ovarian cancer [114]. BAMBI was found to be epigenetically silenced in bladder cancer [115] and is absent in breast cancer [116].

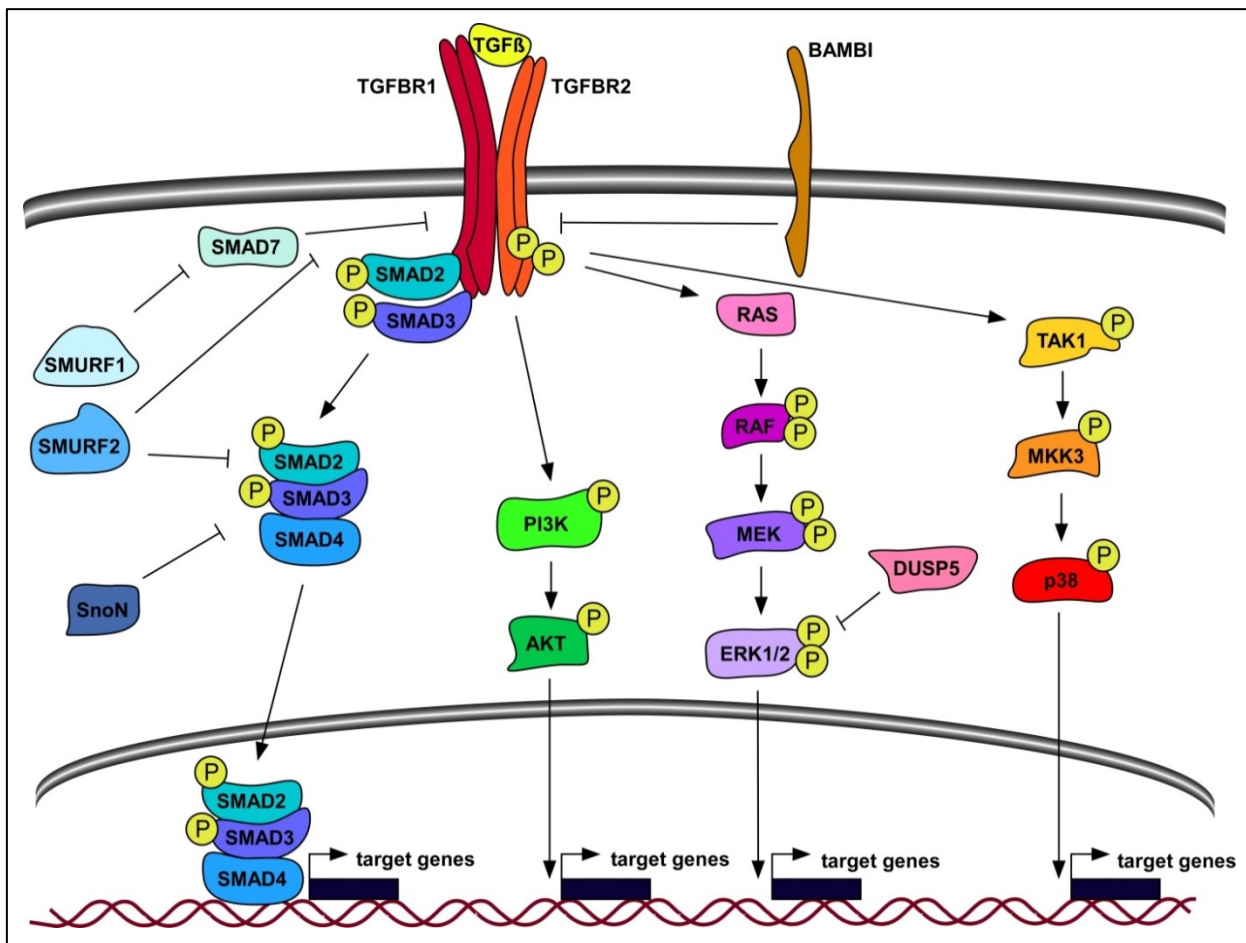


Figure 5: TGF- β signaling: Binding of TGF- β to the receptor hetero-tetramer complex consisting of TGFBR1 and TGFBR2 activates the SMAD, AKT and MAPK signaling pathways. The negative regulators of the TGF- β signaling pathway are SMURF1 and SMURF2, SnoN and SMAD7 and the pseudoreceptor BAMBI.

4.5.2 TGF- β and its role in metastasis by inducing EMT

TGF- β is known to play a dual role in tumor progression by inhibiting tumor growth at early stages but promoting tumor invasiveness and metastasis at later stages of tumor progression for instance by inducing epithelial-to-mesenchymal transition (EMT) [117-122]. EMT is characterized by the development of a fibroblastoid phenotype and the loss of cell-cell-adhesions by suppression of components that built up junctional complexes like E-cadherin [123]. Changes in microfilaments, microtubules and intermediate filaments (e.g. Vimentin) further promote the architectural re-organization and cell motility [121]. In parallel, production of matrix proteins, e.g. fibronectin and collagen is induced. A basic feature of EMT is the nuclear reprogramming which involves transcription factors like Snail and Slug, ZEB1 and ZEB2 [121, 124]. Thus, EMT is suggested to be the main source for invasiveness and metastasis of tumors.

Moreover, genetic alterations like mutations or over-expressed/reduced expression of molecules that are involved in the TGF- β pathway can induce tumorigenesis. For instance, it was shown that high TGF- β levels correlate with poor prognosis in lung cancer [125-127]. The most commonly mutated TGF- β pathway genes in human cancer are *TGFBR2*, *TGFBR1*, *SMAD4* and *SMAD2* [128]. It was shown in lung cancer that *TGFBR2* is frequently down regulated, which is connected to high invasion rates and poor outcome [129]. Furthermore, a regulatory cascade involving microRNAs and EMT regulators is likely to contribute significantly to cancer progression. For instance, the miR-200 family (miR-200a, miR-200b, miR-200c, miR-141 and miR-429) and miR-205 are shown to regulate EMT via e.g. *ZEB1*, *ZEB2*, *CDH1* (E-cadherin) and *VIM* (Vimentin) in several cancer types [130-134]. Moreover, tumor cells that undergo EMT are more resistant to chemotherapy and radiotherapy [135-137]. All these findings demonstrate the importance of TGF- β pathway signaling in tumorigenesis, migration and invasion, yet the exact mechanisms are still undefined and need to be further investigated.

4.6 Systems Biology approach

Every single cell contains a large number of different compounds. Just listing the components does not give any information about the dynamics or explain phenotypic changes. The complexity of a study of a cellular system increases by taking cellular processes, such as signal transduction and regulation processes like DNA methylation, transcription, translation, (de)phosphorylation, or proteolytic degradation, into account. Cancer cells with genetic alterations even complicate the situation in this study. To gain deeper insights into the complexity of signaling and phenotypic changes of lung cancer cells upon different stimuli, such as MEK inhibitors, cisplatin, Epo or TGF- β , a systems biology approach will be applied.

Systems biology aims to understand how cellular systems work and how cellular processes are regulated. Therefore it comprises quantitative information from experiments and computational modeling techniques. It integrates approaches from different fields such as biology, chemistry, physics, medicine, mathematics and computer science showing its interdisciplinary character [138-140]. Kitano defines systems biology as a hypothesis-driven concept (**Figure 6A**) [141, 142]. Data or knowledge is used to establish a computational modeling structure that represents assumptions and hypotheses about a biological system. This hypothesis is tested *in silico* by “dry” experiments such as model simulations. If the model passes the test, it is experimentally validated in the next step (“wet” experiments) and the model is calibrated based on the experimental data. Inadequate models are eliminated and adequate models are refined by using the newly acquired quantitative data.

Mathematical models are an abstract representation of objects and processes. Within the available types of mathematical modeling approaches, models based upon ordinary differential equations (ODEs) are able to describe the biochemical rate laws. Networks of differential equations can model the temporal and spatial dynamics of biochemical processes to achieve a better understanding of chemical mechanism or network dynamics under various conditions [143].

There are two major approaches in systems biology or systems medicine: bottom up and top down (**Figure 6B**) [144-147]:

Top-down approach:

The top-down approach follows a stepwise working plan. The general idea is to start with the big picture followed by the breaking down into smaller segments or sub-systems. Therefore, the starting point is generally a huge data set generated with “-omics”-techniques such as genomics or transcriptomics. Based on this data, a mechanisms, correlation or hidden pattern is tried to be identified or extracted and a hypothesis or model is established. Based on the experimental validation, the hypothesis can either be rejected or supported.

Bottom-up approach:

The bottom-up approach pieces together sub-systems to gain more insights into the big picture of complex systems. For that purpose, prior knowledge about a sub-system is used for a model which is able to predict the behavior of a system. Specific experiments are designed to either validate or refine the hypothesis. At an advanced stage, sub-systems are placed together and information, e.g. about different pathways, are connected to a big and complex model.

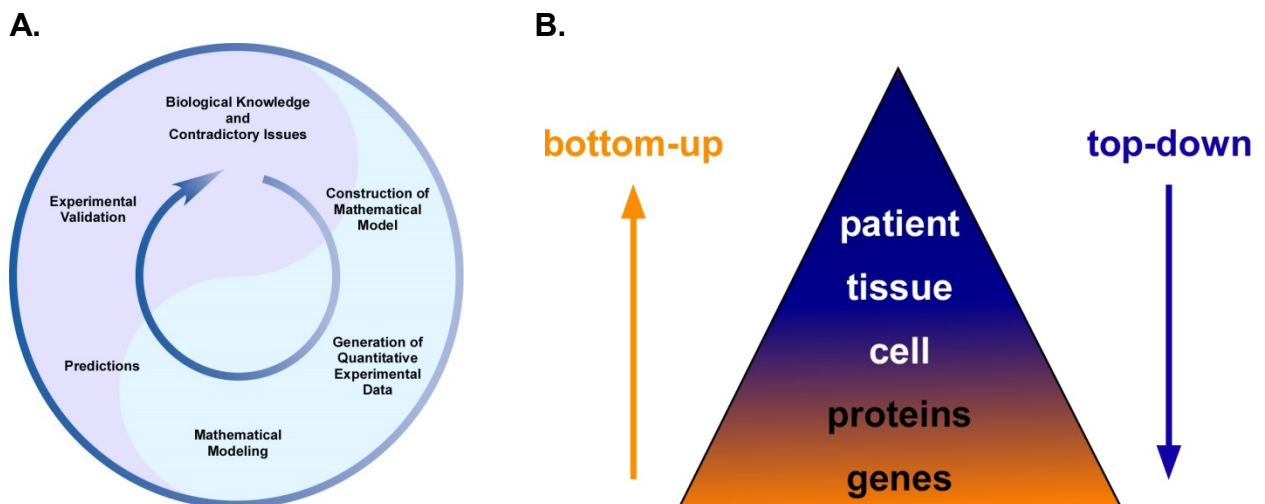


Figure 6: Systems Biology (A) works as a hypothesis-driven cycle in which includes quantitative experimental data generation, mathematical modeling, *in silico* predictions, experimental validation and design of new experiments (adapted from [140]). **(B)** Systems biology can follow either a top-down or a bottom-up approach.

Both approaches are used for biological but also medical and synthetic biology purposes. One criticism of the bottom-up approach in this context is hereby that physiological changes are predicted purely from molecular events in a cell and thus might not be able to fully describe complex phenotypes such as diseases. In contrast, the top-down approach starts at the phenotypic level of a specific disease and breaks down to functional pathways to identify what is important in a specific disorder because it is potentially complete [145, 146]. In general, it is hoped that systems biology and systems medicine will reduce the size and the costs of clinical trials and ensure that clinicians prescribe the right medicines for the right patient at the right time. The improved level of understanding will furthermore result in improved effectiveness in pharmaceutical drug development, molecular diagnostics and personalized medicine [141, 142].

In this work, the integration of large data sets generated by mass spectrometry, quantitative immunoblotting, microarray, quantitative RT-PCR, next generation sequencing, whole genome sequencing and live cell microscopy will be performed by the theoretical cooperation partners in the groups of Prof. Jens Timmer (Freiburg University), Prof. Fabian Theis (Helmholtz Zentrum München), Dr. Hauke Busch and Dr. Melanie Börries (Freiburg University) and Prof. Thomas Höfer (DKFZ Heidelberg) and transferred into mathematical models.

4.7 Objectives

Lung carcinoma with its most prevalent form non-small-cell lung carcinoma (NSCLC) is worldwide one of the leading causes of cancer-related deaths. Due to the fact that lung cancer metastasizes already at early stages, most of the patients receive chemotherapy, e.g. cisplatin. Even if the treatment is quite effective at the beginning, many cancer patients relapse with a cisplatin-resistant disease. Efforts are currently undertaken utilizing co-treatments with specific inhibitors for components of signaling pathways potentially involved in tumorigenesis. Although cisplatin-induced apoptosis is well-understood, the specific mechanisms contributing to therapy resistance or side effects of combined treatments with targeted therapies, e.g. MEK inhibitors, remain unresolved. Moreover, cisplatin treatment frequently results in chemotherapy-induced

anemia which can be treated with erythropoietin (Epo). However, recent studies showed that Epo may have a tumor stimulating effect and therefore the treatment with Epo is controversially discussed.

The aim of this work was to gain insights into signaling pathways that might play a role in tumorigenesis or resistance to cisplatin, Epo- and TGF- β -induced signaling pathways.

The specific aims of this work are:

1. To elucidate whether there is a combinatorial effect of pathway inhibitors, e.g. MEK inhibitors, and the chemotherapeutic agent cisplatin in NSCLC cell lines.
2. To analyze the effect of the presence of a functional EpoR in NSCLC cell lines and its impact on cisplatin-based chemotherapy.
3. To identify the differences in Epo-induced signaling in erythroid progenitor cells and the NSCLC cell line H838 by dynamic pathway modeling to better define the risk of EpoR expression in lung cancer.
4. To determine the impact of TGF- β treatment in NSCLC cell lines.

5. Results

5.1 Establishment of Standard Operating Procedures (SOPs)

To be able to answer the specific aims of this study, such as to elucidate the effect of different treatments alone or in combination with other treatments, standard operating procedures (SOPs) for the cell cultivation and experiments were defined and standardized quantitative assays were established. This includes the agreement on conform culture dishes, protocols for thawing cells from glycerol stocks, subculturing and amplifying cells.

5.1.1 Identification of cell lines as model system for NSCLC

As patient material is very limited and processes in tumorigenesis are rather complex, the two non-small-cell lung carcinoma (NSCLC) cell lines H838 and H1975 with frequent mutations were selected based on literature information (**Table 2**) as experimental model systems to enable specific analysis of single treatments. H838 is known to contain significant amounts of the wild type Epo receptor (*EpoR*), wild type but amplified *KRAS* [148], a mutated *TP53* [149] and a mutated *CDKN2A* [150]. Moreover, the *SOCS3* promoter was reported to be hyper-methylated [92]. In contrast, the NSCLC cell line H1975 has low levels of *EpoR*, mutated *TP53* and an activating mutation in *EGFR* and *PIK3C* [150]. The T790M-EGFR mutation found in H1975 cells is known to induce resistance to EGFR TKIs (tyrosine kinase inhibitors, e.g. erlotinib, gefitinib) [151]. Literature data about *MET* amplification in H1975 is controversial [151, 152].

To confirm the publicly available mutation status in the NSCLC cell lines H838 and H1975 and to generate more detailed information, the cell lines were characterized by whole genome sequencing (WGS), RNA sequencing (RNAseq) and methyl-CpG immunoprecipitation (MCIP)-based methylome sequencing. The analysis was done by Stephen Krämer and Dr. Naveed Ishaque in the group of Benedikt Brors (DKFZ Heidelberg). All mutations reported in the literature were confirmed. However, no hyper-methylation of the *SOCS3* promoter region in the H838 cell line could be measured by MCIP.

Gene	H838			H1975		
	type	variation (PS)	effect	type	variation (PS)	effect
TP53	SNV	p.E62*	stop-gain	SNV	p.R273H	unknown
KRAS	AMP		over-expression	WT		
EGFR	WT			SNV	p.L858R, p.T790M	activating, EGFR inhibitor- resistant
PIK3CA	WT			SNV	p.G118D	activating
PTEN	WT			WT		
MET	SNV	p.I638L	unknown	AMP		over- expression
CDKN2A	DEL		inactivating	SNV	p.E69*	stop-gain

Table 2: Publicly available information of mutations in the NSCLC cell lines H838 and H1975.

Abbreviations: PS: protein sequence, WT: wild type, SNV: single nucleotide variation, DEL: deletion, AMP: amplification, p protein;

Moreover, *SOCS3* mRNA levels could be detected by RNAseq and validated by qRT-PCR (**Figure 7A**). Interestingly, the level of *SOCS3* mRNA in H838 was even higher compared to the other NSCLC cell lines H1975 and H1650 and to the healthy lung alveolar epithelial cells type II (AECII, kindly provided by Prof. Heimo Mairbäurl, University Hospital Heidelberg) that are believed to be the origin of NSCLC. Additionally, the RNA analysis confirmed the over-expression of *KRAS* in H838 and an over-expression of *TP53* in H1975 cells compared to the other two cell lines could be detected (**Figure 7B**). The mRNA levels of *MET* are higher in H1975 compared to H838 but are comparable to H1650 although just H1975 harbors a higher gene copy number. In conclusion, the NSCLC cell lines H838 and H1975 were verified in their representative pattern of mutations for lung cancer and were therefore used for further analysis.

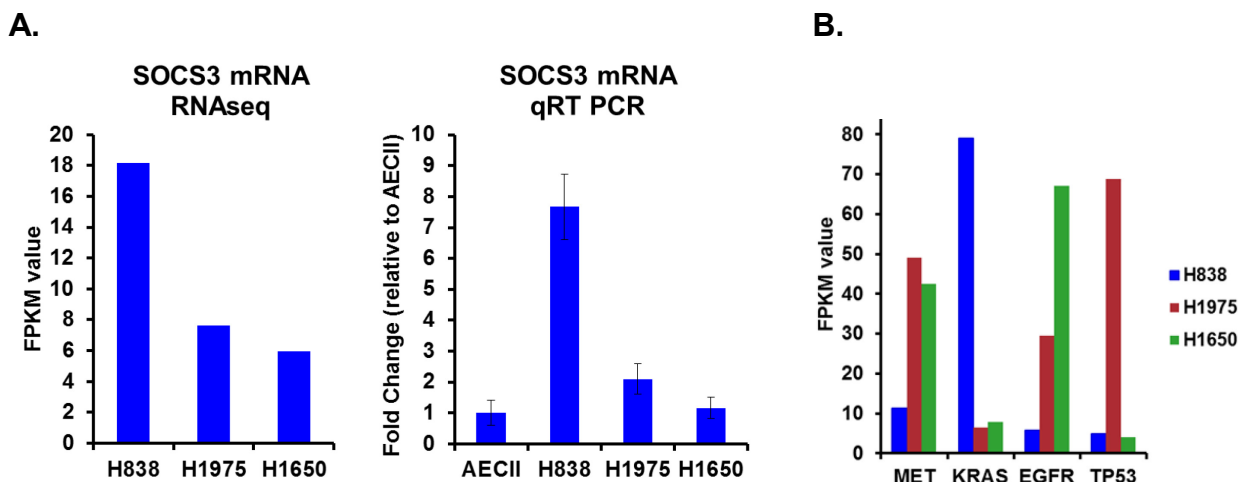


Figure 7: Characterization of NSCLC cell lines. (A) Quantification of the RNAseq data of *SOCS3* mRNA in the NSCLC cell line H838 compared to H1975 and H1650 cells. The validation was performed by qRT-PCR in biological triplicates. The data is plotted relative to the healthy lung control (AECII, alveolar epithelial cells type II). (B) The RNAseq analysis of potential relevant genes with a high mutation frequency in lung cancer is shown in FPKM values for the NSCLC cell lines H838, H1975 and H1650.

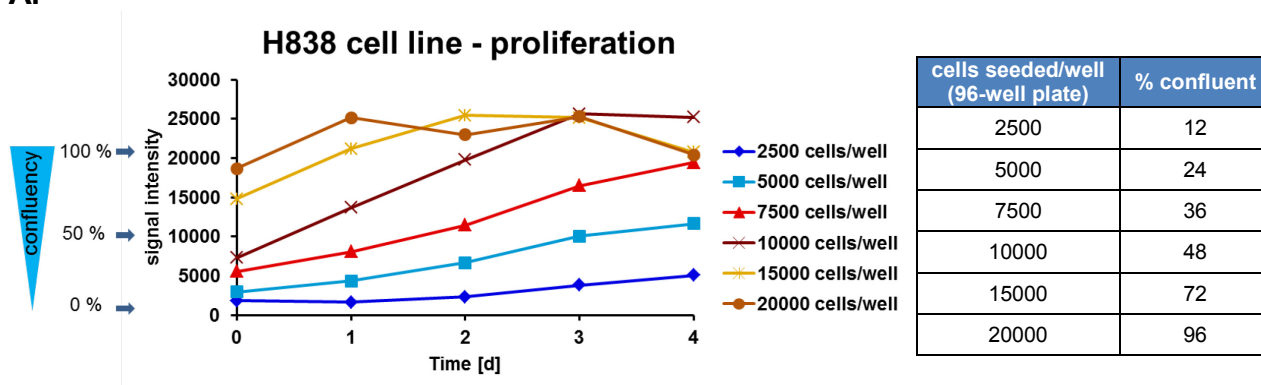
5.1.2 Establishment of optimized confluency conditions for long-term and short-term experiments

To ensure optimal conditions for experiments, different cell confluencies were seeded and cell proliferation was monitored over four days (**Figure 8A**). The cells were washed 24 hours after seeding and kept in growth factor-depleted medium without serum over night before the experiment started (t=0 days). The proliferation was measured using the CellTiter-Blue viability assay. The reduced signal intensity which corresponds to a reduced cell number at t=0 days compared to the time of seeding could be explained by the washing step. The lung cancer cells that were seeded in a very low confluency ($\leq 40\%$) showed low proliferation rates whereas cells at a confluency between 40 and 80% displayed an almost linear increase of proliferation until the maximum confluency was reached.

Further, the influence of the $\geq 100\%$ confluent state on the treatment efficiency was tested. Therefore, cells at a confluency of around 80% and fully confluent cells were treated with 10 U/ml erythropoietin (Epo) and the Epo-induced mRNA *CISH* was measured by qRT-PCR after 2 hours (**Figure 8B**). The 80% confluent condition showed compared to a confluency of $\geq 100\%$ an increased mRNA induction upon treatment.

Thus, a confluency of 80% ($\sim 50,000$ cells/cm² growth area) was selected as optimal condition for experiments over maximal two days (short-term) before the maximum confluency is reached and a confluency of around 50% ($\sim 30,000$ cells/cm² growth area) was established for long-term experiments over several days (see also materials and methods).

A.



B.

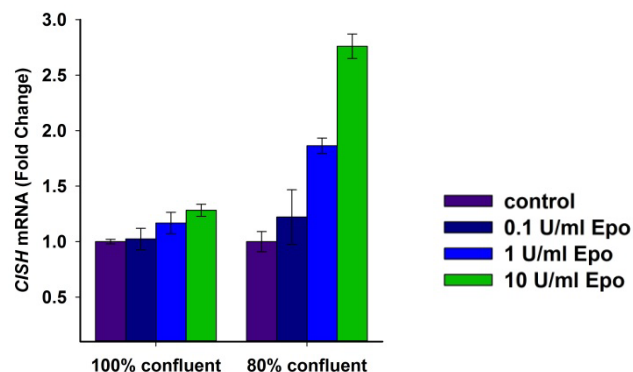


Figure 8: Optimization of experimental conditions. (A) The proliferation was measured with the CellTiter-Blue cell viability assay with different starting confluencies (see table on the right) of the NSCLC cell line H838 in a 96-well format. (B) The Epo-induced target gene *CISH* was measured by qRT-PCR in the H838 cell line in triplicates at a confluency of $\sim 80\%$ and $\geq 100\%$ upon treatment with 0.1, 1 or 10 U/ml Epo ($t = 2$ hours). The data is shown relative to the untreated control ($n=3$).

5.2 Cisplatin-induced apoptosis in NSCLC cell lines

5.2.1 Time- and dose-dependent effect of cisplatin on NSCLC cell lines

Although the pathway of intrinsic apoptosis induced by cisplatin is well known, mechanisms for resistance against this chemotherapeutic compound are poorly understood. Cisplatin is known to induce DNA damage in lung cancer followed by apoptosis when the concentration is high enough. To measure the changes in cell number over time, the sensitive CellTiter-Blue viability assay (Promega) was used. To test the possibility of cell number determination with the CellTiter-Blue assay, the H838 cell line was seeded in different confluencies and the signal intensity was measured. In parallel, the cell number was counted with a Neubauer counting chamber. By plotting the signal intensity against the cell number, a direct linear correlation was observed (**Figure 9A**) that enabled the calculation of the cell number in further experiments when the signal intensity was known.

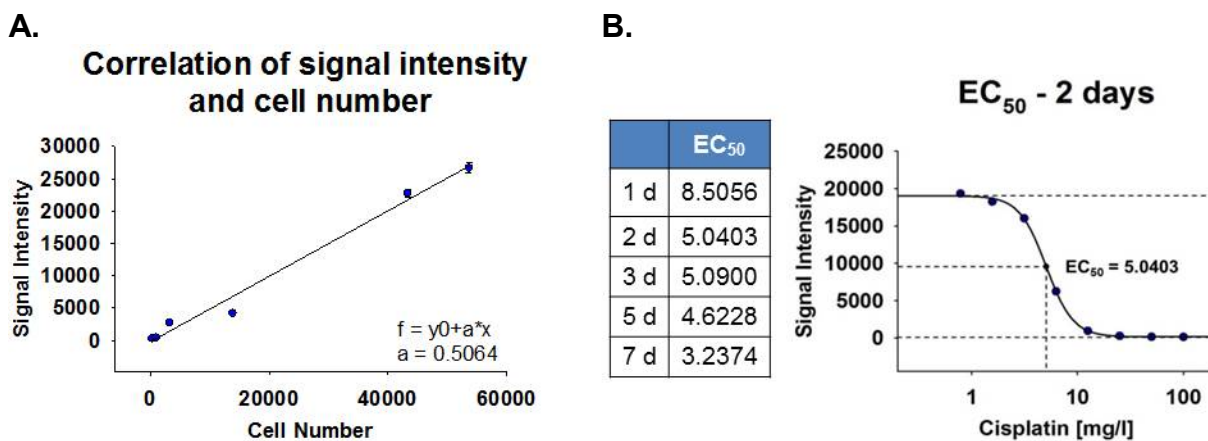


Figure 9: **(A)** The signal intensity of 6 different cell concentrations of the NSCLC cell line H838 was measured with the CellTiter-Blue viability assay and plotted against the cell number that was counted in parallel with a Neubauer counting chamber. The average of the signal intensity of 10 wells (96 well plate) was calculated. **(B)** A dilution series of 100, 50, 25, 12.5, 6.25, 3.125, 1.562, 0.7813 mg/l cisplatin was applied on H838 cells. The signal intensity was measured with the CellTiter-Blue assay and the EC₅₀ values were calculated with the SigmaPlot software for 1, 2, 3, 5 and 7 days (table on the left). The upper and lower dashed lines depict the upper and the lower plateau of the sigmoidal curve that is used to determine the EC₅₀ value.

To investigate the dose- and time-dependent effect of cisplatin on the NSCLC cell line H838, a dilution series of 100, 50, 25, 12.5, 6.25, 3.125, 1.562, 0.7813 mg/l cisplatin was applied according to the SOPs on 10,000 cells/well of a 96-well plate. The plates were incubated for one, two, three, five and seven days and the amount of viable cells was measured with the CellTiter-Blue viability assay. The effective concentration for 50% of the treated cells (EC_{50}) was calculated for different time points (graph and calculation shown representatively for the two days time point, **Figure 9B**). The NSCLC cell line showed an EC_{50} of 8.5 mg/l cisplatin at day one. For further analysis, the EC_{50} that was detected after two days with a starting cell number of 10,000 cells/well (**Figure 9B**) was selected to ensure the initiation of the apoptotic program but also allowing the possibility to start rescue mechanisms if cells are treated in parallel with components with a potential rescue effect. Moreover, this concentration is in the range of clinically relevant doses (see 4.3.1 Cisplatin-induced apoptosis).

5.2.2 Rescue of cisplatin-induced apoptosis by MEK inhibition

5.2.2.1 Influence of signaling pathway inhibitors on cisplatin-induced apoptosis

To gain more insights into resistance mechanisms against chemotherapeutic compounds, the importance of PI3K/AKT and MAPK signaling pathways, which are known to be involved in cisplatin-induced apoptosis signaling [30, 31], was analyzed. Therefore, combined treatment of 5 mg/l cisplatin with inhibitors for PI3K (LY294002, 5 μ M), AKT1/2/3 (AKT inhibitor VIII, 5 μ M) and MEK1/2 (U0126, 2.5 μ M) was applied on the NSCLC cell line H838 for six days (**Figure 10A**) and cell viability was measured with the CellTiter-Blue assay. The growth factor-depleted cells were pre-incubated with the inhibitors for 60 minutes with appropriate concentrations [153, 154]. The inhibition of PI3K and AKT signaling pathway, which is known to play a role in survival and cell cycle regulation, resulted in a decreased proliferation but had no clear effect on the sensitivity to cisplatin. In contrast, inhibition of MEK activity resulted in a strong rescue effect if combined with cisplatin treatment. MEKi alone led to a slightly decreased proliferation that was not detectable before three days upon treatment. As inhibition of the MAPK

pathway seems to be the most promising method to perturb the cisplatin-induced apoptosis, the impact of the MEK inhibitors were studied in more detail.

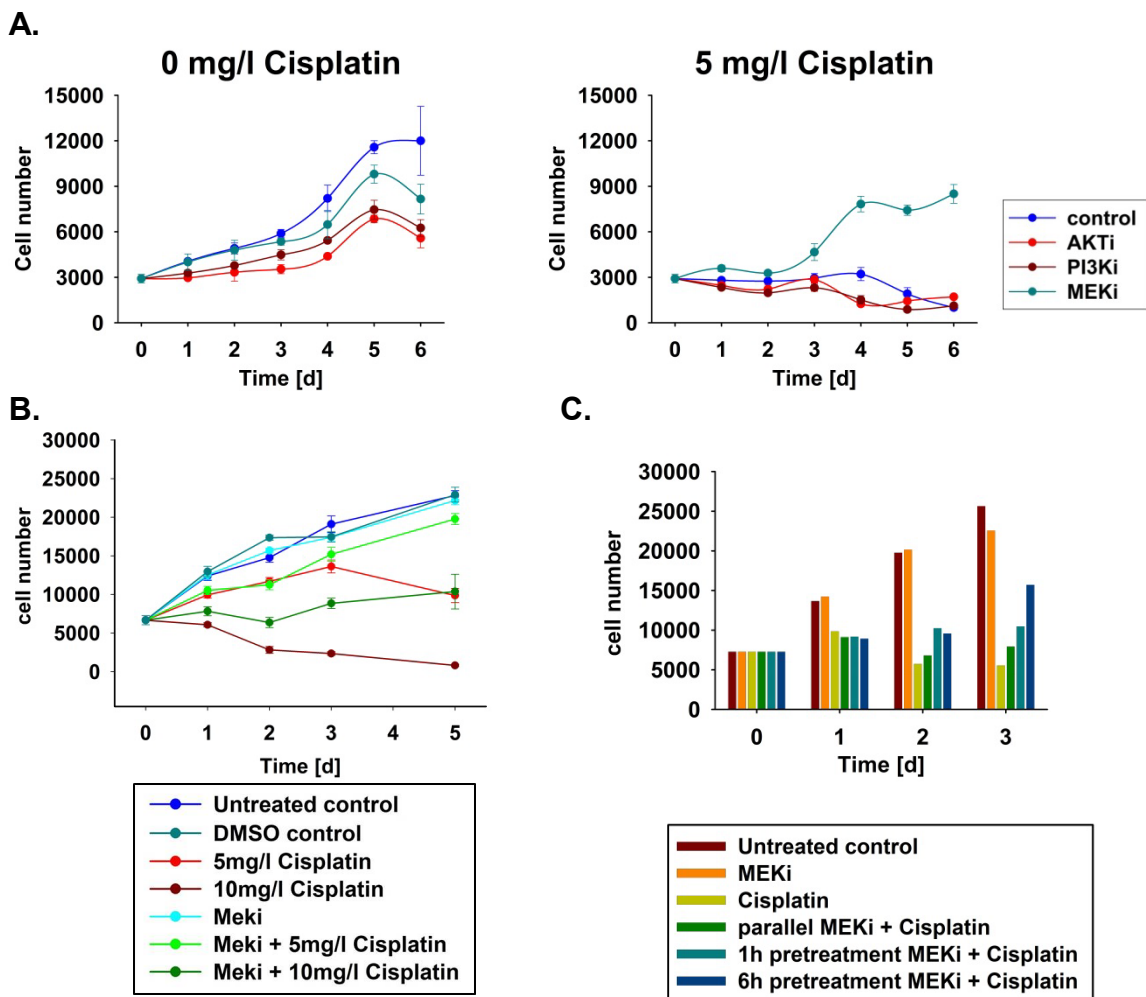


Figure 10: Influence of inhibitors on cisplatin-induced apoptosis in the NSCLC cell line H838 measured by CellTiter-Blue viability assay. (A) Left panel: the cell number is plotted over time upon inhibition of PI3K (LY294002, 5 μ M), AKT1/2/3 (AKT inhibitor VIII, 5 μ M) or MEK1/2 (U0126, 2.5 μ M) compared to the untreated control. Right panel: 5 mg/l cisplatin was added to samples pre-treated for 60 minutes with LY294002, AKT inhibitor VIII and U0126. **(B)** The H838 cell line was pre-treated for 60 minutes with 2.5 μ M MEKi U0126 and either 5 or 10 mg/l cisplatin was added. As controls, the cell number was determined with individual treatments of either 5 mg/l cisplatin, 10 mg/l cisplatin or 2.5 μ M MEKi. Additionally to the untreated control, a DMSO control was included. **(C)** Test of the influence of MEKi pre-treatment times on cisplatin-induced apoptosis (10 mg/l cisplatin). The effect of pre-incubation with 2.5 μ M for 60 minutes was compared to pre-incubation for 6 hours with MEKi and to simultaneous treatment of MEKi and 10 mg/l cisplatin.

To validate these findings and test the reproducibility of this effect, H838 cell line was growth factor-depleted and either treated with 2.5 μM MEKi or pre-treated for 60 minutes with 2.5 μM MEKi before 5 or 10 mg/l cisplatin was added (**Figure 10B**). Individual treatment controls with 5 mg/l cisplatin or 10 mg/l cisplatin without U0126 were included. Additionally to the untreated control, a DMSO control was measured to exclude effects of DMSO, in which the inhibitors are dissolved. Thereby, the DMSO concentration correlated to the DMSO content present upon applying 2.5 μM MEKi. The cells in the untreated control increased their cell number 3-4-fold within 6 days without the addition of growth factors. No effect of DMSO compared to the untreated control could be detected. The negative effect of MEKi on proliferation could not be reproduced. A dose-dependent effect of cisplatin could be observed. Treatment with 5 mg/l cisplatin resulted in a decreased cell number whereas a dose of 10 mg/l cisplatin led to a drastically reduced cell number compared to the untreated control. Pre-treatment with MEKi enabled the cells to completely counteract the treatment with 5 mg/l cisplatin and resulted in a higher cell number after five days compared to 5 mg/l cisplatin alone. The combination of 2.5 μM MEKi and 10 mg/l cisplatin did not affect cell proliferation but showed an increased proliferation after three days. The MEKi rescue effect on the higher dose of cisplatin was already visible after 24 hours, whereas the lower dose resulted only in an effect after three days of treatment.

To study the influence of the MEKi pre-incubation time on the cisplatin sensitivity of H838 cells, the previously tested condition of 60 min pre-treatment was compared to an elongated pre-treatment time of 6 hours before adding 10 mg/l cisplatin and a simultaneous treatment of 2.5 μM MEKi and 10 mg/l cisplatin (**Figure 10C**). As controls, the cell numbers of H838 cells treated individually with 2.5 μM MEKi or 10 mg/l cisplatin were measured additionally to an untreated control. The proliferation of the untreated cells without the addition of growth factors could be reproduced. MEK inhibition showed no significant changes in the cell number compared to the untreated control. The cells that received 10 mg/l cisplatin alone reacted with a slight decline in cell number over time. The effect of pre-incubation for one hour with MEKi on the cisplatin sensitivity could be reproduced as well. The longer pre-incubation time of 6 hours with MEKi increased the rescue effect on the second day compared to cisplatin treatment alone

and was shown to be more effective after 3 days compared to one hour pre-treatment of MEKi. By simultaneous treatment of U0126 and cisplatin, the MEKi-induced rescue effect could not be detected before the third day of treatment but turned out to be less effective compared to pre-treatment with U0126.

In conclusion, the inhibition of the activity of MEK with the MEKi U0126 resulted in a decreased cisplatin sensitivity of the NSCLC cell line H838. This MEKi rescue effect was even more prominent with higher cisplatin doses or increased pre-incubation times with MEKi before adding cisplatin.

5.2.2.2 Influence of MEKi on protein levels of ERK

ERK is the direct, and so far the only known, target of MEK [11] and can be activated upon cisplatin treatment [30]. To determine and quantify the effect of U0126 and cisplatin on ERK phosphorylation in the NSCLC cell line H838, the phosphorylated and total protein levels of ERK (ERK1+ERK2) were detected by quantitative immunoblotting (**Figure 11A**). To this aim, the H838 cell line was pre-treated for 60 minutes with 2.5 μ M MEK inhibitor U0126 (MEKi) before adding 10 mg/l cisplatin (Cis). As controls, the pERK and ERK protein levels were determined for the untreated control (Ctrl) and individual treatments of 10 mg/l cisplatin or 2.5 μ M U0126. Time points were taken 10 minutes, 6 hours, 12 hours and 24 hours after the treatments.

To determine how much ERK is phosphorylated relative to the total ERK level, the bands on the blot were quantified and the pERK-to-ERK-ratio was calculated (**Figure 11B**). The untreated control showed a slight increase in ERK phosphorylation relative to the total ERK level within 24 hours. Cisplatin increased ERK phosphorylation already after 10 minutes of treatment compared to the starting level, with maximum at 6 hours and decreasing over time. In contrast, pre-treatment with 2.5 μ M U0126 resulted in a reduced phosphorylation of approximately 50% compared to the untreated control. This inhibition effect of MEKi diminished over time and was not detectable any more after 24 hours. Moreover, the analysis revealed that the combination of MEKi pre-treatment followed by cisplatin treatment showed comparable ERK phosphorylation as MEK inhibition alone.

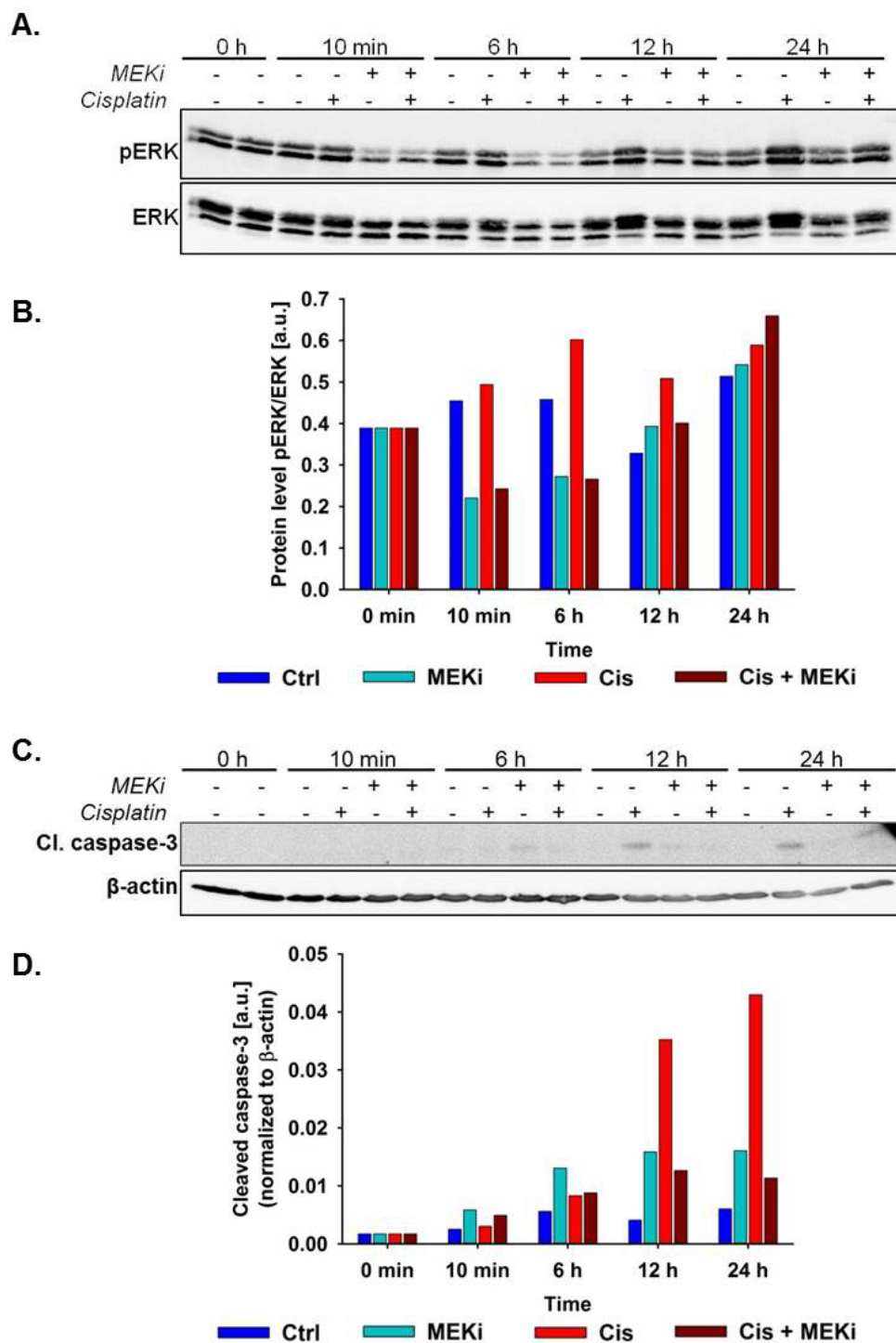


Figure 11: Quantitative immunoblotting in the NSCLC cell line H838. This experiment was performed in triplicates and one representative example is shown. The cells were treated with 10 mg/l Cisplatin (Cis) and/or 2.5 μ M MEK inhibitor U0126 (MEKi) or left untreated (Ctrl). After cell lysis, the proteins were separated by 10% SDS-PAGE, transferred to a nitrocellulose membrane and detected on the Image Quant LAS 4000 by chemiluminescence. **(A)** The phosphorylated and total ERK levels (ERK1+ERK2) were detected. **(B)** The pERK to ERK ratio was calculated of the quantified bands. **(C)** The apoptosis marker cleaved caspase-3 and the housekeeper β -actin are shown. **(D)** Quantification of the cleaved caspase-3 relative to β -actin.

To further test whether the decreasing cell number of cisplatin-treated cells could be ascribed to apoptosis, but also to investigate if additional inhibition of MEK results in decreased apoptosis, the protein level of cleaved caspase-3 as an apoptotic marker was measured by quantitative immunoblotting (**Figure 11C**). To this aim, H838 cells were serum-starved and incubated with the same treatments described in **Figure 11A**. The quantified bands (**Figure 11D**) of the untreated control showed a very slight increase in cleaved caspase-3 levels over time. In contrast, chemotherapeutic treatment with 10 mg/l cisplatin resulted in the cleavage of caspase-3 visible at the 6 hour time point and was still detectable and even stronger after 24 hours. The incubation with 2.5 μ M MEKi U0126 led to moderate increase of active caspase-3 which was reached after 6 hours and stayed constant afterwards in the time observed. The combination of pre-treatment with 2.5 μ M MEKi and 10 mg/l cisplatin showed comparable results as MEK inhibitor treatment alone.

In conclusion, MEK inhibition increases cisplatin-induced phosphorylation of ERK and cleavage of caspase-3 in the NSCLC cell line H838. The combination of MEKi and cisplatin shows comparable results as MEK inhibition alone.

5.2.2.3 Influence of MEKi on the cell cycle

As shown in **Figure 10A**, inhibition of MEK activity can have an influence on proliferation of the NSCLC cell line H838. In combination with the observation that cisplatin targets fast dividing cells [30], it was hypothesized that the rescue mechanism of MEKi on cisplatin-induced apoptosis in NSCLC cells is connected to the regulation of the cell cycle.

To test this, the length of the cell cycle phases were measured in H838 cells that stably express the FUCCI sensor (kindly provided by Dr. Sofia Depner) by live cell microscopy. The FUCCI system is a fluorescent protein-based system that employs both a red (mKate2) fluorescent protein fused to the cell cycle regulator Cdt1 (present in G1-phase) and a green fluorescent protein (EGFP) fused to Geminin (present in S-, G2-, and M-phase) and thus enables the discrimination between the G0/G1- and the S/G2/M-phases (**Figure 12A+B**).

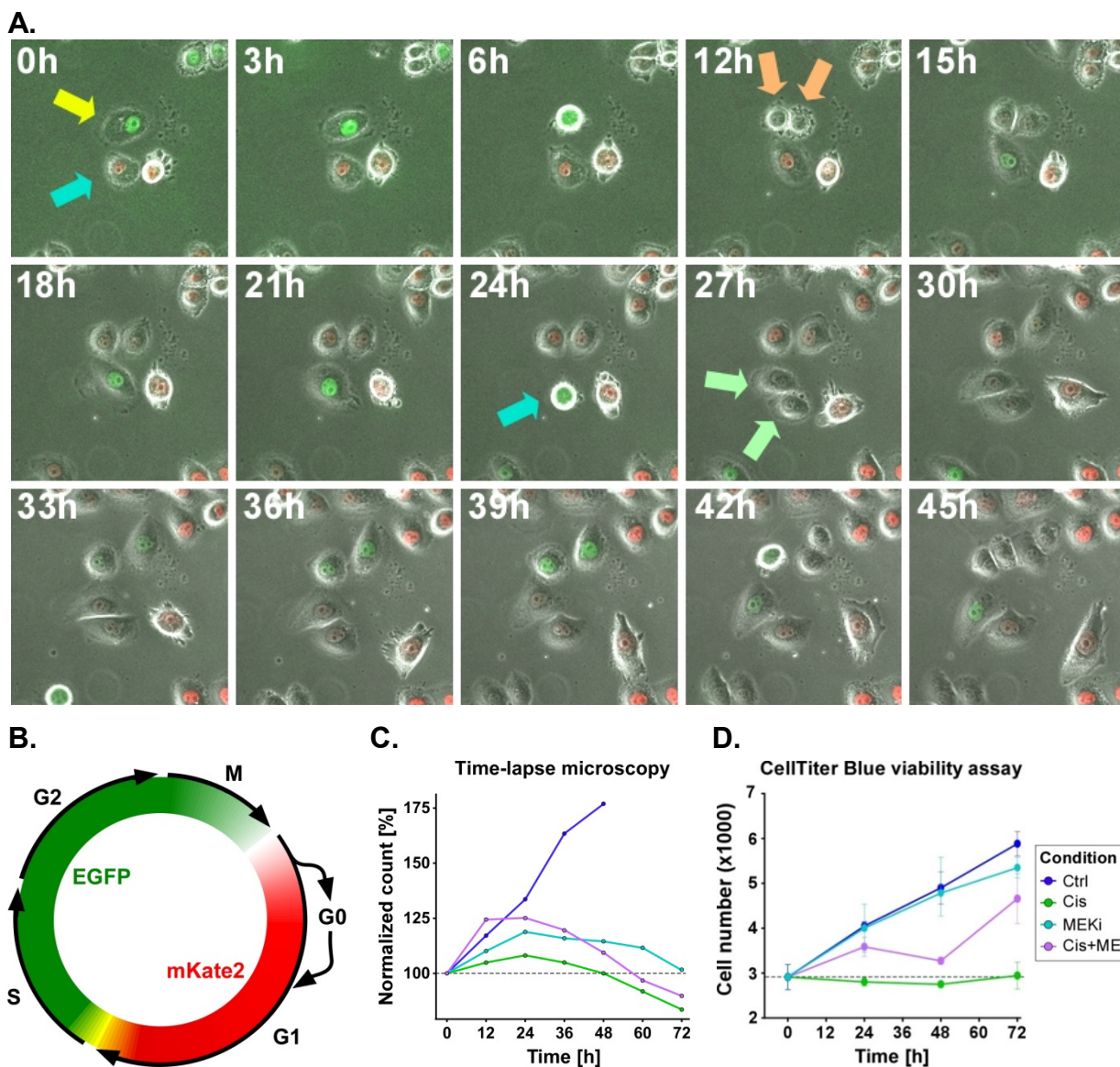


Figure 12: Time-lapse microscopy of the NSCLC cell line H838 expressing the FUCCI sensor enables the measurement of the length of the cell cycle phases. (A) Two mother cells (yellow and blue arrows) were followed until dividing into two daughter cells (orange and green arrows). **(B)** The cell cycle phases were identified by phase-specific expression of EGFP and mKate2. **(C)** The cells were imaged with a confocal microscopy (Nikon Ti eclipse). The images of the time course were taken every 20 minutes. The analysis of the microscopy data sets shows the changes in cell number upon single and combined treatment with 5 mg/l Cisplatin (Cis) and/or 2.5 μ M MEKi (MEKi) in comparison to the untreated control (Ctrl). The experiment was performed twice. **(D)** The CellTiter-Blue viability assay of the wild type cell line H838 with the same treatments is shown in biological triplicates.

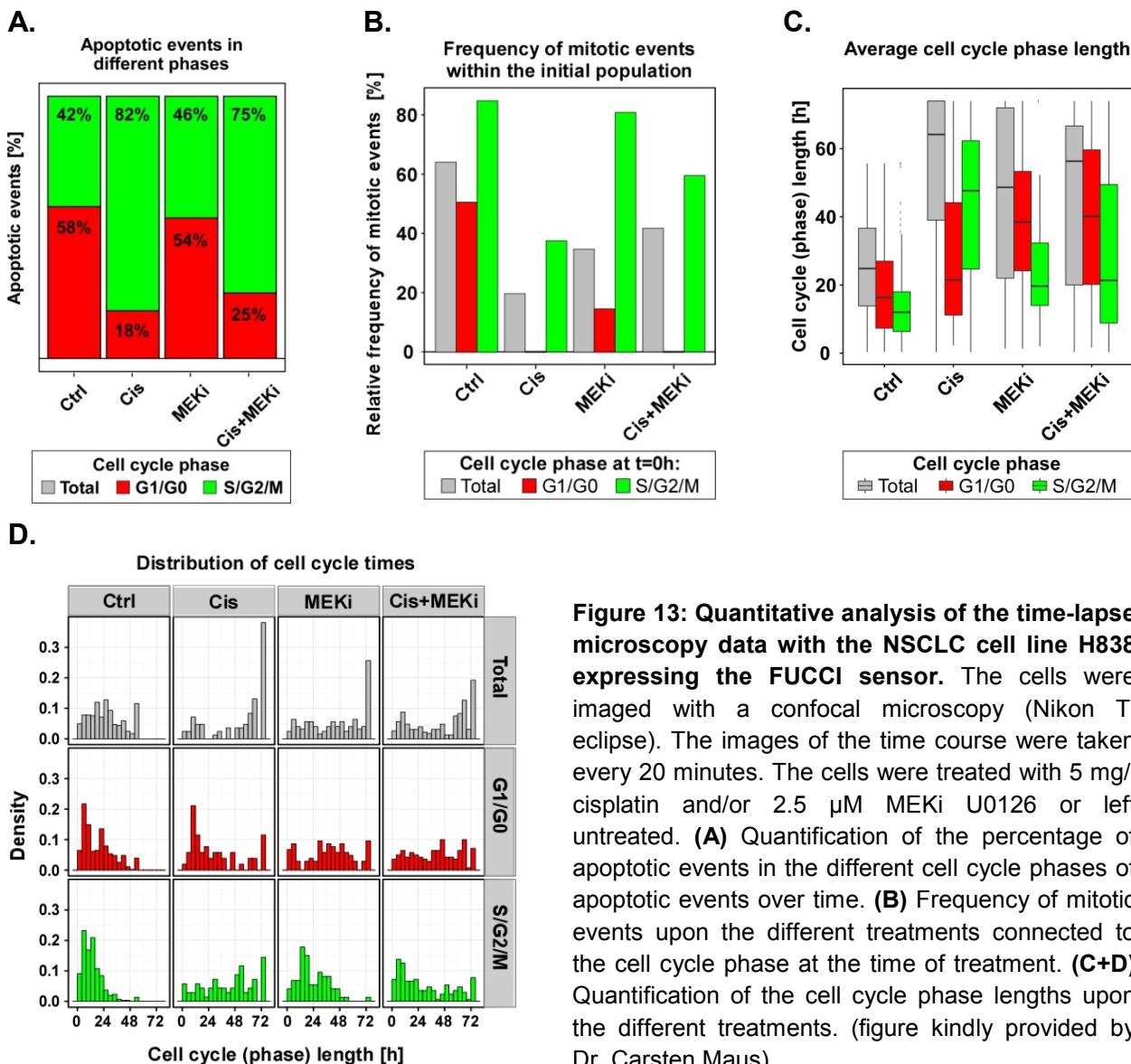
The cells were seeded with 50% confluency according to the SOPs, growth factor depleted, pre-treated with 2.5 μ M MEK inhibitor U0126 (MEKi) and/or 5 mg/l cisplatin (Cis) or left untreated (Ctrl) (**Figure 12C**). The H838-FUCCI cells were imaged with a confocal microscopy (Nikon Ti eclipse). The images of the time course were taken every 20 minutes over 72 hours. As expected, the cells of the untreated control proliferated whereas the cisplatin treatment induced apoptosis. The combination of MEKi pre-treatment and additional cisplatin treatment resulted in an increased cell number compared to cisplatin treatment alone. However, the cells under the microscope showed decreased cell numbers if treated with cisplatin or MEK inhibitor compared to the CellTiter-Blue viability assay (**Figure 12C+D**). Nevertheless, the rescue effect of MEKi on the cisplatin-induced apoptosis was detectable with both assays.

By tracking the cells, mother and daughter cells could be followed and connected in a time-resolved manner to the cell cycle phases, cell divisions and apoptotic events. The cell tracking and the mathematical analysis of the microscopy data was performed by Dr. Carsten Maus in the group of Prof. Thomas Höfer (DKFZ Heidelberg).

The analysis of the connection between the cell cycle phase in which the cells received cisplatin and the apoptotic events revealed that the cells of the untreated controls and the cells that were treated with MEKi did not show a clear preference for the cell cycle phase in which they went into apoptosis (**Figure 13A**). In contrast, the cisplatin-treated cells predominantly died in the block of the S/G2/M-phases. This was true for individual treatment with cisplatin or cisplatin in combination with MEK inhibition, where 82% and 75% of all cells of the initial population that went into apoptosis died in the S/G2/M-phases.

It was further analyzed if the frequency of mitotic events was connected to the applied treatments (**Figure 13B**). Approximately 65% of the initial population of the untreated control underwent mitosis. These 65% were composed of approximately 50% of the cells that were in the G1/G1 cell cycle phase and approximately 80% in the S/G2/M phase of the whole initial population. Cisplatin treatment resulted in a reduced cell division rate of approximately 20% of the initial population and the cells that were in the G1/G0 phase at the time of the treatment did not even divide any more. MEK inhibition decreased the mitotic events of cells that were treated during the G1/G0 cell cycle

phase in comparison to the untreated control. The combination of MEKi and cisplatin resulted in a slightly decreased mitosis rate of cells in the S/G2/M phase whereas cells that were in the G1/G0 phase at the time of the treatment did not undergo mitosis.



Moreover, the lengths of the cell cycle phases were determined for the different treatments (**Figure 13C+D**). The analysis showed that the untreated control showed an average G1/G0 cell cycle phase length of approximately 15 hours and an average S/G2/M cell cycle phase length of approximately 10 hours. The chemotherapeutic drug

prolonged the S/G2/M-phases to approximately 50 hours but did not affect the length of the G1/G0 phase. Inhibition of MEK activity resulted in increased G0/G1 phase lengths and a slight elongation of the S/G2/M phase compared to the untreated control. The combination of MEKi and cisplatin treatment resulted in comparable cell cycle phase lengths like MEKi treatment alone.

In conclusion, MEK inhibition was shown to result in a prolonged G0/G0 cell cycle phase in cisplatin-treated cells. As cisplatin was shown to mainly target cells in the S/G2/M phase, this might hint to an indirect rescue effect by giving the cell more time, for instance for DNA-repair, which results in an increased cell number.

5.2.2.4 Influence of MEKi on gene expression

As shown in **Figure 11**, MEK inhibitor U0126 inhibits cisplatin-induced phosphorylation of ERK on protein level and it is known that this can lead to a G1 arrest in fibroblasts and pancreatic cancer cell lines [14, 155] and activation of ERK is even required to enter the S phase [11-13]. Moreover, we could show that addition of U0126 to the cisplatin-treated NSCLC cell line H838 resulted in a beneficial effect induced by cell cycle arrest compared to chemotherapeutic treatment alone. To investigate how U0126 alone and in combination with cisplatin influences the MAPK signaling and how this effects the cell cycle on RNA level, quantitative RT-PCR was performed (**Figure 14**). Moreover, it was tested whether MEK inhibition, additionally to cell cycle regulation, leads to counteraction of cisplatin-induced apoptosis by altered expression of pro- and anti-apoptotic genes.

To this aim, the NSCLC cell line H838 was pre-treated for 60 minutes with 2.5 μ M MEK inhibitor U0126 (MEKi) before 10 mg/l Cisplatin (Cis) was added. Moreover, individual treatments with 2.5 μ M MEK inhibitor or 10 mg/l cisplatin were included additionally to an untreated control (Ctrl). Time points were taken 0, 1, 2, 4, 8, 12, 24 and 48 hours after the treatments and the quantified mRNA levels were displayed as fold change relative to the untreated control at the beginning of the time course (t=0h). Classical MAPK target genes, transcription factors that are known to be induced by MAPK, cell cycle regulators and mRNAs that are known to be involved in apoptosis signaling were measured.

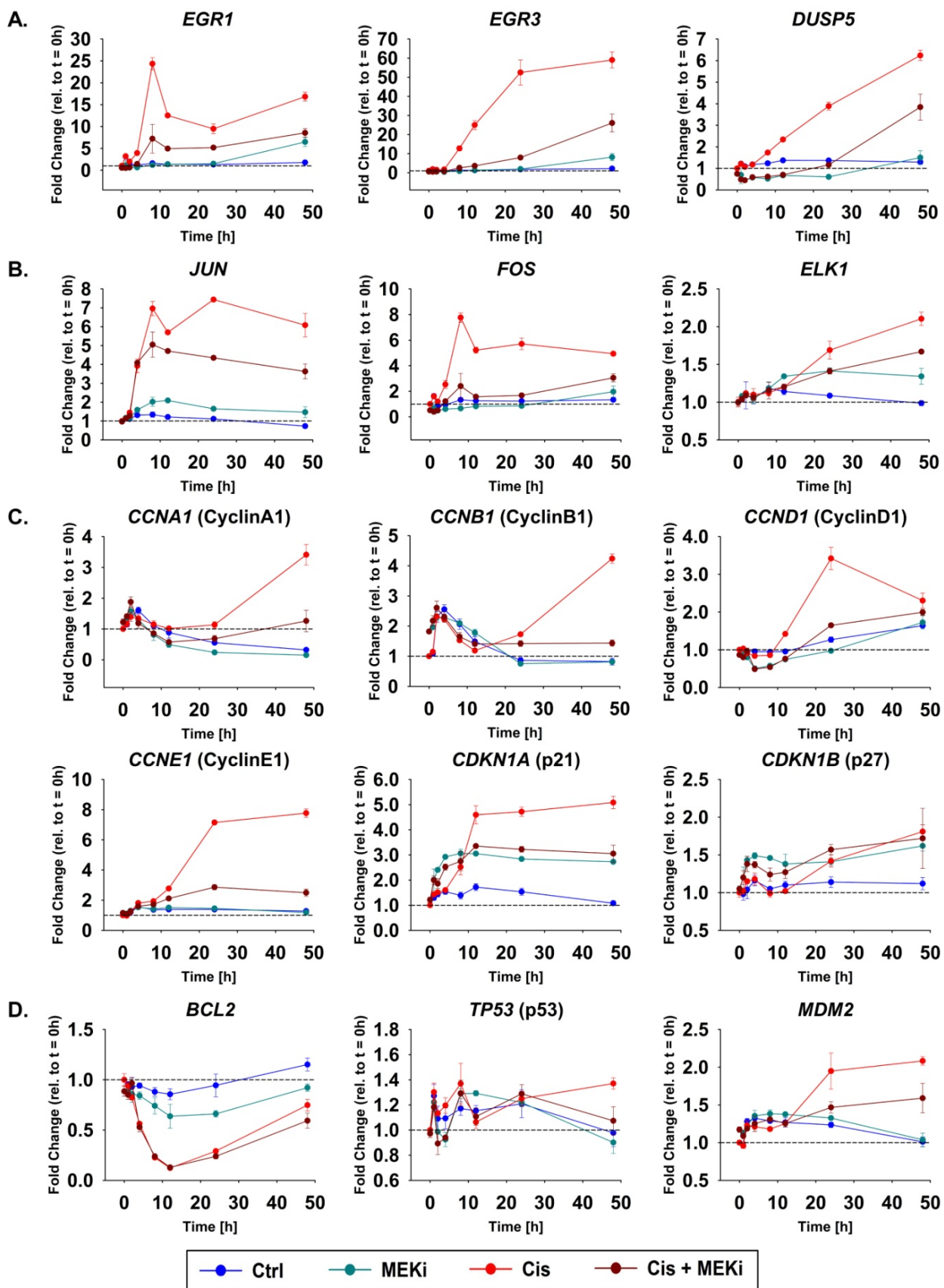


Figure 14: Quantitative RT-PCR of the NSCLC cell line H838 treated with 10 mg/l cisplatin (Cis) and/or pre-incubation for 60 minutes with 2.5 μ M MEK inhibitor U0126 (MEKi) or left untreated (Ctrl) of **(A)** classical MAPK target genes, **(B)** transcription factors that are known to be induced by MAPK, **(C)** cell cycle regulators and **(D)** mRNAs involved in apoptosis signaling (n=3).

First, the inhibitory effect of MEKi and cisplatin alone and in combination on the classical MAPK targets *EGR1*, *EGR3* and *DUSP5* were measured (**Figure 14A**). The mRNA level stayed constant over time in the untreated control. Upon MEK inhibition, *EGR1* and *EGR3* mRNA levels were comparable to the untreated control within the first 24 hours and increased 48 hours after the treatment. *DUSP5* mRNA was slightly down-regulated upon MEKi treatment within the first 24 hours. As expected, the chemotherapeutic agent induced the expression of all three MAPK target mRNAs. The inhibition of the cisplatin-activated MAPK pathway target genes by MEKi was detectable over the whole time course.

Next, the transcription factors *JUN*, *FOS* and *ELK1* that are activated by the RAS–RAF–MEK–ERK-cascade [156] were analyzed (**Figure 14B**). No mRNA expression changes could be observed for the untreated control. MEK inhibition resulted in a slight increase of *JUN* and *ELK1* mRNA levels compared to the untreated control. Upon cisplatin treatment, *JUN* and *FOS* mRNAs were upregulated within the first 8 hours of the time course and showed afterward a sustained expression, whereas *ELK1* mRNA was not induced before 48 hours compared to the untreated control. A pre-treatment with the MEKi U0126 decreases the cisplatin-induced expression of the transcription factor mRNAs analyzed.

Furthermore, the impact of MEKi and cisplatin alone and in combination on cell cycle regulators *CCNA1* (CyclinA1), *CCNB1* (CyclinB1), *CCND1* (CyclinD1), *CCNE1* (CyclinE1), *CDKN1A* (p21) and *CDKN1B* (p27) was verified (**Figure 14C**). The untreated control did not show any changes in the expression of the mRNAs analyzed. The expression of the cyclin mRNAs with MEKi was slightly increased at the later time points compared to the untreated control. Interestingly, *CDKN1A* (p21) and *CDKN1B* (p27), which are known to induce cell cycle arrest in the G1 phase, were the only cell cycle genes tested that were rapidly increased within the first hours followed by a sustained expression with U0126 alone. Cisplatin compared to the untreated control also induced *CDKN1A* mRNA but not before 8 hours and *CDKN1B* mRNA 24 hours

after the treatment. All cyclins analyzed were induced by cisplatin compared to the untreated control with *CCNA1* and *CCNB1* being induced 24 hours and *CCND1* and *CCNE1* being induced already 12 hours upon the treatment. This effect could be decreased by additional pre-incubation with MEKi. The combined treatment of MEKi and cisplatin showed the same effect on *CDKN1A* and *CDKN1B* mRNA expression as MEK inhibition alone.

Finally, mRNAs connected to the apoptotic process, such as *TP53*, *M2MD* and Bcl-2 family members [37, 49, 50] (**Figure 14D**) were analyzed. The mRNA level stayed constant over time in the untreated control. MEK inhibition downregulated the anti-apoptotic *BCL2* mRNA compared to the untreated control. Also cisplatin treatment led to a downregulation of *BCL2* but to a larger extend. The pre-incubation with MEKi did not affect the cisplatin-induced decrease of *BCL2* mRNA expression. *MDM2* mRNA, which is known to be able to downregulate p53, was upregulated 24 hours after the treatment with cisplatin compared to the untreated control and showed a slight decreased expression if cisplatin was combined to U0126. The *TP53* mRNA expression did not change over within the time observed for all treatments tested.

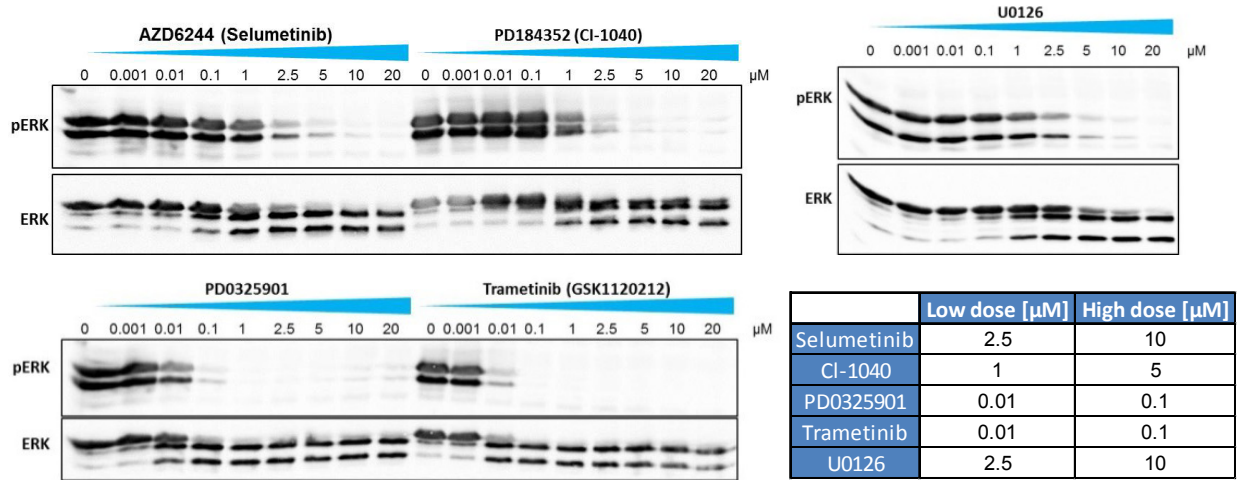
In conclusion, these results are consistent with the previously shown MEKi-induced G1 cell cycle phase elongation. We could also show that U0126 induced *CDKN1A* (p21) and *CDKN1B* (p27) that are known to regulate G1 arrest. The *BCL2* mRNA downregulation upon MEK inhibition is also in line with the previously shown MEKi-dependent cleavage of caspase-3. It can be further excluded that the effect of MEKi on the cisplatin sensitivity is regulated by the anti-apoptotic *BCL2* mRNA as MEKi could not counteract its cisplatin-dependent downregulation.

5.2.2.5 Time- and dose-dependent effect of different clinically relevant MEK inhibitors (MEKi) on cisplatin-induced apoptosis

To better understand the effect of MEK inhibitors on NSCLC and to show that the effect of MEKi U0126 is specific, further experiments with other MEK inhibitors were performed. Therefore, additionally to MEKi U0126, clinically relevant MEK inhibitors like selumetinib (AZD6244), CI-1040 (PD184352), PD0325901 and trametinib (GSK1120212) were tested. First, the efficiency of these MEK inhibitors was determines

qualitatively by measuring the phosphorylation of the MEK downstream targets ERK1 and ERK2 (Figure 15).

A.



B.

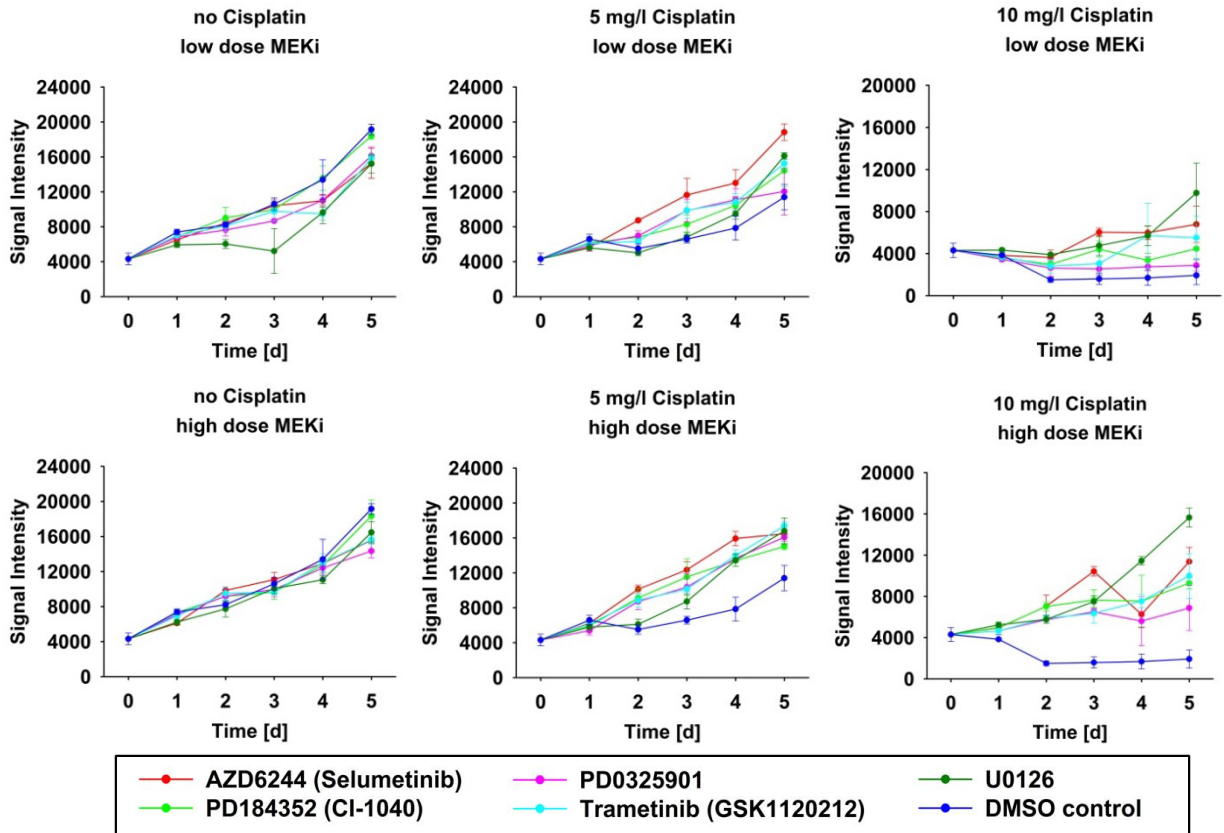


Figure 15: Time- and dose-dependent effect of different MEK inhibitors (MEKi) on the NSCLC cell line H838. (A) The cells were pre-treated for 60 minutes with a MEKi dilution series of 0, 0.001, 0.01, 0.1, 1, 2.5, 5, 10 or 20 μM before 40 ng/ml HGF was added. After cell lysis, the proteins were separated by 10% SDS-PAGE, transferred to a nitrocellulose membrane and ERK and pERK were detected on the Image Quant LAS 4000 by chemiluminescence. Low MEKi doses (half-effective MEK inhibition) and high MEKi doses (complete MEK inhibition) were determined qualitatively. **(B)** CellTiter-Blue viability assay of the H838 cell line upon different treatments; 0, 5 or 10 mg/l cisplatin combined with high or low MEKi doses. The DMSO control with 0.1% DMSO corresponds to the DMSO level of 10 μM MEKi. The experiment was performed in biological triplicates.

To this aim, the NSCLC cell line H838 was pre-incubated for 60 minutes with different doses (0, 0.001, 0.01, 0.1, 1, 2.5, 5, 10, 20 μM) of U0126, selumetinib (AZD6244), CI-1040 (PD184352), PD0325901 and trametinib (GSK1120212) before adding 40 ng/ml HGF to fully activate the MAPK cascade. The cells were lysed after 10 minutes which corresponds to the maximum peak level of ERK phosphorylation [153]. Quantitative immunoblotting of pERK and ERK revealed large differences in the efficiency of the inhibitors. Selumetinib treatment was comparable to U0126 with a half-effective dose (low dose MEKi) of approximately 2.5 μM and a complete inhibition (high dose MEKi) of ERK phosphorylation at a concentration of 10 μM . Interestingly, PD0325901 and trametinib turned out to be around 100-fold more efficient compared to selumetinib and U0126 by completely inhibiting ERK phosphorylation at already 0.1 μM and the half-effective dose for both was determined to be around 0.01 μM . The inhibitor CI-1040 showed a half-effective dose of 1 μM and an almost complete inhibition at a concentration of 5 μM .

To study the influence of half-effective (low dose MEKi) and complete (high dose MEKi) inhibition of MEK activity on cisplatin-induced apoptosis, the NSCLC cell line H838 was pre-treated for 60 minutes with the different MEK inhibitors (high and low doses MEKi, lower right panel (**Figure 15A**) followed by the treatment with either no, 5 or 10 mg/l cisplatin (**Figure 15B**). All MEK inhibitors were dissolved in DMSO and were available in the same stock concentration of 10 mM. As the maximal MEKi concentration used was 10 μM resulting in a final concentration of 0.1% DMSO, all conditions were adjusted to this concentration including the DMSO control. The cell viability was measured using the CellTiter-Blue assay.

The MEK inhibitors alone led to a slightly decreased proliferation compared to the DMSO control. Dependent on high and low doses, the effect of MEKi on cisplatin treatment with 5 mg/l cisplatin differed in efficiency. The half-effective inhibition with all MEK inhibitors led to an increased cell number whereupon selumetinib turned out to be the most effective one and U0126 the weakest showing the rescue effect not before the third day.

The complete inhibition of the MEK activity combined with 5 mg/l cisplatin resulted in a clear effect for all inhibitors compared to the DMSO control with selumetinib again being among the top candidates. Increasing the cisplatin concentration to 10 mg/l resulted in an effect comparable to 5 mg/l but the cells in the DMSO control died already on the second day. In particular, the cells with a full inhibition of MEK activity showed a clear advantage compared to the DMSO control. Again, selumetinib treatment but interestingly also U0126 especially at later time points revealed its rescue potential. PD0325901, which was shown in **Figure 15A** to be quite efficient in MEK inhibition by quantitative immunoblotting, turned out to have less rescue potential if combined with high cisplatin concentrations.

In conclusion, not only the MEKi U0126 but also clinically relevant MEK inhibitors were shown to be able to decrease the cisplatin sensitivity of the NSCLC cell line H838. Furthermore, this effect of the MEK inhibitors became more prominent if the MEK activity was completely inhibited with a high MEKi dose compared to a low MEKi dose that resulted just in a half-effective inhibition.

To sum up, cisplatin treatment could be verified to activate the RAS–RAF–MEK1/2–ERK1/2 cascade. The cisplatin-induced phosphorylation of ERK and the upregulation of the ERK targets *EGR1*, *EGR3*, *DUSP5*, *JUN*, *FOS* and *ELK1* was counteracted by additional pre-treatment with MEKi. Moreover, the study revealed that MEKi was not only able to prolong the G1/G0 cell cycle phase but also upregulated *CDKN1A* mRNA which is known to induce G1 arrest. This might hint to an indirect rescue effect by giving the cell more time, for instance for DNA-repair or cisplatin disposal, which results in an increased cell number.

5.3 Role of Epo in NSCLC

Patients suffering from chemotherapeutic-induced anemia can be medicated either with blood transfusion or Erythropoiesis-stimulating agents (ESA) such as erythropoietin (Epo) to support erythropoiesis and thus increase the number of red blood cells. Unfortunately, recent studies have shown that Epo can have tumor stimulating effects and EpoR expression in NSCLC is associated with poor survival [89, 90]. For this reason, the treatment of patients with Epo in the context of cancer-related anemia is discussed controversially [84, 94-96].

5.3.1 Rescue of cisplatin-induced apoptosis by Epo treatment

To analyze the biological effect of Epo and its receptor (EpoR) on lung cancer cells, which is known to trigger cyto-protective and anti-apoptotic effects [84, 157], NSCLC cell lines were screened for EpoR expression. H838 cells significantly express *EpoR* mRNA compared to healthy lung alveolar epithelial type II cells (AECII) and other lung cancer cell lines, e.g. H1650, H1975, H1944 and H2030. Moreover, detectable protein amounts of the receptor that can be phosphorylated upon Epo- β stimulation could be measured in low (P5) and high (P25) passage numbers of H838 cell line (**Figure 16A+B**). As the sequencing also showed that H838 expresses the wild type receptor, this cell line was selected for further experiments. Additionally, H838 cells that stably over-expresses the Epo receptor (kindly provided by Sofia Depner) (**Figure 16C**) were used to mimic a situation for increased signaling levels upon Epo treatment. This was shown by increased expression levels of the EpoR signaling target gene *CISH* upon stimulation already at low Epo doses (**Figure 16D**). To further test the effect of Epo treatment on H838 cell line, the cells were serum-starved and left either untreated or treated with the clinically relevant cisplatin dose of 5 mg/l and/or 10 U/ml Epo over four days and the cell number was determined by the CellTiter-Blue viability assay (**Figure 16E**). The cells in the untreated control increased their cell number 4-fold within 4 days without the addition of growth factors. Epo treatment showed a comparable proliferation rate to the untreated control. Cells that were incubated with 5 mg/l cisplatin alone showed no significant proliferation and a slight decrease of cell number over time

whereas additional treatment with Epo resulted in a significant rescue effect giving an advantage to parallel-treated cells.

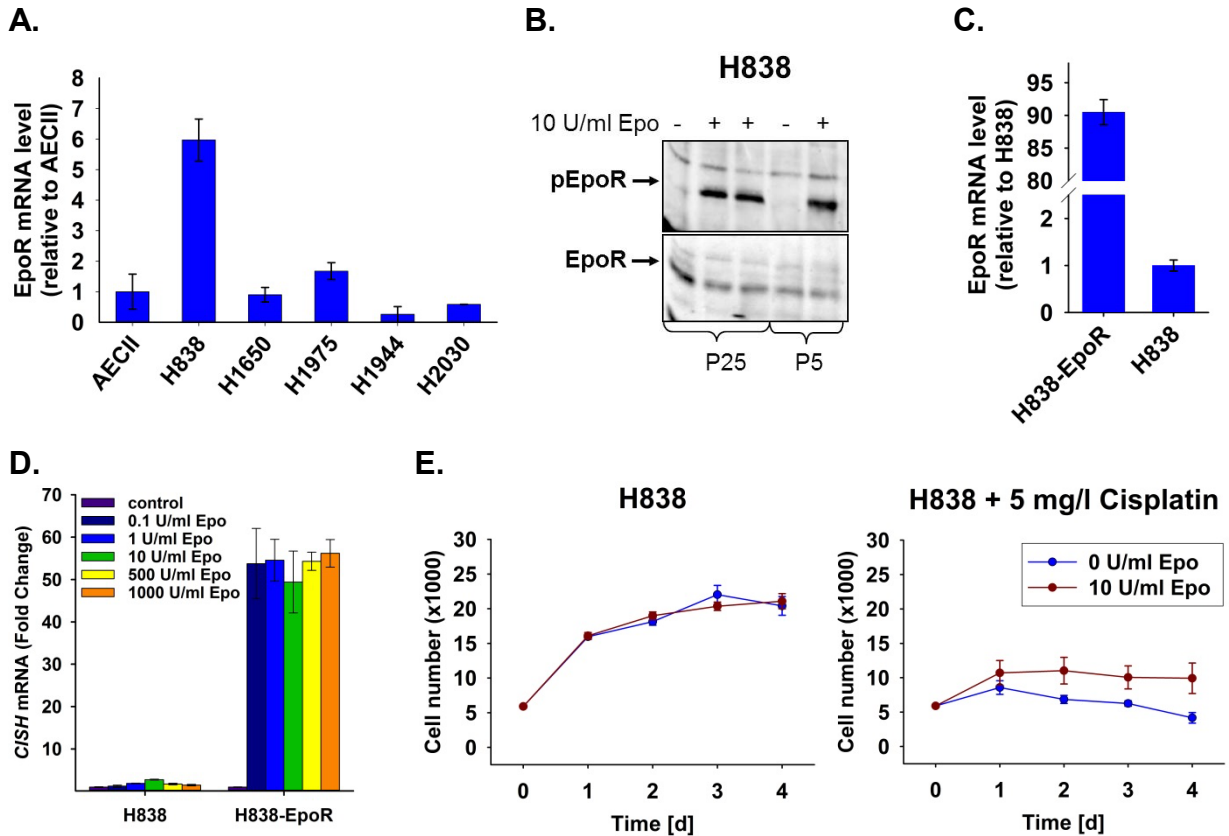


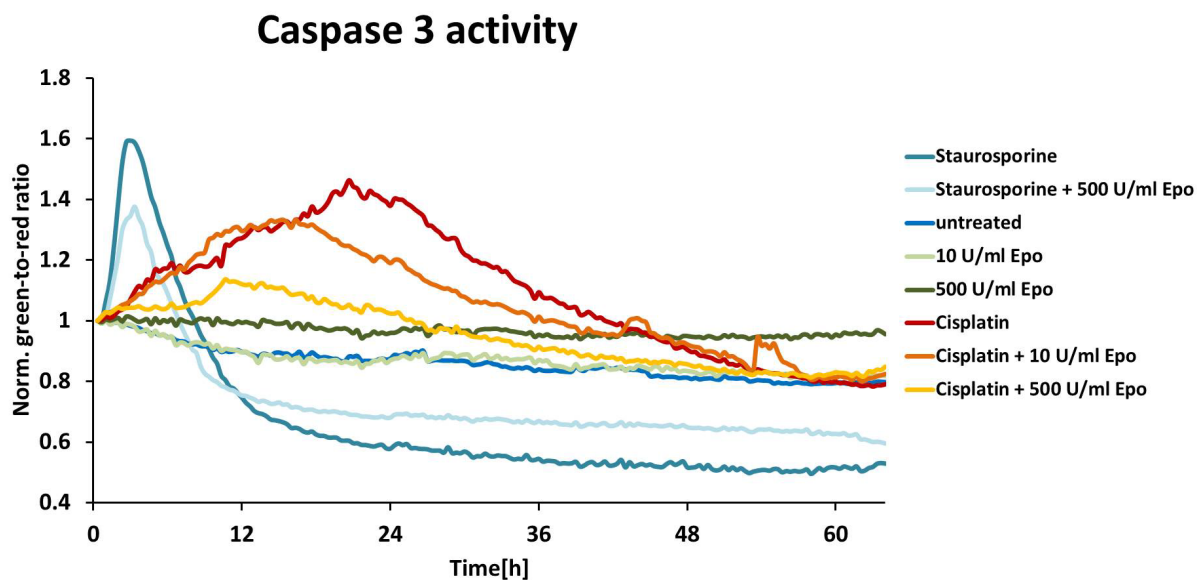
Figure 16: The NSCLC cell line H838 contains the functional Epo receptor (EpoR). (A) *EpoR* mRNA expression was measured by qRT-PCR in lung carcinoma cell lines compared to healthy alveolar epithelial cells type II (AECII) (n=3). (B) H838 cells in different passage numbers (P5 and P25) were serum-starved and either left untreated or stimulated with 10 U/ml Epo-β for 10 minutes. After cell lysis, quantitative immunoprecipitation of EpoR was performed followed by a 10% SDS-PAGE, a transfer to a nitrocellulose membrane and EpoR and pEpoR detection on the Image Quant LAS 4000 by chemiluminescence. (C) qRT-PCR measurements of the *EpoR* mRNA expression level in H838 and H838-EpoR (n=3). (D) The Epo-induced target gene *CISH* was measured by qRT-PCR (n=3) in the cell lines H838 and H838-EpoR upon stimulation with different Epo doses. (E) Measurement of the cell number of H838 cells with the CellTiter-Blue viability assay with or without stimulation with 10 U/ml Epo or additional treatment with 5 mg/l cisplatin (n=3).

Moreover, this rescue effect of Epo on cisplatin-treated cells could also be monitored by live-cell imaging microscopy (**Figure 17**) in a preliminary experiment. Therefore, the NSCLC cell line H838-EpoR was stably transfected with the CasperGR FRET (fluorescence resonance energy transfer)-based sensor (kindly provided by Dr. Sofia Depner) which enables the measurement of cleaved caspase-3 quantitatively in a time-resolved manner in living cells [158]. The sensor consists of green (GFP) and red fluorescent proteins (RFP) connected by the linker containing the caspases-3 cleavage sequence DEVD which leads to FRET between these fluorescent proteins. Caspase-3 activation leads to the cleavage of the DEVD sequence resulting in FRET elimination which is detectable in the changing ratio of green to red. The CasperGR-containing cells were treated either singly or with a combination of 5 mg/l cisplatin, Epo- β in high dose of 500 U/ml or low dose of 10 mg/l or left untreated (**Figure 17A**). As positive control, 10 μ M staurosporine was used that induces apoptosis quite rapidly. Indeed, the low dose of Epo resulted in a rescue effect if combined with cisplatin compared to cisplatin alone. Moreover, the high dose of 500 U/ml Epo almost completely counteracted the effect of cisplatin with only a slight increase in caspase-3 activation. Interestingly, Epo even reduced the cleaved caspase-3 signals if combined with staurosporine compared to staurosporine alone. The maximum peak of caspase-3 activity with cisplatin alone was reached at around 24 hours. After 24 hours, almost all cells with cisplatin underwent apoptosis (**Figure 17B**), which explains why the signal levels decreased afterwards (**Figure 17A**).

Compared to the CellTiter-Blue experiment where some cells survived several days with Cisplatin alone, all cells were dead after two days in the microscopy experiment. This could be explained by the additional stress induced by laser energy of the microscope and the glass surface of the dish where the cells were seeded on.

In conclusion, Epo treatment was shown to decrease the cisplatin sensitivity in the NSCLC cell line H838 that expresses the functional Epo receptor. This effect was shown to be Epo dose-dependent.

A.



B.

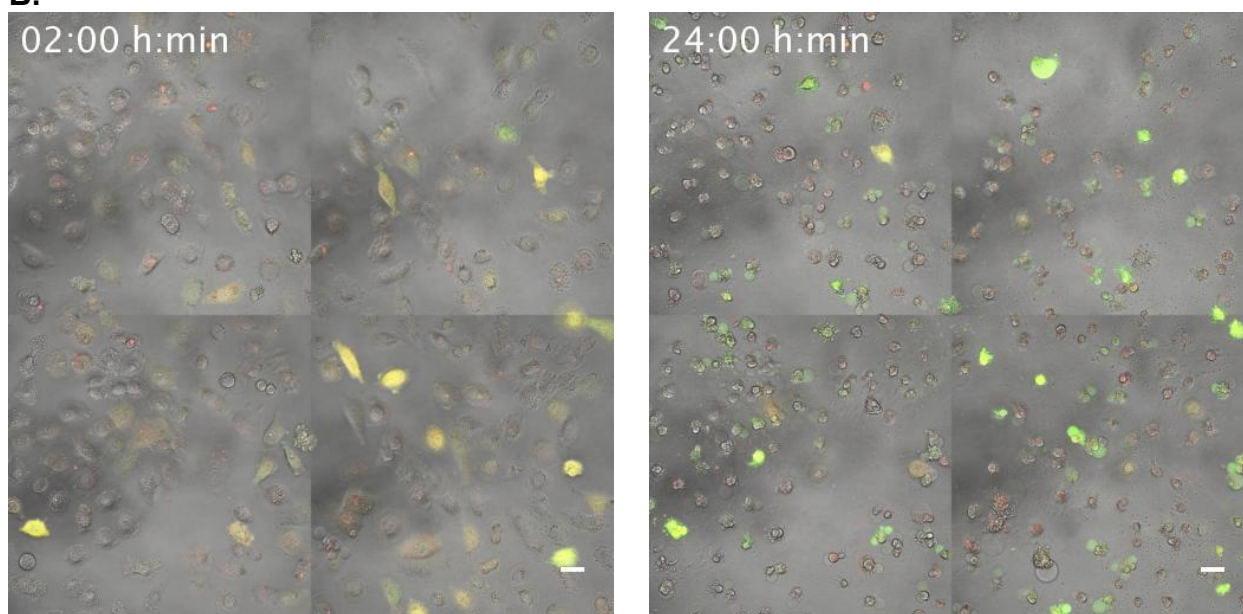


Figure 17: Rescue effect of Epo on cisplatin-treated H838-EpoR cells measured with the CasperGR sensor by live-cell imaging. The cells were imaged on an environment-controlled microscope (Zeiss LSM 710). **(A)** The caspase-3 activity was measured by the CasperGR FRET-based sensor. The cells were treated either singly with Epo- β in high dose of 500 U/ml or low dose of 10 mg/l or or with a combination of 5 mg/l cisplatin or left untreated. 10 μ M staurosporine was used as positive control for apoptosis. **(B)** Microscopy images at the start of the time course measurement ($t = 2$ h) and the maximum peak of active caspase-3 ($t = 24$ h) showing the apoptotic effect of cisplatin (bar = 20 μ m).

5.3.2 EpoR signaling in NSCLC and primary erythroid progenitor cells

To better define the risk of Epo treatment upon chemotherapy-induced anemia for the patients, EpoR signaling in NSCLC cells needs to be understood in more detail. To identify differences in the Epo-induced signaling to primary erythroid progenitor cells and to dissect the complexity of the EpoR system, a mathematical model based on ordinary differential equations (ODEs) for the lung cancer cell line H838 and primary erythroid cells was established.

As already shown in **Figure 16**, the NSCLC cell line H838 expresses not only *EpoR* mRNA but also contains the functional receptor which can be phosphorylated upon Epo stimulation. Furthermore, the rescue effect mediated by Epo on cisplatin-induced apoptosis in the H838 and the EpoR overexpressing H838-EpoR cell line (**Figure 16** and **Figure 17**) demonstrated that Epo has the potential to influence the signaling in cancer cells. Therefore, H838 and H838-EpoR were selected as NSCLC model systems for EpoR signaling. As erythroid model system, the Epo-dependent primary erythroid mouse CFU-Es (mCFU-Es, colony forming unit erythroid) were selected, as human CFU-E cells are very limited.

5.3.2.1 Establishment of a mathematical model for the Epo-induced signaling in lung cancer cells and primary erythroid progenitor cells

The EpoR signaling pathway in CFU-Es has previously been described with a mathematical model [62]. The ODE-based mathematical model is divided into three submodules that represent the cell compartments plasma membrane, cytoplasm and nucleus. As model input, a constant Epo concentration was assumed as it was shown that the effect of the Epo depletion is marginal. The complex formation and activation status of the Epo receptor and JAK2 was considered with a full activation in two steps to be able to describe the effect of the phosphatase. In the first step, EpoR at the plasma membrane undergoes a conformational change upon ligand binding and activates the pre-bound tyrosine kinase JAK2. In the second step, the activated JAK2 phosphorylates EpoR. These processes can be reversed by the phosphatase. The pJAK2pEpoR-complex is now able to bind and phosphorylate the transcription factor STAT5 in the

cytoplasm. In consequence, pSTAT5 translocates into the nucleus (npSTAT5) where it activates the transcription of the negative regulators *CISH* (CIS protein) and *SOCS3* that were modeled with a delay in their production. CIS inhibits STAT5 activation by binding to EpoR, whereas *SOCS3* directly binds to the kinase domain of JAK2 and EpoR, thereby inhibiting tyrosine-kinase activity. A protein tyrosine phosphatases (PTP) also negatively regulates the receptor-JAK2-complex.

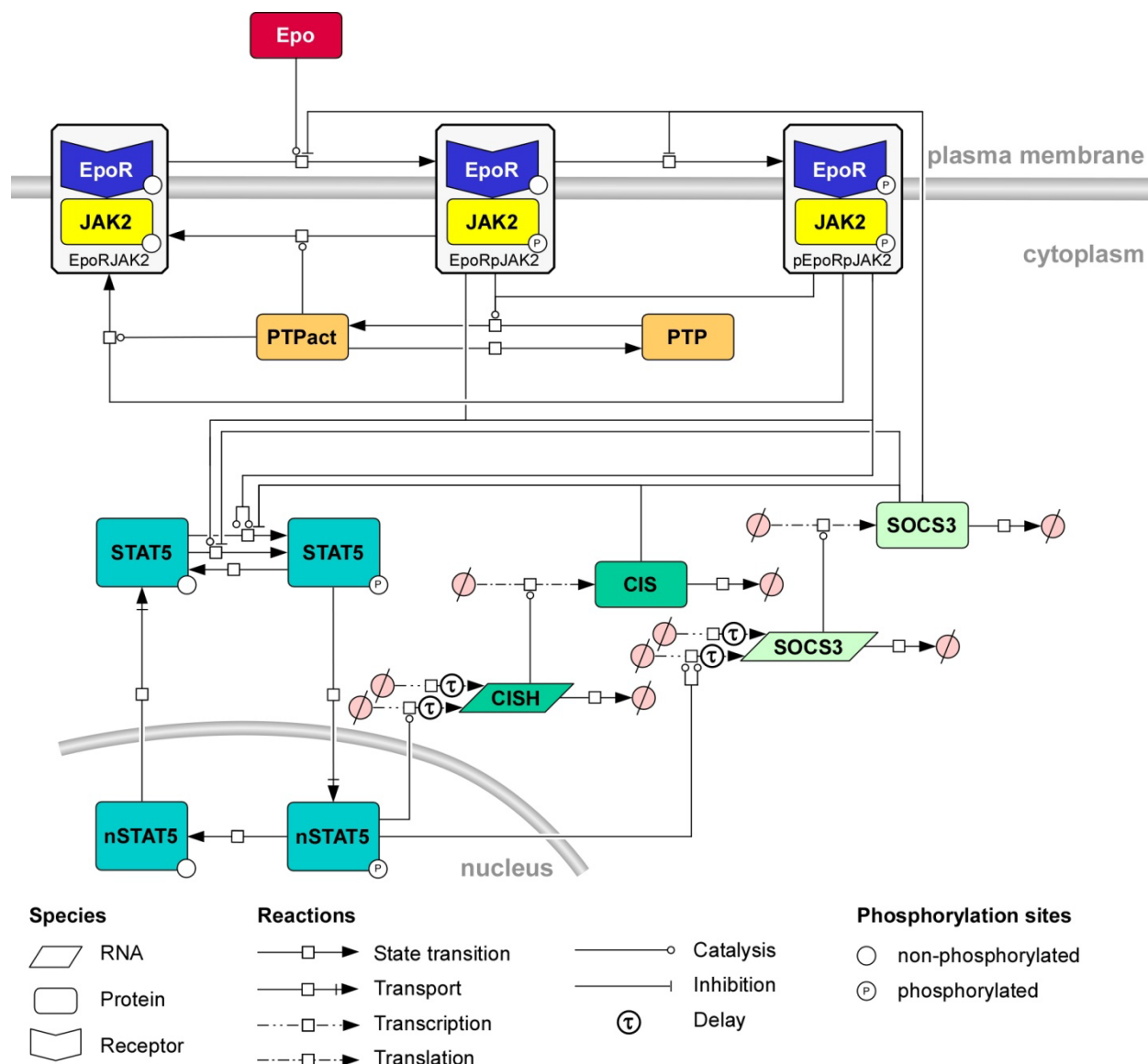
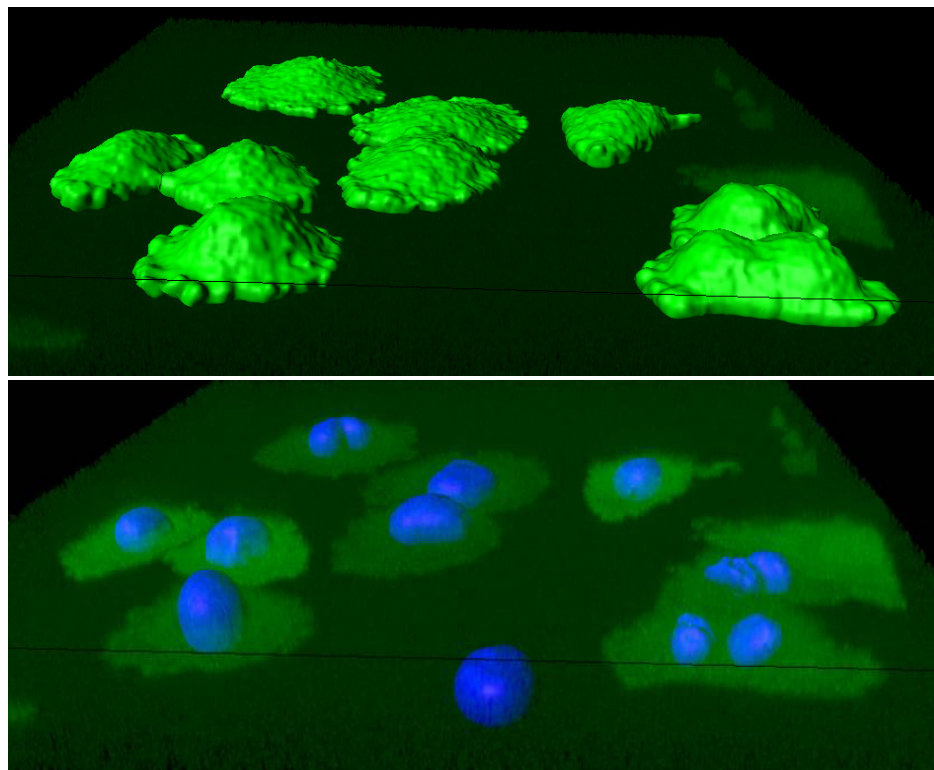


Figure 18: Quantitative dynamic model. The Process diagram of the quantitative dynamic model of the Epo-induced JAK2/STAT5 signaling pathway was drawn with the cell designer software. The binding of the ligand Epo to its receptor results in the phosphorylation of JAK2 and EpoR (EpoRpJAK2). STAT5 is recruited by pEpoR and phosphorylated by pJAK2, dimerizes and translocates to the nucleus where it starts the transcription of the negative feedback regulators CIS and SOCS3.

As a starting point for the cancer cell model in this study, the already existing quantitative dynamic model in CFU-Es [62] was used. The modeling was performed by the theoretical cooperation partner Bernhard Steiert in the group of Prof. Jens Timmer (Freiburg University). The mathematical model (**Figure 18**) is represented as process diagram showing the network structure including transcription, translation, state transition, catalysation and inhibition but also transport processes. The phosphorylation status shows if the protein is available in its active or inactive form.

To adapt the CFU-E-model [62] to the lung cancer cells, biologically-motivated pathway extension and adaptations for H838 and H838-EpoR cells were made. For instance, SHP-1, which is a lineage-specific protein-tyrosine phosphatase (PTP) that is mainly expressed in the hematopoietic system could not be detected by RNAseq analysis in H838 cells. Thus, SHP-1 was replaced in the model by the more general term “PTP”. Further, the volumes of the cytoplasm and the nucleus of H838 cells were measured and compared to the mCFU-E data [62]. To this aim, H838 cells that stably express the green fluorescent protein (H838-GFP, kindly provided by Dr. Sofa Depner) were stained with Hoechst (H33342) and imaged on an environment-controlled microscope (Zeiss LSM 710). The images of single cells were acquired in the blue and green channel applying the z-stack method with a distance of 2 μm between the images. The Imaris software (Bitplane) was used for surface reconstruction that enables the calculation of the volume (**Figure 19**).

The quantification of the total cell volume was generated by using the GFP data and the volumes of the nuclei by Hoechst staining. 24 H838-GFP cells were measured and the total cell volume was calculated. Compared to CFU-E cells, the cancer cells have a much smaller nucleus in relation to the cytoplasm with a nucleus-to-cytoplasm ratio of 0.28 ± 0.007 . The nuclei of CFU-Es constitute more than half of the cells with a nucleus-to-cytoplasm ratio of 0.69 [62].



$$\frac{V_{nuclei}}{V_{cytoplasm}} = \frac{V_{nuclei}}{V_{total\ cell} - V_{nuclei}} = 0.28 \pm 0.007$$

Figure 19: Measurement of cell type-specific parameters. H38-GFP cells were stained with Hoechst (H33342) and imaged on an environment-controlled microscope (Zeiss LSM 710). The volumes of the nucleus and the total cell volume were measured by the z-stack method, displayed and quantified with the Imaris software. The nucleus-to-cytoplasm ratio was calculated as depicted below the image.

5.3.2.2 Generation of quantitative time-resolved data

To calibrate the model with quantitative time-resolved data of the cancer cells, *CISH* and *SOCS3* mRNA was measured upon stimulation with Epo- β by quantitative RT-PCR in the NSCLC cell lines H38 and H38-EpoR (**Figure 21**, black dots). The basal expression of *SOCS3* and *CISH* mRNAs was tested with 1 μ g/ml actinomycin D that inhibits the synthesis of new mRNA (**Figure 20**). Without freshly synthesized mRNA, the levels decreased over time for both mRNAs in both cell types.

Quantitative immunoblotting and mass spectrometry was applied for protein measurements of (p)EpoR, (p)JAK2 and (p)STAT5 (measured by Florian Salopiata). For the CFU-Es, the previously described data [62] was used. The whole model

consists of 36 kinetic, 143 scaling and offset and 16 error parameters describing 57 conditions with 1117 data points.

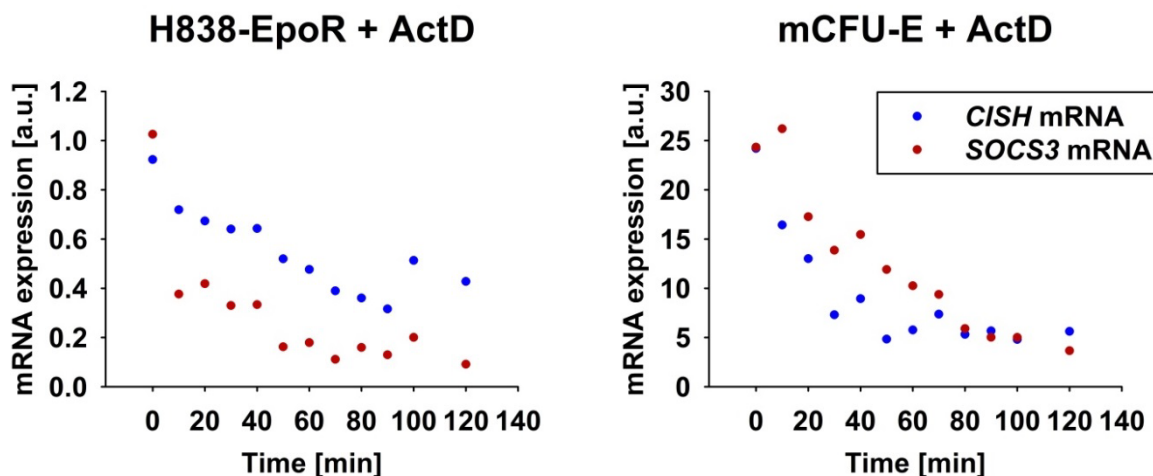


Figure 20: Measurement of the basal level of *CISH* and *SOCS3* mRNA by qRT-PCR. The H838-EpoR and CFU-E cells were treated with 1 $\mu\text{g/ml}$ actinomycin D (ActD) to inhibit new mRNA synthesis. This experiment was performed in triplicates and one representative example is shown.

5.3.2.3 Model selection and calibration

In the next step, the model was calibrated based on the previously generated experimental data by testing whether the model can describe the data of the NSCLC cell lines H838 and H838-EpoR additionally to CFU-Es. Therefore, three model strategies were tested (**Figure 21**). The model fits are shown representatively for *CISH* and *SOCS3* mRNA and pEpoR, pSTAT5, total STAT5 (tSTAT5) protein levels (protein levels were measured by Florian Salopiata).

In the 1st strategy, all parameters were chosen to be different for all cell types suggesting a situation where the cell types have no parameters in common. This model could describe all data sets (**Figure 21**, green curve). On the other hand, some parameters might be estimated to similar values due to too many degrees of freedom. However, the exact value might not be identifiable.

The 2nd strategy was to assume no cell type-specific parameters (**Figure 21**, purple curve). As the model could not describe the data, this model was rejected.

Finally, the 3rd strategy was used to identify the number of cell type-specific parameters that are necessary to describe the data best (**Figure 21**, orange curve). The best description is defined as smallest number of parameters necessary to most accurately describes the data. Thereby, this minimal (=parsimonious) model fit should describe the data to a similar extent as the model of the 1st strategy. All these criteria could be fulfilled with the minimal model. Therefore, this model was selected as the best model.

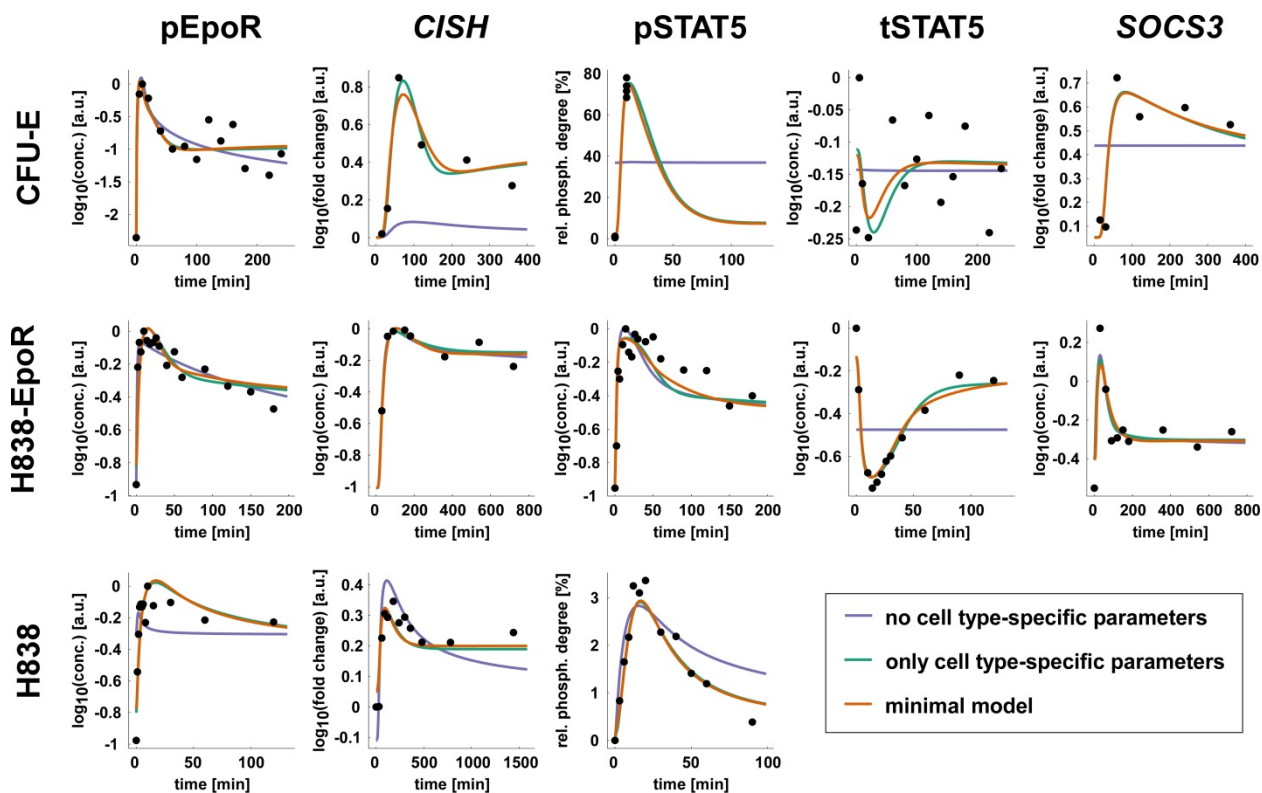


Figure 21: Model selection and calibration: The whole model consists of 36 parameters describing 57 conditions with 1117 data points. Representatively, just the model fits for a couple of species is shown here for the three cell types H838, H838-EpoR and CFU-Es. This includes the EpoR target genes *CISH* and *SOCS3* measured by qRT-PCR and pEpoR, pJAK2 and pSTAT5 protein data measured by quantitative immunoblotting. The dots represent experimentally measured data, solid lines depict the three applied model strategies in purple (no cell type-specific parameters), green (only cell type-specific parameters) and orange (minimal model).

5.3.2.4 Identification of differences in Epo-induced signaling

The minimal model was shown to describe the data best. The parameters were not only optimized to describe the data as accurate as possible, but also cell type-specific differences were penalized using the L1 penalty approach [159-162]. Optimizing for

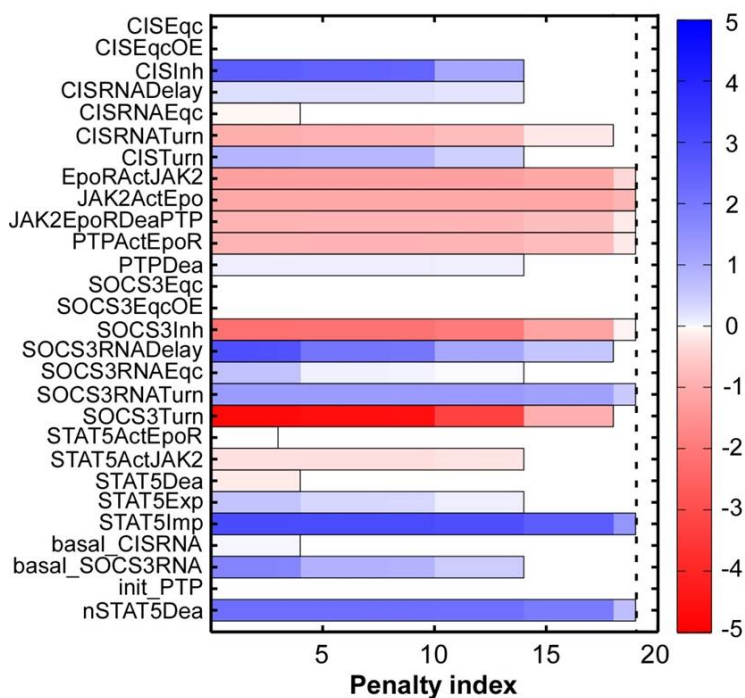
these two criteria, it could be shown that the majority of model parameters are identical and just 8 out of 36 parameters were predicted to be cell type-specific in the cell types H838/H838-EpoR and CFU-Es (**Figure 22A**). These parameters are the activation of EpoR by JAK2 (EpoRActJAK2), the activation of JAK2 by Epo (JAK2ActEpo), the deactivation of the JAK2-EpoR-complex by PTP (JAK2EpoRDeaPTP), the activation of PTP by EpoR (PTPActEpoR), the SOCS3 inhibition rate (SOCS3Inh), the SOCS3 mRNA turnover rate (SOCS3RNATurn), the STAT5 import rate (STAT5Imp) and the deactivation rate of nuclear STAT5 (nSTAT5Dea).

The profile likelihood analysis revealed that 6 out of the 8 identified parameters that were predicted to be different were identifiable and the other two showed a unidentifiability (**Figure 22B**). These two are the deactivation rate of the receptor-kinase complex by the PTP and the activation rate of the PTP by the receptor (JAK2EpoRDeaPTP and PTPActEpoR). If one, in this case the deactivation parameter was selected, was fixed to a certain value, the difference between these two parameters (PTPActEpoR_rel) was identifiable (**Figure 22B**, lower right panel). At least one parameter of these is cell-type specific but both could be cell-type specific.

Most of the predicted differences between the cell types could be explained by biological differences of the erythroid and the lung cancer cell background. The reason for the specific STAT5 import rate (STAT5Imp) in CFU-Es compared to H838/H838-EpoR could be found in the different nucleus-to-cytoplasm-ratios. The deactivation rate of nuclear STAT5 (nSTAT5Dea) is different due to different phosphatases or different amounts of phosphatase. The differences in the activation of JAK2 by Epo (JAK2ActEpo), the activation of the receptor by its kinase (EpoRActJAK2) and inhibition by SOCS3 of the receptor complex (SOCS3Inh) could possibly be explained due to a cell-specific amount of JAK2 and the ratio of JAK2- to EpoR-molecules in H838 and CFU-Es. As no SHP1 is available outside the hematopoietic system, the differences for the deactivation of the JAK2-EpoR complex by PTP or the activation of PTP by EpoR (JAK2EpoRDeaPTP and PTPActEpoR) are not surprising.

The only predicted difference between the cell types that could not be explained is the SOCS3 mRNA turnover rate (SOCS3RNATurn).

A.



B.

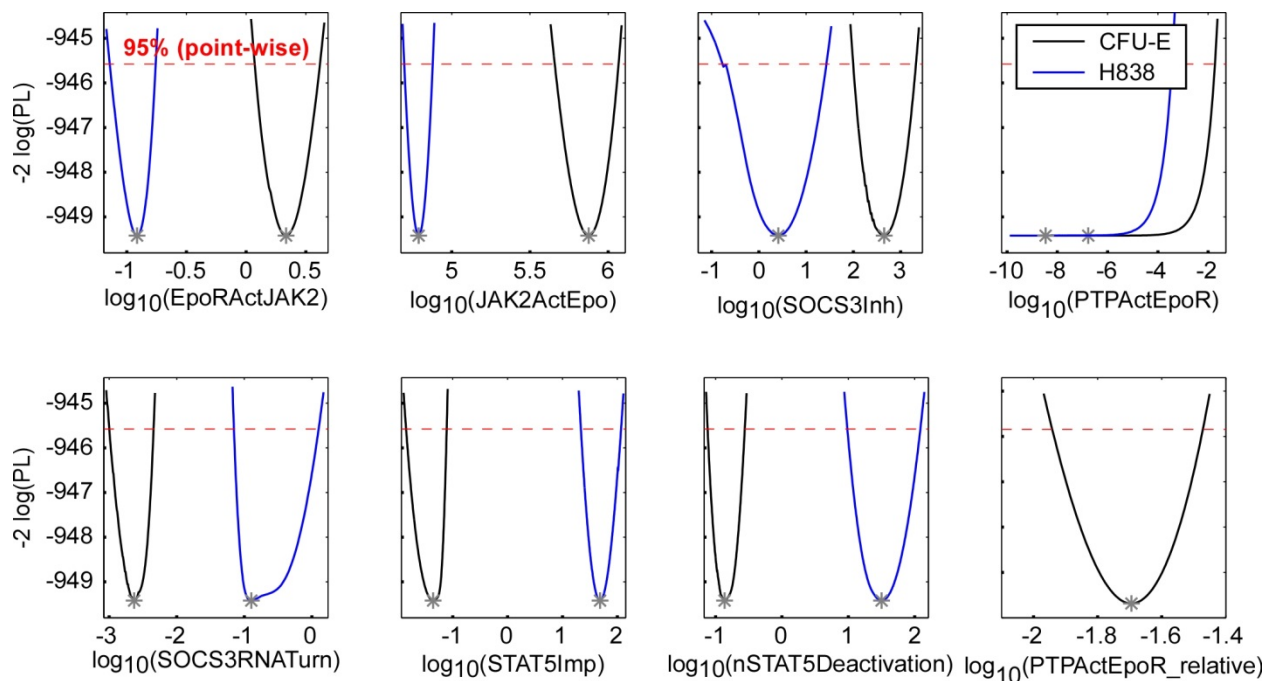


Figure 22: Identification of cell type-specific differences. (A) Identification of differences using the L1 penalty. The parameters are indicated with shades of red (lower in H838/H838-EpoR) to blue (higher in H838/H838-EpoR). **(B)** Profile likelihood analysis of the predicted parameter specificities for the different cell types. All parameters were identifiable except for the deactivation rate of the receptor-kinase complex by the PTP and the activation rate of the PTP by the receptor (JAK2EpoRDeaPTP and PTPActEpoR). The difference of these parameters (PTPActEpoR-relative) is larger than zero and identifiable (lower right panel).

5.3.2.5 Experimental validation of the predicted cell type-specific SOCS3 mRNA turnover rate

The SOCS3 mRNA turnover rate is predicted to be much lower in CFU-Es compared to the lung cancer cells (**Figure 22**, lower panel on the left). In the next step, this model prediction was experimentally validated. The turnover rate is defined as the degradation over time or the mRNA stability.

To enable the measurement of the RNA degradation experimentally, actinomycin D (ActD) treatment was applied at the peak of the signaling dynamic to inhibit further mRNA synthesis. The time of the peak was predicted to be different for the two cell types. The maximal expression of SOCS3 mRNA in CFU-Es was predicted to be after 60 minutes whereas in H838-EpoR the predicted dynamics were faster and reached the peak after 30 minutes upon Epo treatment. The *CISH* mRNA dynamics that was predicted to have the same parameters in the different cell types was used as control.

To validate these predictions, the SOCS3 and *CISH* mRNA was measured upon the treatment with Epo or ActD additionally to Epo by qRT-PCR (**Figure 23**). Both mRNAs in H838-EpoR and CFU-Es showed reduced mRNA levels if the cells were treated with ActD. In H838-EpoR, ActD treatment resulted in even lower SOCS3 mRNA level compared to the starting concentration.

These results confirmed that the selected model can describe the experimental data and predict differences in SOCS3 mRNA half-lives in the lung cancer and the erythroid cells. In conclusion, this mathematical tool can be used to reveal differences between the two cell types which might enable targeting one cell type with a certain drug and leave the other one unaffected.

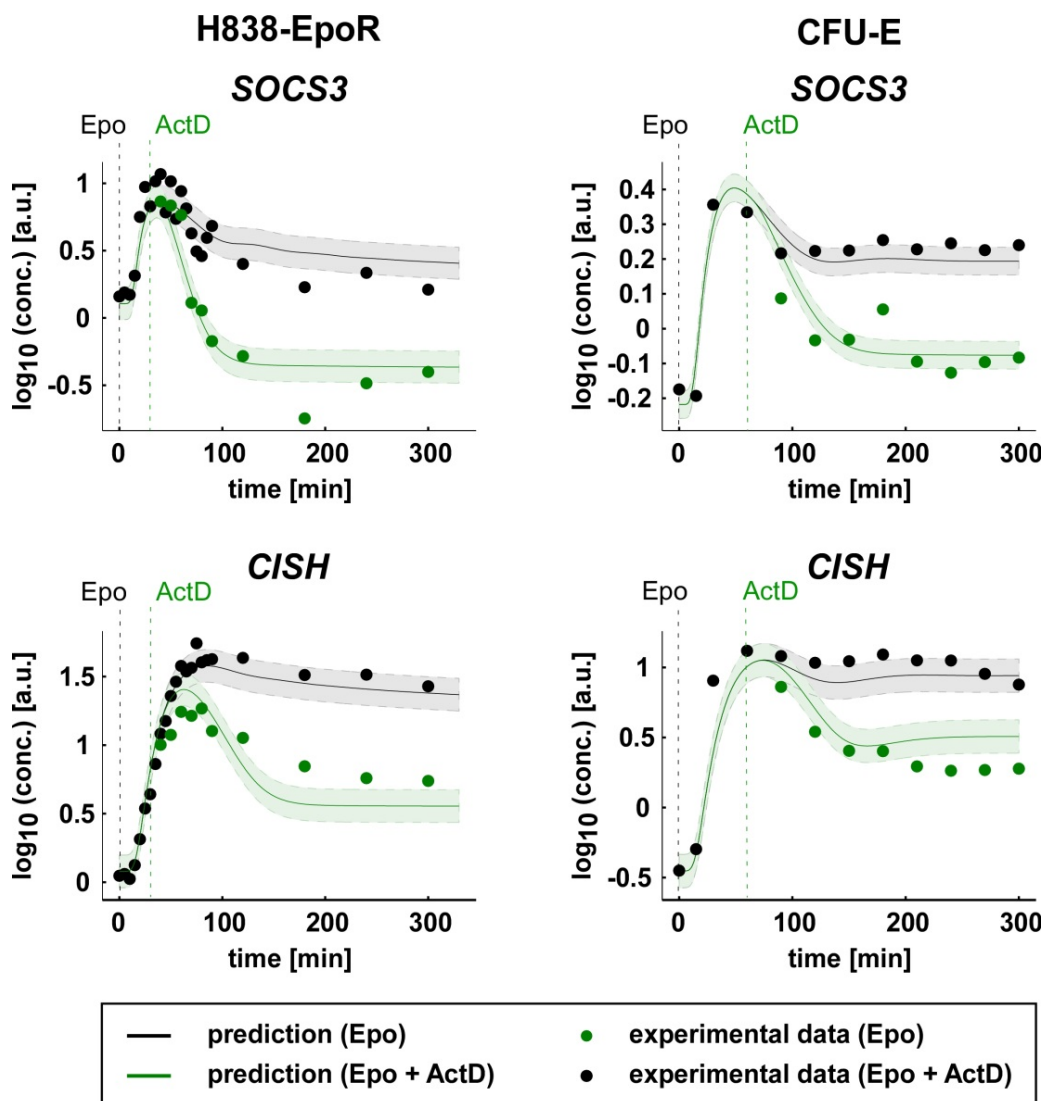


Figure 23: Experimental validation of the cell type-specific SOCS3 turnover rate by qRT-PCR. The H838 cells were stimulated with 10 U/ml Epo- β Epo at $t=0$ min (dashed black line) and new mRNA synthesis was inhibited with the treatment of 1 μ g/ml actinomycin D (ActD, dashed green line) at the predicted peak of SOCS3 mRNA ($t=30$ min) (green and black dots). CFU-E cells were stimulated with 5 U/ml Epo- α and treated with 1 μ g/ml ActD at $t=60$ min. The SOCS3 mRNA level was measured with qRT-PCR and *CISH* mRNA was measured in parallel as control (green and black dots). The model prediction is depicted as black or green line. Shaded areas indicate estimated errors. This experiment was performed in triplicates and one representative example is shown. Model predictions were performed by Bernhard Steiert.

To sum up, the NSCLC cell line H838 expresses significant amounts of Epo receptor that can be phosphorylated upon stimulation with Epo. It was further shown that Epo treatment decreased the cisplatin sensitivity of H838 cells for clinically relevant cisplatin concentrations. In conclusion, the presence of EpoR in NSCLC could pose a risk for lung cancer patients receiving a combined treatment of cisplatin-based chemotherapy and Epo. In order to assess the risk that might be connected to Epo treatment in more detail and to dissect the complexity of EpoR signaling, a mathematical model of Epo-induced signaling was established that was able to identify differences between the NSCLC cell line H838 and the actual therapy target, the erythroid progenitor cells. The SOCS3 mRNA turnover rate was among the predicted cell type-specific parameters. It could be experimentally validated by qRT PCR that SOCS3 mRNA is more stable in CFU-Es than in H838 cells. In conclusion, the study suggests a higher and more sustained pSTAT5 level in H838 cells compared to CFU-Es, that is known to be connected to survival of CFU-Es [62].

5.4 TGF- β signaling in NSCLC cell lines

NSCLC is characterized by a high metastasizing rate. The transforming growth factor beta (TGF- β) induces epithelial-to-mesenchymal transition (EMT) [118-122] which is the key for tumorigenesis, migration and invasion. Moreover, high TGF- β levels are correlated with poor prognosis in lung cancer [125, 127]. Although EMT is quite well-characterized, so far no drug, small molecule or inhibitor has been identified that is able to target this pathway and reduce the metastatic properties of lung cancer. Therefore, the influence of TGF- β on NSCLC cell lines had to be tested to gain more detailed information about how signal is transduced in NSCLC cell lines.

5.4.1 TGF- β is able to induce TGF- β signaling in NSCLC cell lines

As the first step, it was investigated whether TGF- β is able to induce downstream signaling in NSCLC cell lines. This was tested by the measurement of the phosphorylation status of the downstream targets SMAD2 and SMAD3 upon TGF- β stimulation. The NSCLC cell lines H838, H1975 and H1650 were seeded according to the SOPs. The cells were either serum-starved (-FCS-TGF- β), left in serum-containing medium (+FCS-TGF- β) or treated with 1 ng/ml TGF- β for 60 minutes (-FCS+TGF- β). The cells were lysed and prepared for quantitative immunoblotting (**Figure 24A**). Separate immunoprecipitations (IP) were performed for the detection of the TGF- β signaling molecules SMAD2, SMAD3 and SMAD4 followed by immunoblotting against phosphorylated and total species. The housekeeper β -actin was used as a loading control for the total cell lysates (TCL). For all cell lines, the same amount of protein was used for the analysis of the different proteins. The results demonstrated that TGF- β stimulation led to phosphorylation of the downstream components SMAD2 and SMAD3 in all three cell lines. Interestingly, H838 cells contained low levels of total SMAD3 and pSMAD3 in comparison to the other cell lines. The level of SMAD4 was comparable for all the cell lines tested. H1975 cell line that showed the highest level of pSMAD3 and total SMAD3, was selected for further analysis.

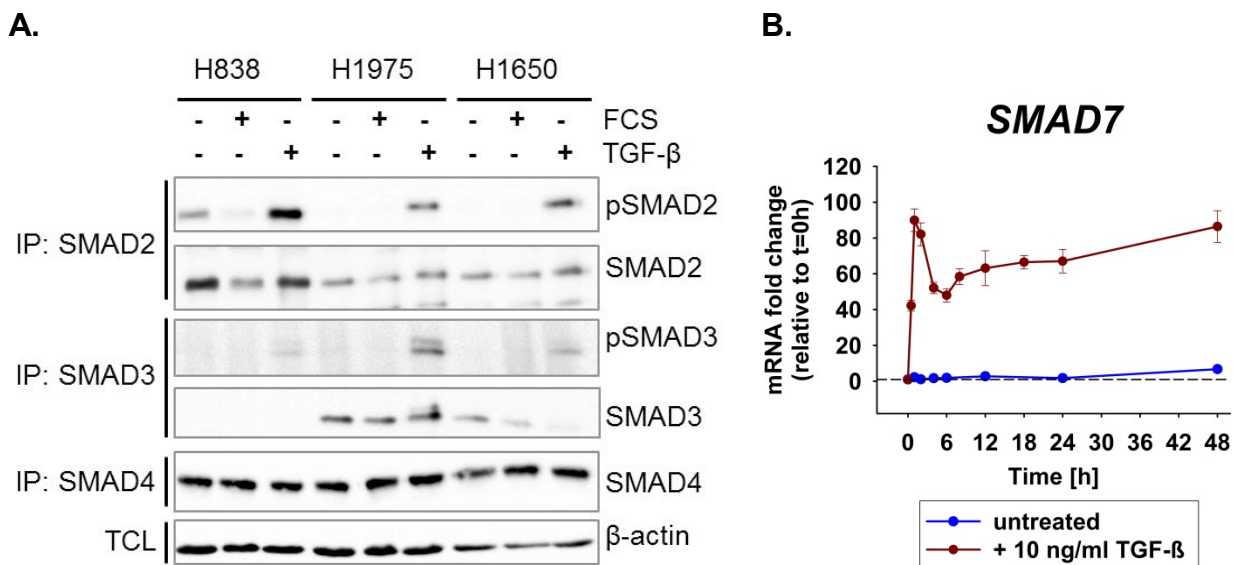


Figure 24: Measurement of TGF- β signaling in NSCLC cell lines. (A) Quantitative immunoblotting of the TGF- β -stimulated NSCLC cell lines H838, H1975 and H1650. The cells were serum-starved (-FCS/-TGF- β) or left in medium with FCS (+FCS/-TGF- β) or treated with 1 ng/ml TGF- β for 60 minutes (-FCS/+TGF- β). After cell lysis, immunoprecipitation was performed for SMAD2, SMAD3 and SMAD4 followed by 10% SDS-PAGE. The proteins were transferred to a nitrocellulose membrane and detected on the Image Quant LAS 4000 by chemiluminescence. β -actin was used as loading control for the individual cells lines. This experiment was performed in triplicates and one representative example is shown. Abbreviations: IP: immunoprecipitation, TCL: total cell lysate, FCS: fetal calf serum. **(B)** Quantitative RT-PCR of the TGF- β target gene *SMAD7* in the cell line H1975. The cells were serum-starved and either treated with 10 ng/ml TGF- β or left untreated. The mRNA levels are shown relative to the starting point of the time course (t=0h).

In the next step, the cell line H1975 was tested for the activation of TGF- β downstream signaling on mRNA level. For this purpose, the most prominent TGF- β target gene *SMAD7* [99, 163] was monitored over time. H1975 cells were seeded according to the SOPs and stimulated with 10 ng/ml TGF- β or left untreated. Samples for the time points 0, 1, 2, 4, 6, 12, 24 and 48 hours after the treatment were taken and total RNA was extracted using TRIzol. The *SMAD7* mRNA was detected by qRT-PCR and depicted relative to the starting point (t = 0 hours) (**Figure 24B**). The untreated control did not show any change in *SMAD7* mRNA expression over time. However, upon TGF- β treatment *SMAD7* mRNA expression was significantly increased with a maximum expression peak within the first hours. However after six hours, the *SMAD7* level decreased but did not decline to the starting level even within the 48 hours of observation.

These results demonstrated that TGF- β was able to activate TGF- β signaling in the NSCLC cell lines H838, H1975 and H1650 and also to induce the mRNA expression of the TGF- β target gene *SMAD7* at least in H1975.

5.4.2 Expression analysis of TGF- β -dependent genes in the NSCLC cell line H1975

To analyze the gene expression pattern in H1975 after TGF- β stimulation, a mRNA time course experiment with different time points (0, 0.5, 1, 2, 4, 6, 12, 24 and 48 hours) was performed and analyzed by a mRNA microarray (GeneChip 2.0 ST, Affimetrix). One replicate of each time point was used for the analysis except of the time points 0, 24 and 48 hours which were measured in triplicates. The microarray data analysis was performed by the theoretical cooperation partners Dr. Hauke Busch and Dr. Melanie B rries (Freiburg University). To identify biological processes that were significantly regulated by TGF- β in comparison to the untreated control, the expression profiles were analyzed using the GO (gene ontology) database.

The analysis is shown as a heatmap (**Figure 25**) for TGF- β -induced downregulated or upregulated processes. The color code depicts the p-value. The first block of genes downregulated by TGF- β (**Figure 25A**) is connected to mitosis and cell cycle. This included genes involved in the general mitotic process, mitotic cell cycle, cell division and the activity of cell cycle checkpoints. Within the first hour, these processes are downregulated, followed by a phase where no significant changes in expression could be observed. However, 6 hours upon the treatment with TGF- β the genes connected to mitosis were again downregulated for the rest of the observed time period.

The second block of downregulated processes connected to mitosis and cell cycle were just downregulated 6 hours after the TGF- β treatment without an initial significance peak within the first hour. These processes included activity of the spindle apparatus, telomere maintenance via recombination, DNA gap filling, mitotic cell cycle spindle assembly checkpoint, mitotic chromosome condensation, M/G1 transition of mitotic cell cycle and G1/S transition of mitotic cell cycle.

The processes connected to DNA repair and DNA replication, such as the activity of DNA damage checkpoint, double-strand break repair, ATP-dependent DNA helicase activity, mismatch repair, nucleotide-excision repair, DNA-directed DNA polymerase activity, double-strand break repair via homologous recombination, DNA repair in general, DNA replication and DNA strand elongation involved in DNA replication are downregulated after 6-12 hours upon TGF- β treatment. Although the p-value differs for different processes, all expression changes compared to the untreated control are significant.

TGF- β also upregulated several biological processes (**Figure 25B**). This includes the organization of the extracellular matrix and cell adhesion, which had the highest p-value for upregulation 6 hours after the stimulation with TGF- β . More distinct but still significant over time, processes connected to adhesion and filament organization, such as skeletal system development, collagen binding, cytoskeleton organization, gap junction and cell adhesion in general were upregulated with TGF- β . Moreover, cell migration and epithelial to mesenchymal transition (EMT) are upregulated.

To sum up, among the downregulated biological processes, mitosis, cell division, cell cycle and DNA repair and replication were detected. In contrast, TGF- β upregulated processes were connected to adhesion, cell junctions, migration and EMT.

The experimental validations of several genes involved in the TGF- β pathway and in EMT processes such as *SMAD7*, *TGFBR1* and *TGFBR2*, *ZEB1*, *SNAI1* (Snail), *SNAI2* (Slug), *FN1* (Fibronectin), *CDH1* (E-cadherin), *CDH2* (N-cadherin), *VIM* (Vimentin) and *SKIL* (SnoN) were performed by qRT-PCR (**Figure 29**).

Figure 25A. Biological processes downregulated upon TGF-β treatment

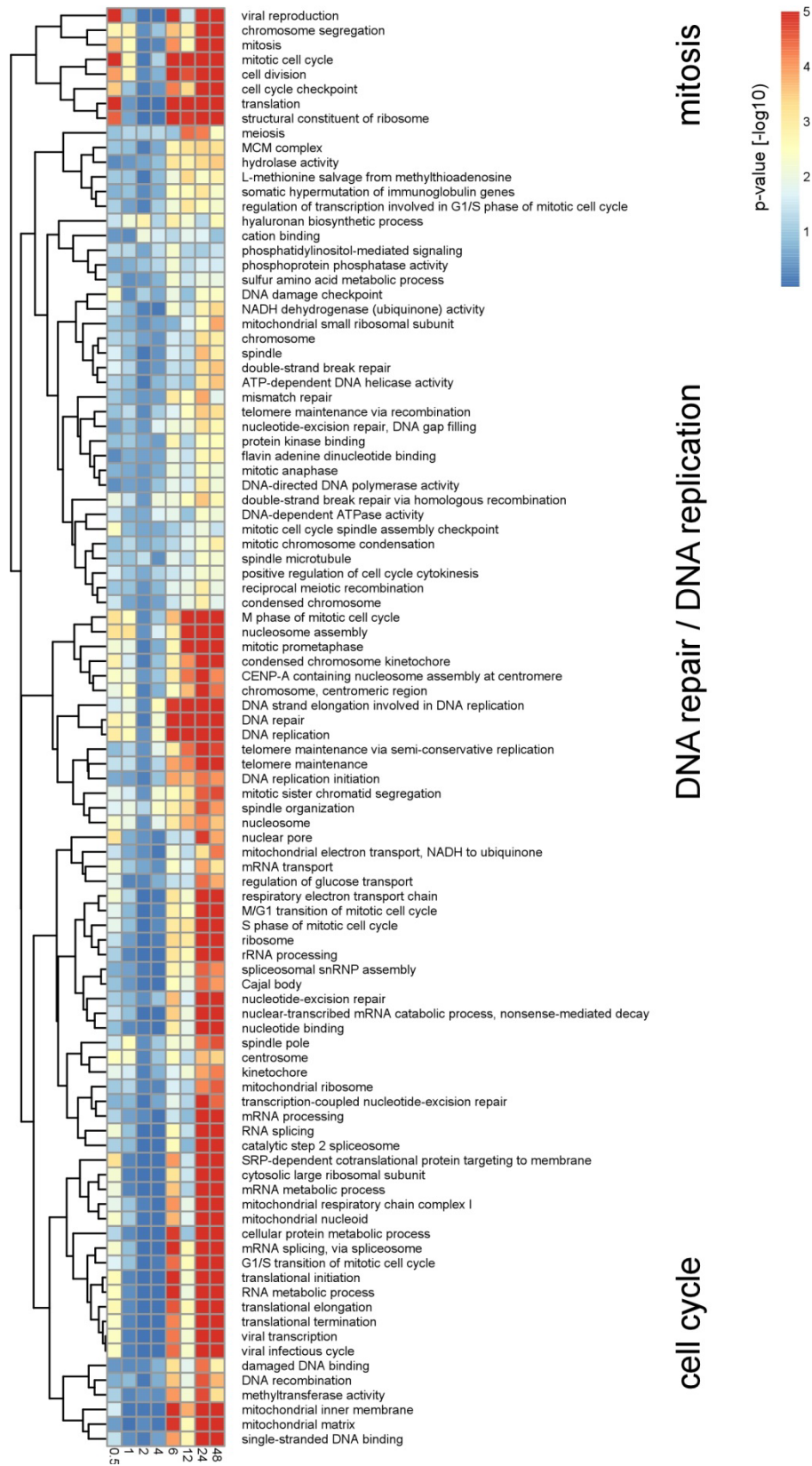


Figure 25B. Biological processes upregulated upon TGF- β treatment

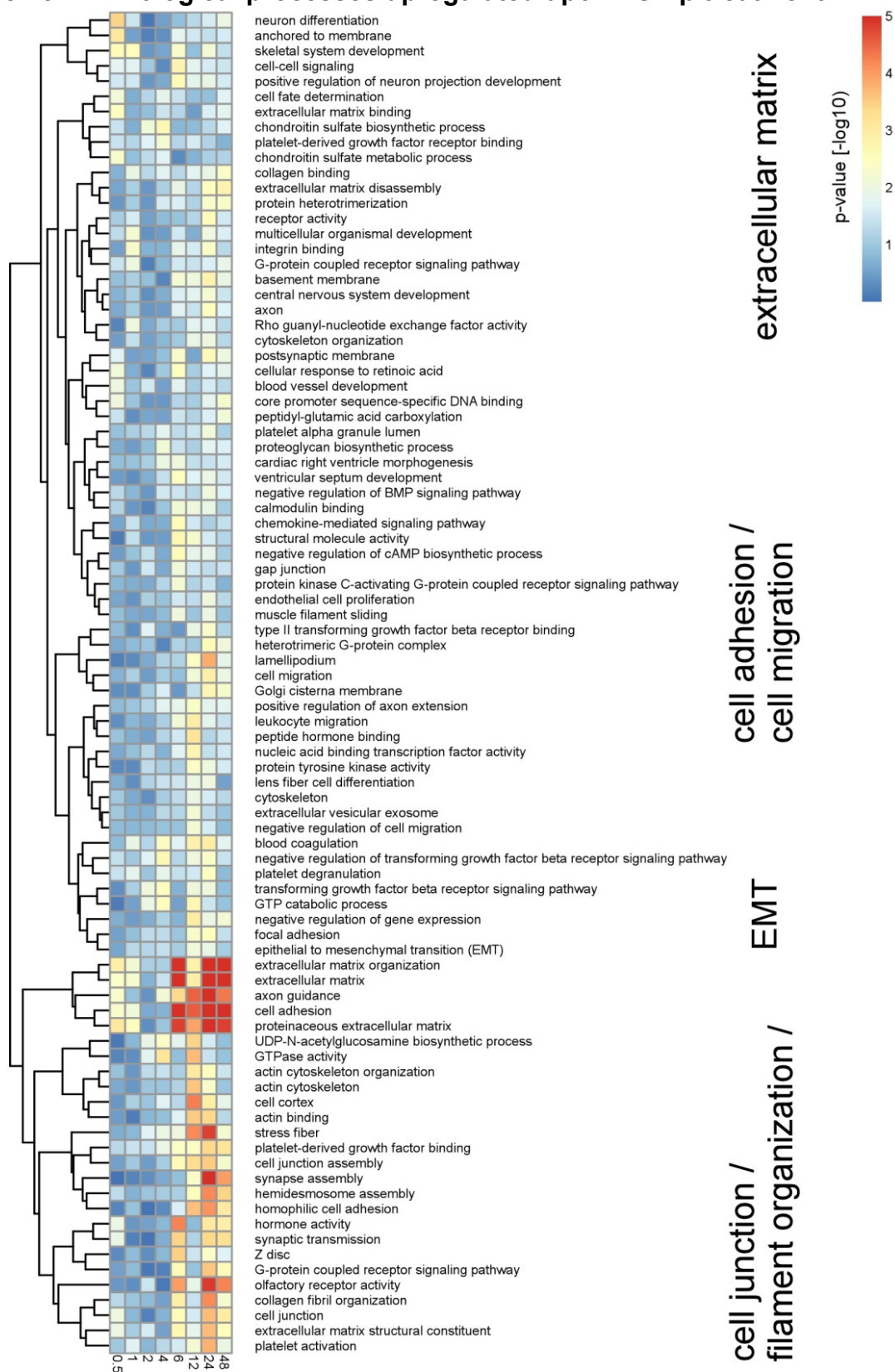


Figure 25: Heatmap of significantly responding genes to TGF- β treatment annotated to (A) downregulated or (B) upregulated biological processes (GO analysis). The NSCLC cell line H1975 was treated with 10 ng/ml TGF- β or left untreated. A mRNA microarray (GeneChip 2.0 ST, Affimetrix) was performed for the time points 0, 0.5, 1, 2, 4, 6, 12, 24 and 48 hours. The terms on the right denote the most significant GO biological processes. The color code depicts the p-value (Figure kindly provided by Dr. Hauke Busch and Dr. Melanie B rries).

5.4.3 Validation of selected target genes induced by TGF- β in NSCLC cell lines

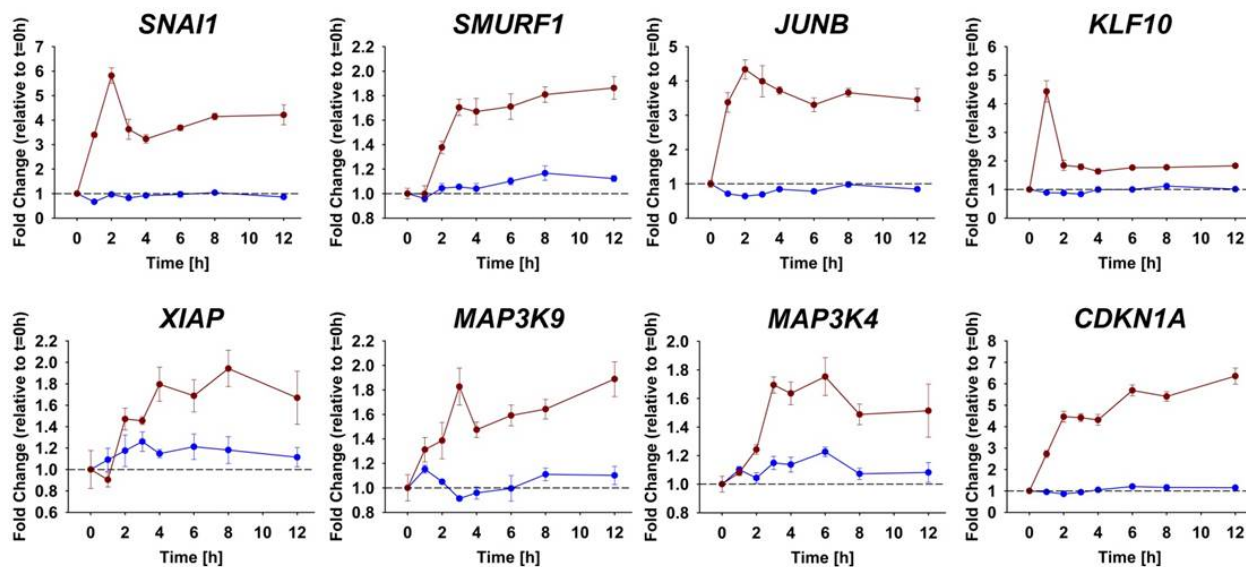
To verify mRNAs that were found to be upregulated in the NSCLC cell line H1975 by microarray analysis, selected mRNA were measured by qRT-PCR (**Figure 26**). The 8 selected candidates included mRNAs that are known to be involved in MAP kinase signaling (*MAP3K4*, *MAP3K9*), TGF- β /SMAD signaling (*SMURF1*, *KLF10*), EMT (*SNAI1*), survival (*XIAP*), transcription factors (*JUNB*) and the cell cycle (*CDKN1A*).

The validation of mRNA dynamics for the first 12 hours was performed by qRT-PCR in biological triplicates with a time course for the NSCLC cell lines H1975 and additionally in the NSCLC cell line H838. To this aim, the cells were seeded according to the SOPs, growth factor depleted and lysed 0, 1, 2, 3, 4, 6, 8 and 12 hours upon the treatment with 1 ng/ml TGF- β . An untreated control was measured in parallel for all time points.

The results showed similar dynamics as observed by microarray. It could be confirmed that all mRNAs were rapidly upregulated within the first hours upon TGF- β treatment in H1975 cells compared to the untreated control. In general, TGF- β treatment was more effective for all mRNAs tested in H1975 cells compared to H838. TGF- β -dependent expression of mRNAs was found to be more reduced in H838 cells. Moreover, no significant changes in the expression levels were detectable for *MAP3K9* and *XIAP* mRNA in H838.

In sum, all selected mRNA candidates could be confirmed to be TGF- β target genes at least in the NSCLC cell lines H1975 and H838. The H1975 cells showed higher mRNA expression upon stimulation with TGF- β compared to H838 cells, which is in line with the phosphorylation pattern of SMAD and SMAD3 proteins measured for both cell lines shown in **Figure 24**. In conclusion, the TGF- β -induced signaling cascade could be activated in the H1975 cell line to a higher extend compared to the cell line H838.

A. H1975



B. H838

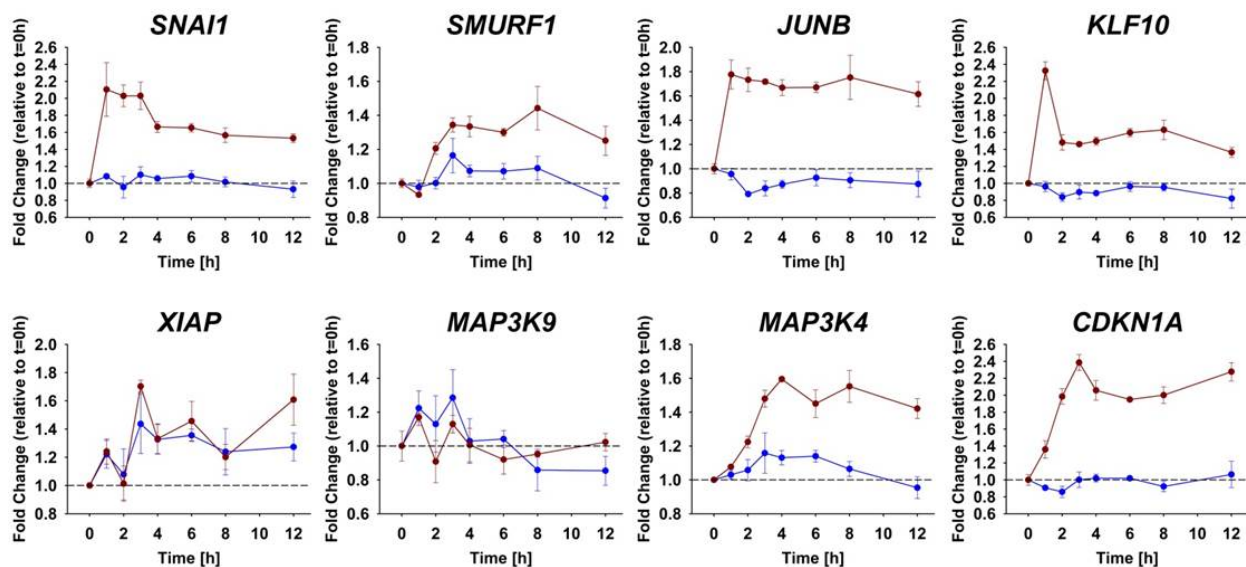


Figure 26: Validation of TGF- β -inducible mRNAs by qRT-PCR in the NSCLC cell lines (A) H1975 and (B) H838. The classical TGF- β targets *KLF10* and *SMURF1*, the EMT marker *SNAI1*, the pro-survival factor *XIAP*, the MAPK pathway members *MAP3K9* and *MAP3K4* and the cell cycle inhibitor *CDKN1A* are shown representatively. The study was performed in triplicates.



5.4.4 The TGF- β pseudoreceptor BAMBI is downregulated in NSCLC

One of the key problems in lung cancer is early spread. EMT, which can be induced by TGF- β , is known to be involved in the development of the metastasis properties of cells. One factor that can negatively influence the TGF- β pathway is the TGF- β pseudoreceptor BAMBI that was shown to be epigenetically silenced in bladder cancer [115] and is absent in breast cancer [116]. As our cooperation partner Dr. Sebastian Marwitz in the group of Prof. Torsten Goldmann (Research Center Borstel, Division of Clinical and Experimental Pathology) could show that BAMBI protein is absent in lung adenocarcinoma patient samples (immunohistochemistry), BAMBI was selected for further analysis.

To determine the mRNA expression level of *BAMBI* and EMT genes in lung adenocarcinoma tumors, matched pairs of tumor and tumor-free lung of 9 patients (cDNA kindly provided by the Research Center Borstel) was tested by qRT PCR (**Figure 27A**). The analysis revealed that not only *BAMBI*, but also the mRNA of TGF- β receptors *TGFBR1* and *TGFBR2* and *SMAD7* were downregulated in all tested adenocarcinoma tumors. Interestingly, also the mRNA for the EMT genes *SNAI1* (Snail), *SNAI2* (Slug), *ZEB1*, *VIM* (Vimentin), *FN1* (Fibronectin) was downregulated in the analyzed adenocarcinomas. *CDH2* (N-cadherin) was found to be downregulated in almost all tumors tested. *CDH1* (E-cadherin) and *SPP1* mRNA were upregulated in the tumor sample compared to its matching tumor-free lung.

To analyze if the BAMBI downregulation observed in the adenocarcinoma tissue samples of patients could be reflected in NSCLC cell lines, the mRNA expression level of *BAMBI* was monitored using quantitative RT-PCR in the cell lines H838, H1650 and H1975 and compared to the *BAMBI* expression level in healthy lung alveolar epithelial type II cells (AECII) (**Figure 27B**). All three cell lines showed significantly lower levels of *BAMBI* mRNA compared to AECII (two-tailed t-test, $p < 0.001 = ***$). The cell lines H838 and H1650 expressed approximately half as much mRNA with 0.5-fold expression for H838 and 0.62-fold expression for H1650 compared to the healthy control. The cell line H1975 showed a dramatic downregulation of *BAMBI* mRNA with an expression level of 0.015-fold lower than AECII.

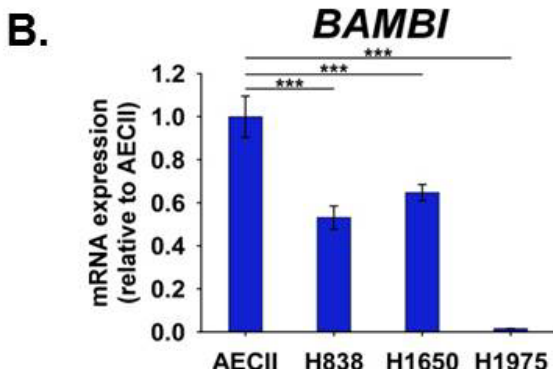
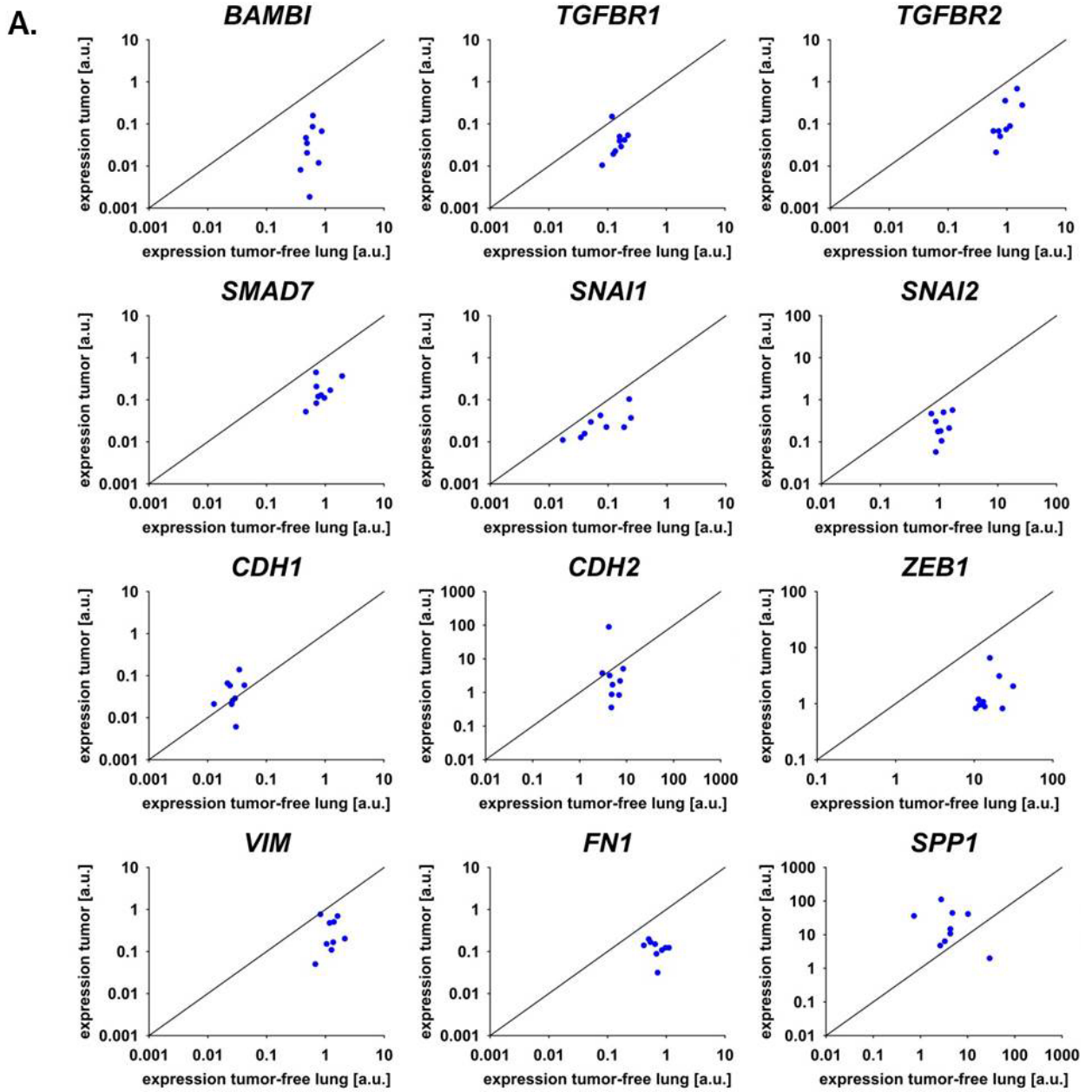


Figure 27: (A) Matching pairs of lung adenocarcinoma tumor and tumor-free lung of 9 patients. The levels of the EMT-related mRNAs were measured by qRT-PCR. One blue dot represents one adenocarcinoma tissue sample of a patient. The black line depicts a ratio of 1, representing comparable amount in the tumor and the tumor-free sample. **(B)** Relative quantification by qRT-PCR of *BAMBI* mRNA in the NSCLC cell lines H838, H1650 and H1975, compared to the healthy AECII cells. $p < 0.001 = ***$ (two-tailed t-test), $n=3$.

5.4.5 BAMBI reconstitution decreases the expression of TGF- β -dependent genes in the NSCLC cell line H1975

The TGF- β pseudoreceptor BAMBI was found to be downregulated in lung adenocarcinoma tumors and also in the NSCLC cell lines H838, H1650 and H1975. To investigate whether this loss of BAMBI expression influences TGF- β -induced signaling, *BAMBI* was reconstituted in the NSCLC cell line H1975 to mimic a “healthy” situation.

To this aim, the NSCLC cell line was transfected with the TET-On system and thus expressed either BAMBI coupled to GFP (H1975-BAMBI-GFP) or as control GFP alone (H1975-GFP) if induced with doxycycline (kindly provided by Dr. Sofia Depner). The reconstitution was effective with a 5349-fold increased expression of *BAMBI* mRNA in H1975-BAMBI-GFP compared to H1975-GFP (**Figure 28**).

To determine the effect of the reconstitution of *BAMBI* in the NSCLC cell line H1975, the H1975-BAMBI-GFP and H1975-GFP cells were seeded according to the SOPs, treated with 5 μ l/ml doxycyclin (DOX) for 24 hours, serum-starved in DOX-containing medium for approximately 16 hours and treated with 0.1 ng/ml TGF- β . The TGF- β -induced expression of the EMT-involved mRNAs *SMAD7*, *TGFBR1* and *TGFBR2*, *ZEB1*, *SNAI1* (Snail), *SNAI2* (Slug), *FN1* (Fibronectin), *CDH1* (E-cadherin), *CDH2* (N-cadherin), *VIM* (Vimentin) and *SKIL* (SnoN) were analyzed for the time points 0, 1, 4, 24 and 48 hours by qRT-PCR (**Figure 29**).

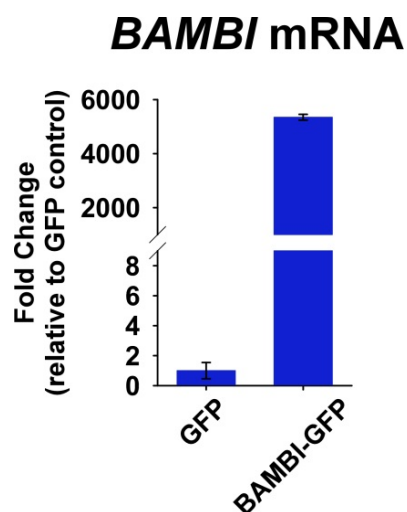


Figure 28: Measurement of the *BAMBI* mRNA expression by qRT-PCR in the cell lines H1975-BAMBI-GFP and H1975-GFP upon the treatment with 5 μ l/ml doxycyclin ($n=3$).

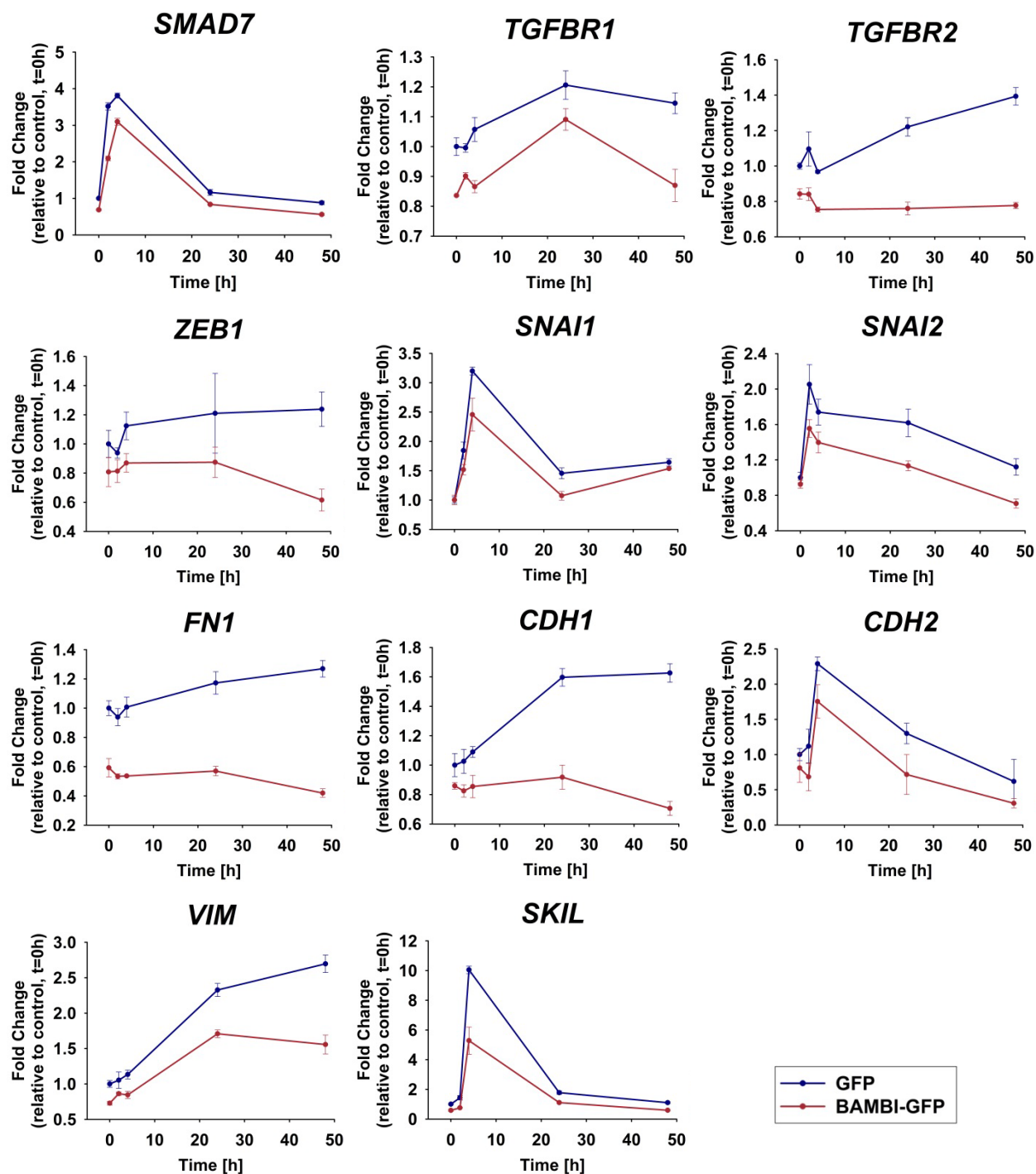


Figure 29: Reconstitution of *BAMBI* in the NSCLC cell line H1975 with the TET-On system (H1975-BAMBI-GFP, depicted in red) in comparison to the control cell line H1975-GFP (depicted in blue) upon stimulation with 0.1 ng/ μ l TGF- β . Signaling dynamics for the EMT-involved mRNAs *SMAD7*, *TGFBR1* and *TGFBR2*, *ZEB1*, *SNAI1* (Snail), *SNAI2* (Slug), *FN1* (Fibronectin), *CDH1* (E-cadherin), *CDH2* (N-cadherin), *VIM* (Vimentin) and *SKIL* (SnoN) were analyzed for the time points 0, 1, 4, 24 and 48 hours by qRT-PCR. The data is shown relative to the GFP-control at t = 0 hours. The experiment was performed in triplicates.

The reconstitution of *BAMBI* resulted in a reduced mRNA starting level for *FN1*, *SKIL*, *VIM*, *TGFBR1*, *TGFBR2* (t-test, $p \leq 0.001$) and *CDH1* 0.05 (t-test, $p \leq 0.05$). All mRNAs of the H1975-GFP control cell line were upregulated upon stimulation with TGF- β . *BAMBI* reconstitution reduced TGF- β -induced mRNA expression although a similar overall dynamics of mRNA expression was observed except for *CDH1*, *TGFBR2* and *ZEB1* mRNA which was no longer inducible upon TGF- β treatment in H1975-BAMBI-GFP cells.

Taken together, the negative regulator of TGF- β signaling *BAMBI* was shown to be downregulated in adenocarcinoma tumors and the NSCLC cell lines H1975, H838 and H1650. The reconstitution of *BAMBI* resulted in decreased expression of EMT markers such as Snail, Slug, Fibronectin, E-cadherin, N-cadherin and Vimentin.

In conclusion, *BAMBI* expression is negatively correlated to the potential for EMT and thus metastasis in NSCLC. *BAMBI* is thereby suggested to act as a tumor suppressor in NSCLC.

6. Discussion

6.1 Effect of MEKi on cisplatin-induced apoptosis in NSCLC cell lines

6.1.1 Cisplatin activates the RAS–RAF–MEK–ERK cascade and induces apoptosis in NSCLC cells

As standard of care, NSCLC patients are treated with platinum-based chemotherapeutic drugs [22], such as cisplatin. In this study, the effect of cisplatin on NSCLC cell lines was tested. The NSCLC cell line H838 was selected as model system for NSCLC as it harbors a representative pattern of mutations for lung cancer.

It was shown by quantitative immunoblotting, that cisplatin treatment led to an increased phosphorylation of ERK1 and ERK2 within 6 hours compared to the untreated control. ERK1 and ERK2, that are known to be direct and the only targets of its upstream kinase MEK [11], were also shown to be phosphorylated by treatment with cisplatin in the lung adenocarcinoma cell line A549 and the NSCLC cell line H460 [34]. The activation of ERK was not only reported for lung cancer cells but also for several other cell types, reviewed by Basu *et al.* [30]. It was further shown that *EGR1* and *EGR3* mRNAs were upregulated 2 hours after cisplatin treatment in ovarian cancer cells [164] and *EGR1* mRNA after 24 hours in osteosarcoma cells [165]. However, little is known about cisplatin-induced mRNA expression in NSCLC cells. To this aim, the cisplatin-induced upregulation of the mRNA expression of MAPK target genes *EGR1*, *EGR3* and *DUSP5* was confirmed by quantitative qRT-PCR in the NSCLC cell line H838.

Moreover, cisplatin was verified to mediate apoptosis in the NSCLC cell line H838. This was expected, as cisplatin is an FDA-approved chemotherapeutic agent for NSCLC and Tsai *et al.* already showed by using the tetra-zolium dye colorimetric assay that cisplatin induces apoptosis in H838 cells [166]. The time- and dose-dependent effect of cisplatin on the cell viability of H838 cells was confirmed with the colorimetric CellTiter-Blue viability assay. Furthermore, the protein level of cleaved caspase-3 as an apoptotic marker was established by quantitative immunoblotting in H838 cells. A slight increase of cleaved caspase-3 was observed after 6 hours and a strong increase after 12 hours of treatment with cisplatin. Moreover, it was shown by qRT-PCR that cisplatin treatment

resulted in downregulation of anti-apoptotic factor BCL2. This confirmed the initiation of the apoptotic program in the NSCLC cell line H838 upon cisplatin treatment.

Furthermore, an analysis by live cell imaging with H838 cells that express the FUCCI cell cycle sensor revealed that cisplatin affects primarily cells in the S/G2/M cell cycle phases in which DNA is replicated and cell division occur. This was not surprising as cisplatin is known to bind to purine bases and to intercalate in DNA which interferes with cell division and consequently leads to induction of apoptosis in dividing cells [30].

6.1.2 Pre-incubation with MEKi decreases the cisplatin sensitivity of NSCLC cells

Although cisplatin-based chemotherapy is initially rather effective, many cancer patients relapse with a cisplatin-resistant disease [23, 53]. Several mechanisms contributing to therapy resistance are discussed in the literature, such as an activating mutation in the MAPK pathway [15]. *KRAS* for instance, is with 17% one of the most frequently mutated genes in lung cancer [16] and 30% of the NSCLC were found to harbor RAS mutations. Therefore, several MEK inhibitors (MEKi) that block signaling downstream of MEK, have been tested in clinical trials also in combination with chemotherapeutic drugs [15] (ClinicalTrials.gov, Identifier: NCT01809210).

In this study, the influence of MEKi on the effect on NSCLC cells of treatments with clinically relevant cisplatin doses was examined. By quantitative immunoblotting, it was shown that pre-incubation for 60 minutes with MEKi U0126 of the NSCLC cell line H838 resulted in a decreased cisplatin-induced ERK phosphorylation. Moreover, MEKi was found to counteract the expression of the MAPK target genes *EGR1*, *EGR3* and *DUSP5* upon cisplatin treatment in H838 cells.

Interestingly, MEKi not only influenced cisplatin-induced signaling, but also affected cellular processes. For instance, live cell imaging with the FUCCI cell cycle sensor revealed that MEK inhibition alone or in combination with cisplatin resulted in an elongated G1 cell cycle phase in H838 cells. Moreover, *CDKN1A* mRNA, that is known to induce a G1 cell cycle arrest, was found to be upregulated upon stimulation with MEKi. This suggests that MEK inhibition might induce G1 arrest in the NSCLC cell line H838. This would be in line with literature where it was reported that MEK inhibition can

lead to a G1 arrest in fibroblasts and pancreatic cancer cell lines [14, 155] and activation of ERK is even required to enter the S phase [11-13].

The study further revealed that pre-treatment with MEK inhibitor U0126 is able to rescue H838 cells from cisplatin-induced apoptosis. This effect could be measured with the CellTiter-Blue viability assay and by microscopy-based live cell imaging. Moreover, reduced levels of cleaved caspase-3 were obtained by quantitative immunoblotting for the combined treatment of cisplatin and MEKi compared to cisplatin treatment alone. However, the cisplatin-mediated downregulation of *BCL2* mRNA could not be counteracted with MEKi. Furthermore, CellTiter-Blue measurements revealed that the MEKi-mediated rescue effect on cisplatin-induced apoptosis could be increased with elongated MEKi pre-incubation times. This effect could also be monitored in the NSCLC cell line H838 for the clinically relevant MEK inhibitors selumetinib (AZD6244), CI-1040 (PD184352), PD0325901 and trametinib (GSK1120212) [15].

A MEKi-mediated rescue of cisplatin-induced apoptosis was already observed in mouse liver cells [167], mouse renal cells [168], human testicular germ cell tumor cell lines [39], human hepatocellular carcinoma [169] and in the human lung cancer cell lines A549 and H460 [34]. In contrast, in human ovarian cancer cells U0126 treatment in addition to cisplatin resulted in increased apoptosis rates [170]. It was also demonstrated that the elevated expression of RAS, an upstream component of the MEK-ERK signaling pathway, was connected with enhanced sensitivity to cisplatin [36]. Moreover, HeLa cell variants that were selected for cisplatin resistance, showed reduced activation of ERK following platinum treatment [36]. In sum, these studies showed that decreased signaling via the RAS–RAF–MEK1/2–ERK1/2 cascade was correlated to decreased cisplatin sensitivity. However, there are also contrary observations about the role of ERK in influencing cell survival of cisplatin-treated cells. It was shown that the MEK1-specific inhibitor PD98059, sensitizes human melanoma cells [171], human ovarian carcinoma cell lines [172, 173], human pancreatic cancer cells [174] and human cervical carcinoma cells [175] to cisplatin-induced apoptosis.

Different possibilities are conceivable how the MEK inhibitor was able to decrease the sensitivity of the NSCLC cells to cisplatin. For instance, the inhibition of the MAPK pathway with MEKi might either lead to a downregulation of pro-apoptotic molecules or

an upregulation of anti-apoptotic molecules as the RAS–RAF–MEK–ERK pathway is known to be involved in the regulation of pro- and anti-apoptotic Bcl-2 family members in the lung adenocarcinoma cell line A549 [176] and pancreatic cancer cells [174]. This possibility might not be very likely as it was shown by qRT-PCR that MEKi could not counteract the cisplatin-mediated downregulation of *BCL2* mRNA.

The studies rather suggest a rescue mechanism in which the NSCLC cell lines is arrested in the G1 cell cycle phase and can therefore not be targeted by cisplatin, as it was shown that the chemotherapeutic agent attacks cells in the S/G2/M phase. Furthermore, the cells might also benefit from the increased time for the repair of damaged DNA strands.

In conclusion, MEK inhibitor treatment leads to an indirect rescue effect on cisplatin-induced apoptosis in the NSCLC cell line H838. The study shows that MEKi treatment in combination with cisplatin-based chemotherapy poses a potential risk for lung cancer patients.

6.2 Role of Epo-induced signaling in NSCLC cell lines

6.2.1 Epo treatment decreases the cisplatin sensitivity of the EpoR-expressing cell line H838

Lung cancer patients often suffer from cisplatin-induced anemia [177, 178]. Anemia is characterized by a decrease in the amount of erythrocytes or the amount of hemoglobin in the blood. The symptoms are caused by the lower oxygen levels in the blood and may include fatigue, shortness of breath or a general weakness and often come along with reduced quality of life. A toxicity grading system, including the grades mild (grade 1), moderate (grade 2), serious/severe (grade 3) or life threatening (grade 4), was established by the World Health Organization [178]. Anemia has to be treated in grade 3 and 4 (≤ 6.5 - 7.9 g hemoglobin /dl blood), as at this point not only quality of life is impaired but also further planned chemotherapeutic cycles have to be dose-decreases or even cancelled. One possible treatment against anemia is thereby blood transfusion. Unfortunately, blood transfusions carry several risks, such as a viral or bacterial infection, acute hemolytic reactions, delayed hemolytic reactions and transfusion-related

acute lung injury [178-182]. Therefore, the erythropoietin-stimulating agent Epo was suggested as preferred treatment as it decreases chemotherapy-induced anemia in patients [183-187]. Unfortunately, recent studies have shown that Epo can have tumor stimulating effects [89] and Epo and EpoR co-expression is shown to be associated with poor survival of non-small cell lung cancer patients [90]. The expression of EpoR on mRNA and protein level was reported for several cell types. Hardee *et al.* reviewed the expression levels of EpoR in several other tumor types and cancer cell lines of different origins including bladder, breast, the female reproductive tract, the gastrointestinal tract, head and neck, hematologic, kidney, liver, lung, melanoma, nervous system, pancreatic, prostate, sarcoma and thyroid [188]. However, also the specificity of antibodies for EpoR, e.g. the Santa Cruz antibody C20 (catalogue number SC-695) [97, 189], and consequently the proof for EpoR expression was discussed controversially [98].

In this study, the NSCLC cell line H838 was selected as model system to enable the analysis of the biological effect of Epo and its receptor on NSCLC cells. Dunlop *et al.* already described the EpoR expression in H838 cells and showed that Epo binding activates the three pathways JAK2/STAT5, RAS/ERK and PI3K/AKT [91]. It was confirmed by qRT-PCR and quantitative immunoblotting that H838 cells express significant amounts of Epo receptor. Moreover, the EpoR was shown to be functional as it was phosphorylated upon stimulation with Epo.

Interestingly, Epo decreased the sensitivity of H838 cells to cisplatin. The analysis with the CellTiter-Blue viability assay showed a clear increased cell number for the combined treatment of Epo and cisplatin compared to cisplatin treatment alone. This rescue effect could also be observed by live cell imaging with a sensor for active caspase-3 under the microscope and was even shown to be dependent on the Epo dose. High Epo doses completely counteracted the cisplatin-induced activation of caspase-3. The applied cisplatin concentration was thereby in a range of clinical relevance.

However, Epo was already shown to reduce the sensitivity to cisplatin of several cancer cells for cisplatin-induced apoptosis [190], including renal cell carcinomas [157, 191], melanoma [192], cervical cancer cells [193] and ovarian cancer cell lines [194].

Phosphorylated STAT5A might be a key regulator of the Epo-induced rescue of cisplatin-induced apoptosis in lung cancer. Bittorf *et al.* showed that erythroleukemic cell lines lacking STAT5 docking sites in Epo receptors, have a diminished ability for the mediation of anti-apoptotic signals [195]. Moreover, STAT5 was reported to activate the anti-apoptotic factor Mcl-1 in B cell development [61] and anti-apoptotic Bcl-2 family members Bcl-2 and Bcl-xL in erythroid progenitor cells [84, 196-198] and myeloid leukemia [199].

To sum up, the EpoR-expressing NSCLC cell line H838 was shown to be less sensitive for cisplatin in clinically relevant doses upon treatment with Epo. In conclusion, the combined treatment of cisplatin-based chemotherapy and Epo might pose a risk for NSCLC patients with tumors expressing EpoR.

6.2.2 A mathematical model of the Epo-induced signaling pathway predicts differences between NSCLC cell line H838 and erythroid progenitor cells

As the intention of Epo treatment in the case of chemotherapy-related anemia is to target the erythroid system, the focus of this study was on the comparison of the activation of JAK2/STAT5 signaling in H838 cells and in primary erythroid cells (CFU-E). To be able to analyze the complex EpoR networks dynamics in both cell types, a dynamic pathway model was applied.

EpoR signaling has already been described using a systems biology approach. Becker *et al.* [79] focused on the receptor level of EpoR signaling in BaF3-EpoR cells, a murine proB cell line that expresses high EpoR levels. The applied model contains parameters for receptor mobilization, recycling, and turnover. It was shown that after EpoR binds its ligand, the EpoR-Epo complex is internalized and degraded followed by a replenishment of the receptor from intracellular receptor pools [79]. It was previously shown by Yoshimura *et al.* that only a small proportion of EpoR is present on the cell surface and the majority is located in intracellular receptor pools [200]. Bachmann *et al.* [62] worked on the JAK2/STAT5 signaling pathway that is activated upon Epo binding and the specific function of the negative feedback regulators CIS and SOCS3 in murine CFU-Es. The applied mathematical model contains information about the processes at

the membrane, in the cytoplasm and the nucleus upon ligand binding. In CFU-Es, EpoR signaling upon Epo binding is essential for survival, proliferation and differentiation. It was further shown that there is a direct correlation of cell survival and the integrated response of STAT5 in the nucleus [62].

In this study, the JAK2/STAT5 dynamic pathway model established by Bachmann *et al.* [62] was used as starting point and adapted to the NSCLC cell lines H838 and the EpoR overexpressing cell line H838-EpoR that was included to mimic a lung cancer situation with high EpoR expression in tumor cells. The mathematical model was further adapted to the lung cancer cells lines. This included the protein-tyrosine phosphatase SHP-1 that was replaced by the more general term “PTP” as SHP1 was shown by RNAseq to be absent in H838 cells. However, this might not be true for all NSCLC cell lines, indicated by recent publications that found SHP-1 transcripts in epithelial cancer cells [201] including epithelial ovarian cancer [202] As there is strong evidence that NSCLC cells derived from alveolar epithelial cells type II (AECII) [2-5], some other NSCLC cell lines might express SHP-1. Cao *et al.* also detected SHP-1 in the lung cancer cell line A549 [203].

For model calibration, quantitative time-resolved data of the NSCLC cell lines H838 and H838-EpoR was measured using three different experimental techniques. The time-resolved protein dynamics and the initial values were detected by quantitative immunoblotting. The quantitative mass spectrometry was applied to determine the absolute phosphorylation degree of STAT5 and qRT-PCR was performed to determine the mRNA dynamics of *SOCS3* and *CISH*. Together with the CFU-E data taken from Bachmann *et al.* [62], the model was calibrated using the data of the different cell types. As the aim was to identify differences between the cancer cells and the erythroid system, the emphasis was placed on the identification of cell type-specific parameters. Therefore, different model strategies were applied to test how many parameters have to be different to be able to describe the data. The discrepancy between a fitted model and a data set, also called the goodness of fit, was quantified by the chi-square value [204, 205]. The best model predicted 8 cell type-specific parameters for both cell types. All differences could be explained except of the *SOCS3* mRNA turnover rate. A qRT-PCR

analysis validated that the SOCS3 mRNA was more stable in CFU-Es compared to the NSCLC cell lines.

One possible mechanism for the cell type-specific SOCS3 mRNA turnover rate might be a cell type-specific expression level of miR-203, that was shown to specifically target and downregulate SOCS3 in keratinocytes [206], hepatocytes [76] and epidermal progenitors [207]. Moreover, miR-203 expression was correlated to higher SOCS3 levels and increased cisplatin resistance in breast cancer cells [75]. Another hypothesis for the higher SOCS3 mRNA turnover rate in the NSCLC cells would be an increased activation of the MAP kinase p38, that is known to be able to stabilize SOCS3 mRNA by binding to its AU-rich elements [73, 208].

In this study, the applied mathematical was shown to be a useful tool that was able to pinpoint differences between the NSCLC cell line H838 and erythroid progenitor cells, e.g. the SOCS3 mRNA turnover rate. SOCS3 levels might be a potential marker for cell survival as it negatively targets STAT5 activity that is known to correlate with increased survival rates. The direct correlation of pSTAT5 levels and survival was already shown for B cell development and leukemia and primary erythroid cells [61, 62].

In conclusion, this model strategy can also be generalized and applied as a tool for the identification of pathway differences in other cell types or for different pathways. Thereby, potential therapeutic targets, e.g. tumor cells, might be identified.

6.3 Role of TGF- β signaling in NSCLC cell lines

6.3.1 TGF- β treatment induces EMT in NSCLC cell lines

TGF- β is known to play a crucial role in tumorigenesis [209] and high TGF- β levels are correlated to poor prognosis in lung cancer [125, 127]. Therefore, the NSCLC cell lines H838, H1975 and H1650 were tested for their ability to signal via the TGF- β receptor. As markers for the activation of TGF- β signaling, the phosphorylation of SMAD2 and SMAD3 upon stimulation with TGF- β examined and it was shown that at the protein level TGF- β was able to start the TGF- β signaling cascade in all analyzed cell lines. However, in the cell line H1975 high pSMAD2 levels additionally to pSMAD3 could be detected in contrast to H1650 and H838 that showed only weak phosphorylation of

SMAD3 upon TGF- β stimulation. Moreover, the TGF- β target gene *SMAD7* [99, 163] that is known to serve as negative feedback regulator of the SMAD complexes and TGFBR1 [111] was rapidly expressed upon TGF- β stimulation in H1975 cells and remained sustained over the 48 hours observed.

Further insights into the impact of TGF- β signaling on mRNA expression were obtained by categorizing the TGF- β -induced target genes in H1975 cells using the gene ontology database. The identified biological processes were clustered into “up- or downregulated by TGF- β ”. Among the downregulated biological processes, mitosis, cell division, cell cycle and DNA repair as well as replication were detected. In contrast, TGF- β upregulated processes were connected to cell adhesion, cell junctions, cell migration and epithelial-to-mesenchymal transition (EMT).

The TGF- β -induced expression of some mRNAs was verified by qRT-PCR in H1975 and additionally in H838 cells. TGF- β mediated up-regulation of the mRNA expression was verified for *SNAI1* (Snail protein), *SMURF1*, *JUNB*, *KLF10*, *MAP3K4* and *CDKN1A* (p21 protein) in H1975 cells. In the cell line H838, *MAP3K9* and *XIAP* mRNAs were not significantly changed and all tested mRNAs showed weaker inducibility upon TGF- β treatment in comparison to H1975 cells. These findings suggest that in general the TGF- β pathway can be activated to a higher extent in H1975 compared to H838 cells correlating with higher pSMAD2 and pSMAD3 levels in H1975 cells compared to H838 cells.

Previous microarray analysis showed that the adenocarcinoma cell line A549 compared to the lung epithelial cell line HPL1D expressed upon TGF- β stimulation not only expressed regulators of the cytoskeleton and cell-cell junctions, but also genes involved in the MAPK pathways [210]. A mRNA microarray analysis of in lung fibroblasts showed that TGF- β induces several genes involved in matrix formation, cytoskeletal remodeling, cell adhesion and metabolism [211].

The key process that was found to be up-regulated upon stimulation with TGF- β in the NSCLC cell line H1975 was EMT. This was not surprising as it is known that TGF- β induces EMT in many cell types including mammary epithelial cells and cancer, including lung cancer [118-122]. Moreover, the results of the mRNA expression analysis are in line with observed loss of the epithelial character during EMT (Reference) that is

known to be connected to cell cycle arrest and disassemble of cell junctions and adhesion. For instance, it was reported that stimulation with TGF- β results in cell cycle attenuation via the expression of the EMT marker Snail in embryogenesis [212] which is known to induce p21 expression and thereby arrests the cell cycle in human mammary cells [213] and in pancreatic cancer cell lines [214]. Snail, that was also found to be upregulated in the qRT-PCR studies in H1975 cells, is further known to be a key regulator of the disassemble of cell junctions in human embryonic kidney cells, mouse keratinocytes [215] and mouse embryogenesis [216]. SMURF1, that was also monitored by qRT-PCR to be upregulate in H1975 cells upon TGF- β treatment, was shown to negatively regulate SMAD proteins, but also to be essential for the loss of tight junctions in mammary gland epithelial cells [217]. The loss of epithelial cell junctions was shown to lead to acquired motility and invasive properties [209, 218]. Moreover, MAP kinases were also shown to be significantly induced by TGF- β in H1975 cells. This is in agreement with reports that TGF- β was able to induce MAPK pathways in epithelial cells [219] and in the lung adenocarcinoma cell line A549 [210]. The importance of the MAP kinases for TGF- β -induced EMT was shown by the inhibition of MEK, which resulted in the loss of the ability to disassemble adherent junctions in murine mammary and epithelial cells [220] and in pancreatic cancer cell lines [221]. MAP3K4 was even shown to correlate with TGF- β -mediated phosphorylation of the p38 MAPK in mouse embryonic fibroblasts and keratinocytes [222].

In conclusion, TGF- β treatment resulted in the downregulation of genes involved in mitosis, cell division, cell cycle and DNA repair and replication and upregulation of genes that are connected to cell adhesion, cell junctions and migration. All these processes can be connected to EMT, which was also among the detected upregulated processes.

6.3.2 Role of BAMBI as a potential tumor suppressor

This study showed that TGF- β induced the development of mesenchymal properties by EMT in the NSCLC cell line H1975. As it was shown that the BAMBI protein, a negative regulator of the TGF- β signaling pathway, is absent in lung adenocarcinoma tissue

sample of patients, the expression level of BAMBI and its influence on NSCLC cells was tested.

BAMBI mRNA was shown by qRT-PCR to be downregulated in lung adenocarcinoma tumors of matched pairs of tumor and tumor-free lung of tissues from 9 patient. In agreement with these results, BAMBI was significantly lower expressed in the NSCLC cell lines H838, H1650 and H1975 compared to the control healthy lung epithelial cells type II. Interestingly, BAMBI was found to be epigenetically silenced in bladder cancer [115] and is absent in breast cancer [116]. Moreover, BAMBI was shown to be upregulated in the lung upon treatment with nontypeable haemophilus influenzae [223]. In contrast, BAMBI was reported to be over-expressed in ovarian cancer [114] and colorectal cancer tissues [224, 225].

The measurements further revealed that the TGF- β receptors 1 and 2, as well as *SMAD7* and the EMT markers *SNAI1* (Snail), *SNAI2* (Slug), *ZEB1*, *VIM* (Vimentin), *FN1* (Fibronectin) and *CDH2* (N-cadherin) were downregulated in the tumors tested. It was shown for NSCLC that loss of *TGFBR2* is associated with more aggressive tumor behavior [226] and is connected to high invasion rates and poor outcome in lung adenocarcinoma [129].

BAMBI was reconstituted in the NSCLC cell line H1975 with the intention to reestablish the healthy status in the cancer cell. A TGF- β -treated mRNA time course, including the measurement of *SMAD7*, *TGFBR1* and *TGFBR2*, *ZEB1*, *SNAI1*, *SNAI2*, *FN1*, *CDH1*, *CDH2*, *VIM* and *SKIL* revealed the effect of different BAMBI expression levels. The tested genes showed similar signaling dynamics but in a reduced manner with BAMBI reconstitution compared to the wild type H1975 cells. However, the EMT markers analyzed were shown to be upregulated upon TGF- β treatment, which confirms the mRNA expression analysis by microarray where EMT was shown to be the key process upregulated by TGF- β .

It was hypothesized that low BAMBI levels sensitize NSCLC cells to TGF- β . In conclusion, the treatment with TGF- β results in increased activation of the EMT markers that is connected to increased EMT and thus tumorigenesis. As *ZEB1*, Snail, Slug, Vimentin, E-cadherin and N-cadherin are EMT key regulators, it can be concluded that the BAMBI expression is negatively correlated to the potential for EMT and thus

metastasis in NSCLC. BAMBI is thereby suggested to act as a tumor suppressor in NSCLC.

6.4 Conclusions and outlook

In this study, the impact of growth factors, therapeutic inhibitors and cytostatic compounds on the response of non-small-cell lung carcinoma cell lines was analyzed (**Figure 30**). In detail, the transforming growth factor beta (TGF- β) was shown to induce EMT in NSCLC cells that is connected to the attenuation of the cell cycle, the disassemble of cell-cell contacts and increased metastatic properties. The standard of care for metastasizing NSCLC tumors is the chemotherapeutic agent cisplatin that was shown to induce apoptosis via the cleavage of caspase-3 predominantly in dividing NSCLC cells. The cisplatin-induced induction of the RAS–RAF–MEK–ERK cascade could be blocked with MEK inhibitors that are currently tested in clinical trials to determine their potential for the inhibition of constitutive activated MAP kinase signaling that might lead to uncontrolled cell proliferation or resistance to chemotherapeutic agents. Unfortunately, MEKi treatment was shown to decrease the sensitivity of NSCLC cells to cisplatin. As mechanism, an indirect rescue effect by arresting the cells in the G1 cell cycle phase was suggested. Furthermore, the presence of EpoR in the NSCLC cell line H838 resulted in response to Epo stimulation in a rescue effect of cisplatin-induced apoptosis that is believed to be mediated by phosphorylated STAT5. However, a verification of these findings in primary tumor cells or *in vivo* mouse models, as well as with patient samples might be required, as almost all experiments were performed with NSCLC cell lines.

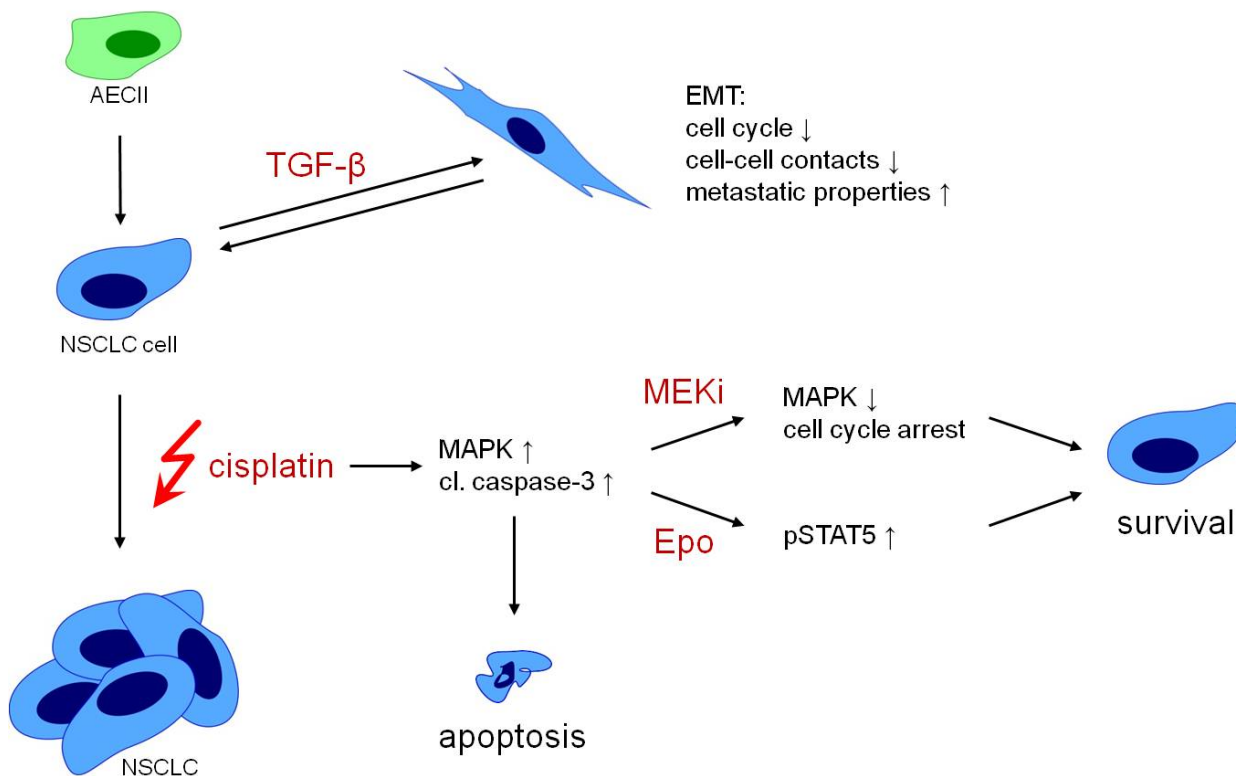


Figure 30: Impact of growth factors, therapeutic inhibitors and cytostatic compounds on the response of non-small-cell lung carcinoma cells. The origin of NSCLC cells is believed to be lung alveolar epithelial cells type II (AECII). NSCLC cells undergo EMT upon TGF- β treatment, which is connected to repression of the cell cycle, the disassembly of cell-cell contacts and increased metastatic properties. Treatment with the chemotherapeutic agent cisplatin induces apoptosis predominantly in dividing cells. The sensitivity for cisplatin can be decreased in NSCLC cells by the treatment with MEK inhibitors (MEKi) or upon Epo treatment.

In conclusion, the complexity of signaling pathways upon different or even combined treatments is quite high and may result in unintended effects. For instance, MEKi treatment in combination with cisplatin-based chemotherapy was shown to pose a potential risk for lung cancer patients. Furthermore, genetic alteration, such as the presence of EpoR in NSCLC cell lines results in response to Epo stimulation in a decreased sensitivity to cisplatin. To unravel complex signaling properties and to identify regulatory network, a systems biology approach might be required.

7. Materials and methods

7.1 Software and general equipment

Canvas 15 (for graphics)

CellDesigner 4.4 (for graphical representation of ODE model)

LightCycler 480 (for qRT-PCR, Roche Diagnostics)

Imaris (for image processing of confocal stacks)

ImageJ (for image analysis, <http://imagej.net/>)

SigmaPlot (for graphs, significance test)

I control (for fluorescence measurements at the infinite F200 pro Reader, TECAN)

Image Quant LAS 4000 (for the quantification of immunoblots, GE Healthcare)

7.2 Cell culture chemicals, solutions and media for NSCLC cell lines

Substance	Additional information	Cat. No (company)
DMEM	without phenol red, without glutamine	BE12-917F (Lonza)
DMEM	with phenol red	BE12-604F (Lonza)
HEPES BUFFER 1M		15630056 (Invitrogen)
Pen/Strep 100x	10,000 µg/ml Strep., 10,000 U/ml Pen.	Cat# 15070063 (Invitrogen)
L-Glutamin 200mM		Cat# 25030024 (Invitrogen)
BSA		A9418 (Sigma)
PBS (DPBS)	-Mg ²⁺ , -Ca ²⁺	PO4-36500I (PAN Biotech)
Trypsin/EDTA	0.05% Trypsin, 4Na EDTA	25300054 (Invitrogen)
Puromycin		P7255 (Sigma)
Doxycyclin		D9891 (Sigma)
Staurosporine		380-014-M001 (Enzo)
G418 (Neomycin)		A1720 (Sigma)
EDTA		E5134 (Sigma)
Glycerol		15523 (Sigma)
Old FCS	Australian origin	10099141 (Invitrogen)
New FCS	South American origin	10270098 (Invitrogen)

Table 3: List of chemicals, solutions and media

Three different media types were used depending on the application (**Table 4**). For selection purposes, puromycin and/or neomycin was additionally added. For instance, H838-GFP and H838-EpoR cells were cultured with 1 µg/ml puromycin and H838-

EpoR-CasperGR cells received 1 $\mu\text{g/ml}$ puromycin and 400 $\mu\text{g/ml}$ neomycin. The expression of either BAMBI-GFP or GFP from either H1975-TRET-BAMBI-GFP or H1975-TRET-GFP cells was induced by addition of 5 $\mu\text{l/ml}$ doxycyclin.

Medium type	DMEM Cat. No. (company)	Supplemented with:
Amplification medium	BE12-604F (Lonza)	10 % FCS, 100 $\mu\text{g/ml}$ Penicillin, 100 U/ml Streptomycin
Medium to seed cells for experiments	BE12-917F (Lonza)	10 % FCS, 100 $\mu\text{g/ml}$ Penicillin, 100 U/ml Streptomycin, 2mM L-Glutamin
Growth factor depletion medium	BE12-917F (Lonza)	100 $\mu\text{g/ml}$ Penicillin, 100 U/ml Streptomycin, 2mM L-Glutamin, 1 mg/ml BSA

Table 4: List of different medium types, its composition and application.

7.3 Cell culture plastic ware and volumes for the amplification and experiments with NSCLC cell lines

	diameter of plate			multi well plates			
	15 cm	10 cm	6 cm	6 well	12 well	24 well	96 well(flat)
company	TPP	TPP	TPP	TPP	TPP	TPP	TPP
plastic type	PS	PS	PS	PS	PS	PS	PS
coating	yes	yes	yes	yes	yes	yes	yes
product number	93150	93110	93060	92006	92012	92024	92096
growth surface [cm^2]	147.8	60.1	22.1	8.96	3.6	1.86	0.34
internal diam. [mm]	137	87	53	33.78	21.4	15.4	6.54
volume [ml]	25	10	3.5	1.5	0.6	0.3	0.06
ml/ cm^2 growth area	0.2	0.2	0.2	0.2	0.2	0.2	0.2

Table 5: List of the plastic ware including dimensions and appropriate volumes.

7.4 Inhibitors

For experiments that include inhibitor treatments, cells were pre-incubated with the according inhibitor for 60 minutes. All inhibitors were diluted in DMSO with a stock concentration of 10 mM. 5 μM LY294002 and Akt Inhibitor VIII were applied for the treatment of the NSCLC cell lines. The standard working concentrations for the inhibitors U0126 and selumetinib were 2.5 or 10 μM , for CI-10-40 1 and 5 μM and for PD0325901 and trametinib 0.001 and 0.1 μM .

Inhibitor	Additional information	Cat. No (company)
LY294002	PI3 Kinase Inhibitor	9901 (Cell Signaling)
Akt Inhibitor VIII	Akt-1/2/3 Inhibitor	124017 (Millipore)
U0126	MEK1/2 Inhibitor	9903 (Cell Signaling)
Selumetinib (AZD6244)	MEK1 Inhibitor	2234-5 (BioVision)
CI-1040 (PD184352)	MEK1/2 Inhibitor	1585 (BioVision)
PD0325901	MEK1/2 Inhibitor	SPD131 (System Biosciences)
Trametinib (GSK1120212)	MEK1/2 Inhibitor	sc-364639 (Santa Cruz)
U0126	MEK1/2 Inhibitor	9903 (Cell Signaling)

Table 6: List of inhibitors.

7.5 Treatments

The standard working concentrations for cisplatin were 5 or 10 mg/ml. 5 U/ml Epo- α was applied for mouse experiments and 10 or 500 U/ml Epo- β was used for the treatment of human NSCLC cell lines. 1 or 10 mg/ml TGF- β was applied on NSCLC cell lines. 40 ng/ml HGF was applied on NSCLC cell lines. 1 μ g/ml actinomycin D was used to block RNA synthesis.

Treatment	Additional information	Cat. No (company)
Cisplatin	chemotherapeutic drug	CisTeva (Ratiopharm)
Epo- α	applied on mCFU-Es	ERYPO FS 10 000 I.E./ml (Janssen-Cilag)
Epo- β (EPOsf)	applied on NSCLC cell lines	36016762 (Roche)
TGF- β	applied on NSCLC cell lines	240B (R&D systems)
HGF	applied on NSCLC cell lines	294HG (R&D systems)
Actinomycin D	applied on NSCLC cell lines	A1410 (Sigma)

Table 7: List of treatments.

7.6 Antibodies

For the detection of cleaved caspase-3 and pERK1/2, the primary antibodies were diluted 1:1000. For EpoR, ERK1/2, pEpoR and β -actin detection, a 1:10,000 dilution was used. Either horseradish peroxidase conjugated goat anti-rabbit (Dianova, 111-035-144), goat anti-mouse (Dianova, 115-035-146) or protein A HRP (Amersham Biosciences) were applied as secondary antibodies in 1:10,000 dilution.

Prot. detected	Antibody	Mol. weight	Company	Article #	Source
Cl. caspase-3		18	Cell signaling	9664	rabbit
EpoR	C20	65	Santa Cruz	sc-695	rabbit
ERK1/2	p42/44	44, 42	Cell signaling	9102	rabbit
pEpoR	pTyr	80	Upstate (millipore)	16-101	Mouse (protein A HRP)
pERK1/2	pp42/44	44, 42	Cell signaling	9101	rabbit
β -actin		42-45	Sigma	A5441-.2ML	mouse

Table 8: List of immunoblot antibodies.

7.7 Cell culture SOPs and cell-based techniques

7.7.1 NSCLC cell lines

The NSCLC cell lines H838, H1975 and H1650, were purchased from ATCC and cultivated in DMEM amplification medium (**Table 4**, **Table 5**). Cells were always incubated at 37°C with CO₂.

Cell line	ATCC no	Smoker	Age	Stage	Gender	Tissue
H1975	CRL-5908	no			female	lung
H838	CRL-5844	yes	59	3b	male	lung; metastatic site (lymph node)
H1650	CRL-5883	yes	27	3b	male	lung; derived from metastatic site

Table 9: NSCLC cell lines selected for the main experiments.

The cell lines H838-GFP, H838-EpoR, H838-EpoR-CasperGR, H1975-TRET-GFP and H1975-TRET-BAMBI-GFP were kindly provided by Dr. Sofia Depner.

7.7.2 Detaching and amplification of NSCLC cells

Medium was aspirated and EDTA/PBS was added according to medium volumes (**Table 4**, **Table 5**) and incubated for 5 minutes at 37°C with CO₂. EDTA/PBS was replaced by 0.025% Trypsin/EDTA/PBS (0.05% Trypsin/EDTA stock diluted with PBS 1:2) and incubated for 5 minutes at room temperature. Cells were washed down in Trypsin/EDTA/PBS before medium was added to stop the trypsinization. After centrifugation (5 minutes, 1000 rpm, room temperature), the supernatant was discarded and the cells were resuspended in pre-warmed medium and counted using a Neubauer

counting chamber. For amplification, cells were splitted 1:4 (for 3 days) or 1:5 (for 4 days) and plated in amplification medium (**Table 4, Table 5**).

7.7.3 Freezing and thawing of NSCLC cells

Cells were detached (see **Detaching and amplification of NSCLC cells**) and frozen at the concentration of 2.5×10^6 cells/ml. A Neubauer counting chamber was used to determine the cell number. The freezing medium contained 80% amplification medium (**Table 5**) with 10% FCS and 10% glycerol. The cells were aliquoted into a cryo tube and incubated for one day at -80°C in freezing containers containing isopropanol. Cells were stored in liquid nitrogen.

For the amplification, freshly thawed cells were mixed with 9 ml pre-warmed medium and seeded on appropriate 10cm-plastic plates (**Table 4, Table 5**). Medium was exchanged on the next day to remove residual glycerol.

7.7.4 Seeding NSCLC cells for experiments

NSCLC cells were seeded in medium to seed cells for experiments (**Table 4, Table 5**) three days before the experiment to have them about 80% confluent at the day of the experiment (**Table 10, Table 11**). Before each experiment and prior to any treatment or stimulation (**Table 7, Table 7**), growth factor depletion over night was applied without phenol red. Cells were always incubated at 37°C with CO_2 . A Neubauer counting chamber was used to determine the cell number.

	seed	cells/cm2	after 3d	cells/cm2
15 cm plate	2.00E+06	1.35E+04	7.39E+06	5.00E+04
10 cm plate	8.11E+05	1.35E+04	3.01E+06	5.00E+04
6 cm plate	2.98E+05	1.35E+04	1.11E+06	5.00E+04
6 well-plate	1.20E+05	1.35E+04	4.46E+05	5.00E+04
12 well-plate	4.86E+04	1.35E+04	1.80E+05	5.00E+04
24 well-plate	2.51E+04	1.35E+04	9.30E+04	5.00E+04
96 well-plate	4.52E+03	1.35E+04	1.68E+04	5.00E+04

Table 10: SOPs for the seeding of the H838 cells.

	seed	cells/cm ²	after 3d	cells/cm ²
15 cm plate	2.21E+06	1.50E+04	5.17E+06	3.50E+04
10 cm plate	9.00E+05	1.50E+04	2.10E+06	3.50E+04
6 cm plate	3.31E+05	1.50E+04	7.74E+05	3.50E+04
6 well-plate	1.33E+05	1.50E+04	3.12E+05	3.50E+04
12 well-plate	5.39E+04	1.50E+04	1.26E+05	3.50E+04
24 well-plate	2.79E+04	1.50E+04	6.51E+04	3.50E+04
96 well-plate	5.02E+03	1.50E+04	1.17E+04	3.50E+04

Table 11: SOPs for the seeding of the H1975 cells.

7.7.5 AECII cells

Freshly isolated human alveolar epithelial type II cells (AECII) were kindly provided by Prof. Heimo Mairbäurl (University of Heidelberg, Sports medicine). The cells were cultivated in low glucose medium (provided by the group of Prof. Heimo Mairbäurl, DMEM Low Glucose from Sigma-Aldrich Cat.No. D5546, supplemented with 10 % FCS) for two days. Afterwards, low glucose medium was replaced by DMEM medium for experiments (**Table 5** and **Table 5**).

7.7.6 Tumor samples adenocarcinoma

The cDNA of matched pairs of tumor and tumor-free lung of 9 patients were kindly provided by the cooperation partner Dr. Sebastian Marwitz in the group of Prof. Torsten Goldmann (Research Center Borstel, Division of Clinical and Experimental Pathology).

7.7.7 Preparation of murine fetal liver cells (CFU-Es)

At E13.5 Balb/c mouse embryos were dissected from the uterus of killed females. Fetal livers were resuspended in PBS/0.3% BSA and passed through a 40- μ m cell strainer (BD Biosciences). Fetal liver cells were treated with 9 ml Red Blood Cell Lysis Buffer (Sigma-Aldrich) to remove erythrocytes. For sorting TER119⁻ erythroid progenitors, FLCs were incubated with rat antibodies against the following surface markers: GR1, CD41, CD11b, CD14, CD45R/B220, CD4, CD8 and Ter119 (BD Pharmingen), and 42.2.2 for 30 min at 4°C. After washing, cells were incubated for 30 min at 4°C with anti-

rat antibody-coupled magnetic beads and negatively sorted with MACS columns according to the manufacturer's instructions (Miltenyi Biotech). Sorted CFU-E cells were cultivated for 12–14 h in Panserin401 (PAN-biotech) supplemented with 50 μ M β -mercaptoethanol and 0.5 U/ml Epo- α . For experiments, the CFU-Es were seeded at a cell density of 4×10^6 cells/ml in Panserin401. Before the experiments, the CFU-Es were growth-factor-starved for 60 minutes.

7.7.8 CellTiter-Blue cell viability assay

The cells for the experiment were seeded according to the SOPs (**7.7.4 Seeding NSCLC cells for experiments, Table 4, Table 5**). For the determination of the EC_{50} in the cell line H838, a dilution series of 100, 50, 25, 12.5, 6.25, 3.125, 1.562, 0.7813 mg/l cisplatin (**Table 7**) was applied. Apoptosis was induced in further experiments by applying 5 or 10 mg/l cisplatin. In combination with 10 U/ml Epo, 5 mg/l cisplatin was used. The determination of the sensitivity of MEK inhibitors was performed with 5 and 10 mg/l cisplatin and 2.5 or 10 μ M U0126 and selumetinib, 1 and 5 μ M CI-10-40 and 0.001 and 0.1 μ M PD0325901 and trametinib (**Table 6**).

To measure the viability of cells, CellTiter-Blue Viability Assay (Promega, #G8081) was applied according to the manufacturer's instructions. Incubation with the dye for 60 min was followed by measurement of the fluorescence with the infinite F200 pro Reader (TECAN). A blank well without cells was measured to determine the background. After subtraction of the background, cell dilution series enabled due to a direct correlation of the signal intensities with the cell number, the verification of absolute cell numbers.

7.8 Molecular biology: RNA

7.8.1 RNA extraction

The cells for the experiment were seeded according to the SOPs (**7.7.4 Seeding NSCLC cells for experiments, Table 4, Table 5**). Treatments were applied as described (**Table 6** and **Table 7**). For the determination of the effect of MEK inhibition on cisplatin-induced apoptosis on RNA level, 2.5 μ M U0126 was applied in combination

with 10 mg/l cisplatin. The standard working concentration for all experiments including Epo was 10 U/ml Epo- β for human cells and 5 U/ml Epo- α for mouse cells. For the TGF- β -treated time course analyzed by qRT-PCR, the standard working concentration was 1 ng/ml TGF- β and the time course analyzed by microarray, was stimulated with 10 ng/ml TGF- β (**Table 6, Table 7**).

To extract total RNA, including small RNAs like miRNAs, miRNeasy Mini Kit (QIAGEN) was employed according to the manufacturer's instructions. If just the mRNA was needed, RNA was extracted using the RNeasy Mini Plus Kit (QIAGEN) according to the manufacturer's instructions.

7.8.2 Quantitative Real Time PCR (qRT-PCR)

The concentration and sample purity of total RNA samples were determined by measuring the absorbance at 260 and 280nm ($A_{260/280}$) by NanoDrop (Thermo scientific). For quantitative RT-PCR, complementary DNA was generated with the High Capacity cDNA Reverse Transcription Kit (Applied Biosystems) and analyzed using the LightCycler 480 with the Universal ProbeLibrary (UPL) platform (Roche Applied Science).

In general, qRT-PCR amplifications were performed in 384-well format in an 11 μ l reaction volume containing 5 μ l of diluted template cDNA, 0.2 μ M of forward and reverse primer, 0.2 μ l of the appropriate UPL probe and 6 μ l LightCycler 480 Probes (**Table 12, Table 13**). Master solution (Roche Diagnostics, Mannheim) according to the manufacturer's manual. Primer pairs were generated using the automated UPL Assay Design Center (www.roche-applied-science.com).

Crossing point values were calculated using the second derivative maximum method of the LightCycler 480 Basic Software (Roche Diagnostics, Mannheim). PCR efficiency correction was performed for each PCR setup individually based on a dilution series of template cDNA. For the relative correlation between different cell types, the efficiency was assumed to be 100%.

The values were normalized for the NSCLC cell lines individually if not compared amongst each other by using the geometric mean of *ESD* and *GUSB* mRNA levels.

If not other stated, primers target all transcript variants of the according gene.

Gene	Protein	Primer forward/reverse	UPL Probe
<i>BAMBI</i>	BAMBI	cgccactccagctacatctt/cacagtagcatcgaattca	71
<i>BCL2</i>	Bcl-2	tacctgaaccggcactctg/gccgtacagttccacaaagg	75
<i>CCNA1</i>	CyclinA1	tcagtaccttaggaagctgaaa/ccagtcaccagaaatcgtg	71
<i>CCNB1</i>	CyclinB1	acatggtgcacttctctct/aggtaagtgtgagagttggtgtcc	18
<i>CCND1</i>	Cyclin D1	gctgtgcatctacaccgaca/ttgagctgttcaccaggag	17
<i>CCNE1</i>	CyclinE1	ggccaaaatcgacaggac/gggtctgcacagactgcat	36
<i>CDH1</i>	E-Cadherin	tggaggaattctgtcttgc/cgctctcctccgaagaaac	84
<i>CDH2</i>	N-Cadherin	ggtggaggagaagaagaccag/ggcatcaggctccacagt	66
<i>CDKN1A</i>	p21	tcactgtctgtaccctgtgc/ggcgtttggagtggtagaaa	32
<i>CDKN1B</i>	p27	tcactgtctgtaccctgtgc/ggcgtttggagtggtagaaa	32
<i>FOS</i>	cFos	actaccactaccgacagac/ccaggtcgtgcagaagt	67
<i>CISH</i>	Cis	agccaagacctctctctacct/tggcatctctgcaggtgt	20
<i>DUSP5</i>	DUSP5	caaatggatccctgtggaa/ccctttccctgacacagtc	5
<i>DUSP7</i>	DUSP7	cccatctctgaccactggag/caggacaccacactcttg	14
<i>DUSP8</i>	DUSP8	gaccattgcgagctcat/tcatagaccaccagctctgt	39
<i>EGR1</i>	Egr1	agcctacgagcactgac/gtttggctgggtaactg	22
<i>EGR3</i>	Egr3	tggaggacttgggtgttct/agcttccatggctcatct	74
<i>ELK1</i>	Elk1	tgcttctacgcatactga/ggtgtccagaagtgaatgc	16
<i>EpoR</i>	Epo receptor	caatctgtaccgaggaga/cagaccgatgcccattacattc	69
<i>ESD</i>	ESD	ttagatggacagtactcctgataa/ggttgaatgaagtagtagtatgat	27
<i>FN1</i>	Fibronectin	ctgcccgaataacattgtaaa/ccacagtcgggtcaggag	32
<i>GUSB</i>	GUSB	cgccctgcctatctgtattc/tccccacaggagtgtag	57
<i>JUNB</i>	JunB	atacacagctacgggatacgg/gctcggttcaggagttgt	49
<i>KLF10</i>	KLF10	tctgaaggcccacacagac/acctcttccacaaccttcc	2
<i>LTBP1</i>	LTBP1	tgctacgagggtacaggtt/gcagagggttggacctga	6
<i>LTBP2</i>	LTBP2	agggtccttcaactgtctatg/ccatagtcctcacactctgcaa	11
<i>MAP3K1</i>	MAP3K1	caccaccactgcatgcaa/gatctcaaaaggggacatattaaagg	29
<i>MAP3K2</i>	MAP3K2	tctggctcaggaagtgtcc/agctctgagccctaggcatt	58
<i>MAP3K4</i>	MAP3K4	ggctttcagcccagtttag/taaccaggaatttgacact	79
<i>MAP3K9</i>	MAP3K9	cagggttcaccagccttag/cacctctcaatgtcgatgg	71
<i>MAP4K4</i>	MAP4K4	tggcttctgtggcattacagc/gctctcattggatgcatgct	29
<i>MDM2</i>	Mdm2	gactccaagcgcgaaaac/cagacatgttggtattgcacatt	68
<i>SKIL</i>	SnoN	gaggctgaatatgcaggacag/cttgcctatcggcctcag	13
<i>SMAD7</i>	SMAD7	accgatggatttctcaaa/aggggccagataaactggtc	69
<i>SMURF1</i>	SMURF1	ttccaaggcccatact/cagcttctctgtagagcttctca	31
<i>SMURF2</i>	SMURF2	agaaattacatgagcagaacacatt/tgttgcgtgtcctctgttc	25
<i>Snai1</i>	Snail	gctgcaggacttaaccaga/atctccggagggtgggatg	11
<i>Snai2</i>	Slug	tggttgctcaaggacacat/gttgcagtgagggaagaa	7
<i>SOCS3</i>	SOCS3	agacttcgattcgggacca/aactgctgtgggtgacca	36
<i>SOX4</i>	SOX4	agccggaggaggagatgt/tctcgggtcatttcttagc	20
<i>SPP1</i>	SPP1	gagggtctgggtgtcagc/caattctatggtagtgtttcc	18
<i>TGFBR1</i>	TGF- β receptor 1	gcagactaggactggcagtaag/agaactcaggggcatgt	5
<i>TGFBR2</i>	TGF- β receptor 2	caccgcagttcagaagtc/tggatgggcagtcctattaca	43
<i>TP53</i>	p53	aggcctggactcaaggat/cccttttggactcagggtg	12
<i>VIM</i>	Vimentin	tacaggaagctgtggaagg/accagagggagtgaatccag	13
<i>XIAP</i>	XIAP	tttgggacatggatatactcagtt/agcactttactttacacctcacc	68
<i>ZEB1</i>	ZEB1	ttttctgaggcactgaa/aaaatgcatctggtgttccat	34

Table 12: List of primers and probes used for qRT-PCR.

PCR step		Temperature	Time
initial denaturation		95°C	5 min
50 cycles	melting	95°C	10 s
	primer annealing	60°C	30 s
	DNA synthesis and data acquisition	72°C	1 s
cooling		40°C	2 min

Table 13: PCR programm for qRT-PCR

7.8.3 Gene expression arrays

The mRNA microarray (GeneChip 2.0 ST, Affimetrix) was performed by the group of Prof. Gretz (Heidelberg University, Medical Faculty Mannheim) for the NSCLC cell lines H838, H1650 and H1975 (**Table 9**). The normalization and data analysis was done by Dr. Melanie Börries and Dr. Hauke Busch (Freiburg University). The miRNA microarray (Agilent) was performed by the Genomics & Proteomics Core Facility (DKFZ Heidelberg) and normalized and analyzed by Dr. Nikola Müller in the group of Prof. Fabian Theis (Helmholtz Zentrum München).

7.8.4 RNA sequencing (RNAseq)

The RNA sequencing (RNAseq) was performed by the Genomics & Proteomics Core Facility (DKFZ Heidelberg) for the NSCLC cell lines H838, H1650 and H1975 (**Table 9**). The analysis was done by Stephen Krämer and Dr. Naveed Ishaque in the group of Benedikt Brors (DKFZ Heidelberg).

7.9 Molecular biology: DNA

7.9.1 DNA extraction

The NSCLC cell lines H838, H1650 and H1975 for the experiment were seeded according to the SOPs (**7.7.4 Seeding NSCLC cells for experiments**). The DNA

extraction was performed with the DNeasy Tissue Kit (QIAGEN) according to the manufacturer's instructions.

7.9.2 WGS and MChp

The whole genome sequencing (WGS) and methyl-CpG immunoprecipitation (MChp)-based methylome sequencing was performed by the Genomics & Proteomics Core Facility (DKFZ Heidelberg) for the NSCLC cell lines H838, H1650 and H1975 (**Table 9**). The analysis was done by Stephen Krämer and Dr. Naveed Ishaque in the group of Benedikt Brors (DKFZ Heidelberg).

7.10 Molecular biology: proteins

7.10.1 Preparation of total cell lysates (TCL)

The cells for the experiment were seeded according to the SOPs (**7.7.4 Seeding NSCLC cells for experiments, Table 4, Table 5**). The effect of MEK inhibition (**Table 6**) on cisplatin-induced ERK phosphorylation and cleavage of caspase-3, was measured with 2.5 μ M U0126 and 10 mg/l cisplatin (**Table 6, Table 7**). For the determination of the effect of MEK inhibition on HGF-induced phosphorylation levels of ERK1/2, 40 ng/ml HGF in combination with a dilution series of 0, 0.001, 0.01, 0.1, 1, 2.5, 5, 10, 20 μ M U0126, selumetinib (AZD6244), CI-1040 (PD184352), PD0325901 or trametinib (GSK1120212) were applied (**Table 6**). The detection of Epo receptor phosphorylation was performed with 10 U/ml Epo- β (**Table 7**).

Detergent lysates of cells were prepared with 2x 1% NP40 buffer (1x buffer: 1% NP40, 150 mM NaCl, 20 mM Tris pH 7.4, 10 mM NaF, 1 mM EDTA pH 8.0, 1 mM ZnCl₂ pH 4.0, 1 mM MgCl₂, 1 mM Na₃VO₄, 10% Glycerol) supplemented with 2 μ g/ml aprotinin and 200 μ g/ml AEBSF. After 20 min of rotation at 4°C, the lysates were centrifuged for 10 min at 20,000 g and 4°C. The supernatant was either used directly, processed further by immunoprecipitation or total cellular lysates were stored at -80°C.

7.10.2 Protein quantification

To determine protein concentrations of cellular lysates the BCA Protein Assay Kit (Pierce) was used according to the manufacturer's instructions.

7.10.3 Immunoprecipitation of EpoR

Immunoprecipitation was performed by adding 5 μ l of the EpoR antibody MAB307 (R&D) and 25 μ l of Protein A sepharose (GE Healthcare) to the TCL and rotate over night at 4°C. The immunoprecipitates were washed twice with 1x 1% NP40 lysis buffer and once with TNE buffer (10 mM Tris pH 7.4, 100 mM NaCl, 1 mM EDTA, pH 8.0, 100 μ M Na₃VO₄). Immunoprecipitates were immediately subjected to protein gel electrophoresis or stored at -80°C.

7.10.4 SDS-PAGE

Proteins were separated according to their electrophoretic mobility in a denaturing SDS-PAGE. Protein samples were boiled for 3 min in SDS sample buffer. Protein samples were separated by 10% SDS-PAGE with low bis-acrylamide (GE Healthcare) and separated in a electric field in running buffer (192 mM glycine, 25 mM Tris, 0.1% SDS) (**Table 14**). The samples were centrifuged for 2 min at 15,700 g before loading. For total cell lysates, an amount of 50-100 μ g protein resuspended in SDS sample buffer were separated by SDS-PAGE.

	Stacking gel	Separating gel 10%
40% acrylamide	1 ml	5 ml
2% w/v methylenebisacrylamide	0.5 ml	1.3 ml
1M Tris-HCl, pH 6.8	1.25 ml	-
1.5M Tris-HCl, pH 8.8	-	5 ml
10% SDS	0.1 ml	0.2 ml
ddH ₂ O	7.15 ml	8.5 ml
APS (10 %)	100 μ l	200 μ l
Temed	10 μ l	20 μ l

Table 14: 10% polyacrylamide gels for SDS-Page.

7.10.5 Immunoblotting

Immunoblotting was performed in semi-dry chambers (GE Healthcare) on nitrocellulose membranes with a pore size of 0.2 μm (Schleicher&Schuell) except of cleaved caspase-3, which was detected on a nitrocellulose membrane with a pore size of 0.1 μm (Whatman).

The blotting was performed in transfer buffer (192 mM glycine, 25 mM Tris, 0.075% SDS, 0.5 mM Na_3VO_4 , 15% methanol) for 1 hour at approximately 1.3 mA/cm². Proteins were reversibly stained with Ponceau Red. After blocking unspecific antibody binding with 5% BSA diluted in TBS-T (10 mM Tris pH 7.4, 150 mM NaCl, 0.2% Tween-20), membranes were incubated with the appropriate first and secondary antibodies (**Table 8**) and proteins were visualized with the ECL or ECL Prime/select Western Blotting Detection Reagents (GE Healthcare) and subsequently detected on Image Quant LAS 4000 (GE Healthcare). The quantification was performed using the specific software (GE Healthcare). To evaluate total protein levels, membranes were incubated in stripping buffer (62.5 mM Tris pH 6.8, 2% SDS, 100 mM β -mercaptoethanol) for 20-25 min at 65°C, blocked with 5 % BSA diluted in TBS-T, and reprobated with the appropriate first and secondary antibody.

7.11 Microscopy

7.11.1 Caspase-3 assay

For the caspase-3 activity assay, H838 cells over-expressing EpoR and additionally expressing the FRET-based CasperGR sensor (H838-EpoR-CasperGR, kindly provided by Dr. Sofia Depner). The sensor consists of green (GFP) and red fluorescent proteins (RFP) connected by the linker containing the caspase-3 cleavage sequence DEVD which leads to FRET between these fluorescent proteins. Caspase-3 activation leads to the cleavage of the DEVD sequence resulting in FRET elimination which is detectable in the changing ratio of green to red. The cells were seeded in 8-well plates (Thermo scientific, #155411) at a density of 20,000 cells/well. 24 hours after the seeding, the cells were growth factor-depleted for 16 hours and afterwards treated with 5 mg/l cisplatin and/or treated with 10 or 500 U/ml Epo- β or left untreated (**Table 7**). The cells

were imaged on an environment-controlled microscope (Zeiss LSM 710). Images were acquired every 20 minutes for 64 hours. Analysis was performed using ImageJ software.

7.11.2 Volume measurements with GFP and Hoechst staining

For the cell volume measurements, H838 cells stably expressing GFP (H838-GFP, kindly provided by Dr. Sofia Depner) were seeded in 8-well plates (Thermo scientific, #155411) at a density of 10,000 cells/well. 24 hours after the seeding, the cells were growth factor-depleted for 16 hours. The cells were stained with 1 µg/ml Hoechst (H33342, Sigma) and imaged on an environment-controlled microscope (Zeiss LSM 710). Images were acquired with an EC Plan-Neofluor 40x/1.30 oil objective lens applying the z-stack method. The total cell volume (GFP) and the volume of the nucleus (Hoechst) were calculated with the Imaris software (Bitplane).

7.11.3 Cell cycle analysis with the FUCCI sensor

For the measurement of the cell cycle, H838 cells expressing the FUCCI sensor (kindly provided by Dr. Sofia Depner) were seeded in 8-well plates (Thermo scientific, #155411) according to the SOPs. 24 hours after the seeding, the cells were growth factor-depleted for 16 hours before the time course with different treatments started. To test the effect of MEKi on cisplatin induced apoptosis, the cells were pre-incubated with 2.5 µM U0126 for 60 minutes followed by the treatment with 5 mg/l cisplatin. The cells were imaged on an environment-controlled Nikon Ti eclipse microscope in cooperation with Dr. Erika Kuchen in the group of Prof. Thomas Höfer (DKFZ Heidelberg). The analysis was performed by Dr. Carsten Maus in the group of Prof. Thomas Höfer (DKFZ Heidelberg)

7.12 Dynamic pathway modeling

The reactions listed below are adapted for H838 and H838-EpoR from Bachmann *et al.* [62].

$$\begin{aligned} d[\text{EpoRJAK2}] / dt = & - \frac{[\text{Epo}] \cdot [\text{EpoRJAK2}] \cdot \text{JAK2ActEpo}}{[\text{SOCS3}] \cdot \text{SOCS3Inh} + 1} + [\text{EpoRpJAK2}] \cdot \text{JAK2EpoRDeaPTP} \cdot [\text{PTPAct}] \\ & + \text{JAK2EpoRDeaPTP} \cdot [\text{PTPAct}] \cdot [\text{pEpoRpJAK2}] \end{aligned} \quad (1)$$

$$\begin{aligned} d[\text{EpoRpJAK2}] / dt = & + \frac{[\text{Epo}] \cdot [\text{EpoRJAK2}] \cdot \text{JAK2ActEpo}}{[\text{SOCS3}] \cdot \text{SOCS3Inh} + 1} - [\text{EpoRpJAK2}] \cdot \text{JAK2EpoRDeaPTP} \cdot [\text{PTPAct}] \\ & - \frac{\text{EpoRActJAK2} \cdot [\text{EpoRpJAK2}]}{[\text{SOCS3}] \cdot \text{SOCS3Inh} + 1} \end{aligned} \quad (2)$$

$$d[\text{pEpoRpJAK2}] / dt = + \frac{\text{EpoRActJAK2} \cdot [\text{EpoRpJAK2}]}{[\text{SOCS3}] \cdot \text{SOCS3Inh} + 1} - \text{JAK2EpoRDeaPTP} \cdot [\text{PTPAct}] \cdot [\text{pEpoRpJAK2}] \quad (3)$$

$$d[\text{PTP}] / dt = -[\text{PTP}] \cdot \text{PTPActEpoR} \cdot ([\text{EpoRpJAK2}] + [\text{pEpoRpJAK2}]) + [\text{PTPAct}] \cdot \text{PTPDea} \quad (4)$$

$$d[\text{PTPAct}] / dt = +[\text{PTP}] \cdot \text{PTPActEpoR} \cdot ([\text{EpoRpJAK2}] + [\text{pEpoRpJAK2}]) - [\text{PTPAct}] \cdot \text{PTPDea} \quad (5)$$

$$\begin{aligned} d[\text{STAT5}] / dt = & - \frac{[\text{STAT5}] \cdot \text{STAT5ActJAK2} \cdot ([\text{EpoRpJAK2}] + [\text{pEpoRpJAK2}])}{[\text{SOCS3}] \cdot \text{SOCS3Inh} + 1} - \frac{[\text{STAT5}] \cdot \text{STAT5ActEpoR} \cdot [\text{pEpoRpJAK2}]^2}{([\text{CIS}] \cdot \text{CISInh} + 1) \cdot ([\text{SOCS3}] \cdot \text{SOCS3Inh} + 1)} \\ & + \text{STAT5Dea} \cdot [\text{pSTAT5}] + \text{STAT5Exp} \cdot [\text{nSTAT5}] \cdot \frac{\text{nuc}}{\text{cyt}} \end{aligned} \quad (6)$$

$$\begin{aligned} d[\text{pSTAT5}] / dt = & + \frac{[\text{STAT5}] \cdot \text{STAT5ActJAK2} \cdot ([\text{EpoRpJAK2}] + [\text{pEpoRpJAK2}])}{[\text{SOCS3}] \cdot \text{SOCS3Inh} + 1} + \frac{[\text{STAT5}] \cdot \text{STAT5ActEpoR} \cdot [\text{pEpoRpJAK2}]^2}{([\text{CIS}] \cdot \text{CISInh} + 1) \cdot ([\text{SOCS3}] \cdot \text{SOCS3Inh} + 1)} \\ & - \text{STAT5Dea} \cdot [\text{pSTAT5}] - \text{STAT5Imp} \cdot [\text{pSTAT5}] \end{aligned} \quad (7)$$

$$d[\text{nSTAT5}] / dt = +\text{nSTAT5Dea} \cdot [\text{npSTAT5}] - \text{STAT5Exp} \cdot [\text{nSTAT5}] \quad (8)$$

$$d[\text{npSTAT5}] / dt = +\text{STAT5Imp} \cdot [\text{pSTAT5}] \cdot \frac{\text{cyt}}{\text{nuc}} - \text{nSTAT5Dea} \cdot [\text{npSTAT5}] \quad (9)$$

$$d[\text{CISnRNA1}] / dt = +\text{basal_CISRNA} + \text{CISRNAEqc} \cdot \text{CISRNA} - \text{CISRNA} \cdot \text{CISRNA} \cdot \text{Turn} \cdot [\text{npSTAT5}] - \text{CISRNA} \cdot \text{CISRNA} \cdot \text{Delay} \cdot [\text{CISnRNA1}] \quad (10)$$

$$d[\text{CISnRNA2}] / dt = +\text{CISRNA} \cdot \text{CISRNA} \cdot \text{Delay} \cdot [\text{CISnRNA1}] - \text{CISRNA} \cdot \text{CISRNA} \cdot \text{Delay} \cdot [\text{CISnRNA2}] \quad (11)$$

$$d[\text{CISnRNA3}] / dt = +\text{CISRNA} \cdot \text{CISRNA} \cdot \text{Delay} \cdot [\text{CISnRNA2}] - \text{CISRNA} \cdot \text{CISRNA} \cdot \text{Delay} \cdot [\text{CISnRNA3}] \quad (12)$$

$$d[\text{CISnRNA4}] / dt = +\text{CISRNA} \cdot \text{CISRNA} \cdot \text{Delay} \cdot [\text{CISnRNA3}] - \text{CISRNA} \cdot \text{CISRNA} \cdot \text{Delay} \cdot [\text{CISnRNA4}] \quad (13)$$

$$d[\text{CISnRNA5}] / dt = +\text{CISRNA} \cdot \text{CISRNA} \cdot \text{Delay} \cdot [\text{CISnRNA4}] - \text{CISRNA} \cdot \text{CISRNA} \cdot \text{Delay} \cdot [\text{CISnRNA5}] \quad (14)$$

$$d[\text{CISRNA}] / dt = +\text{CISRNA} \cdot \text{CISRNA} \cdot \text{Delay} \cdot [\text{CISnRNA5}] \cdot \frac{\text{nuc}}{\text{cyt}} - [\text{CISRNA}] \cdot \text{CISRNA} \cdot \text{Turn} \quad (15)$$

$$d[\text{CIS}] / dt = +\text{CISEqc} \cdot [\text{CISRNA}] \cdot \text{CIS} - \text{CIS} \cdot \text{CIS} \cdot \text{Turn} \quad (16)$$

$$d[\text{SOCS3nRNA1}] / dt = +\text{basal_SOCS3RNA} + \text{SOCS3RNAEqc} \cdot \text{SOCS3RNA} - \text{SOCS3RNA} \cdot \text{SOCS3RNA} \cdot \text{Turn} \cdot [\text{npSTAT5}]^2 - \text{SOCS3RNA} \cdot \text{SOCS3RNA} \cdot \text{Delay} \cdot [\text{SOCS3nRNA1}] \quad (17)$$

$$d[\text{SOCS3nRNA2}] / dt = +\text{SOCS3RNA} \cdot \text{SOCS3RNA} \cdot \text{Delay} \cdot [\text{SOCS3nRNA1}] - \text{SOCS3RNA} \cdot \text{SOCS3RNA} \cdot \text{Delay} \cdot [\text{SOCS3nRNA2}] \quad (18)$$

$$d[\text{SOCS3nRNA3}] / dt = +\text{SOCS3RNA} \cdot \text{SOCS3RNA} \cdot \text{Delay} \cdot [\text{SOCS3nRNA2}] - \text{SOCS3RNA} \cdot \text{SOCS3RNA} \cdot \text{Delay} \cdot [\text{SOCS3nRNA3}] \quad (19)$$

$$d[\text{SOCS3nRNA4}] / dt = +\text{SOCS3RNA} \cdot \text{SOCS3RNA} \cdot \text{Delay} \cdot [\text{SOCS3nRNA3}] - \text{SOCS3RNA} \cdot \text{SOCS3RNA} \cdot \text{Delay} \cdot [\text{SOCS3nRNA4}] \quad (20)$$

$$d[\text{SOCS3nRNA5}] / dt = +\text{SOCS3RNA} \cdot \text{SOCS3RNA} \cdot \text{Delay} \cdot [\text{SOCS3nRNA4}] - \text{SOCS3RNA} \cdot \text{SOCS3RNA} \cdot \text{Delay} \cdot [\text{SOCS3nRNA5}] \quad (21)$$

$$d[\text{SOCS3RNA}] / dt = +\text{SOCS3RNA} \cdot \text{SOCS3RNA} \cdot \text{Delay} \cdot [\text{SOCS3nRNA5}] \cdot \frac{\text{nuc}}{\text{cyt}} - [\text{SOCS3RNA}] \cdot \text{SOCS3RNA} \cdot \text{Turn} \quad (22)$$

$$d[\text{SOCS3}] / dt = +\text{SOCS3Eqc} \cdot [\text{SOCS3RNA}] \cdot \text{SOCS3} - \text{SOCS3} \cdot \text{SOCS3} \cdot \text{Turn} \quad (23)$$

8. Abbreviations

μ	micro
ActD	actinomycin D
AECII	alveolar epithelial cells type II
ALK	anaplastic lymphoma kinase
Bad	Bcl-2-antagonist of cell death
BAMBI	BMP and activin membrane-bound inhibitor homolog
Bax	BCL2-associated X protein
Bcl-2	B-cell lymphoma 2
Bid	BH3 interacting domain death agonist
Bik	BCL2-interacting killer
BSA	bovine serum albumin
CCN	cyclin
CDH1	E-cadherin
CDH2	N-cadherin
CDK	cyclin-dependent kinase
CDKN	cyclin-dependent kinase inhibitor
CFU-E	colony forming unit-erythroid
Cis	cisplatin
CISH	cytokine-inducible SH2-containing protein
cm	centi meter
CTR1	copper transporter 1
Ctrl	control
d	day(s)
DMEM	Dulbecco's modified Eagle's medium
DMSO	dimethyl sulfoxide
DNA	deoxyribonucleic acid
DOX	doxycyclin
DUSP	dual specificity protein phosphatase
EC ₅₀	half effective concentration

ECL	enhanced chemiluminescence
EDTA	ethylenediaminetetraacetic acid
EGFR	epidermal growth factor receptor
EGR1	early growth response 1
ELK1	ETS domain-containing protein
EMT	epithelial-to-mesenchymal transition
Epo	erythropoietin
EpoR	erythropoietin receptor
ERK	extracellular signal-regulated kinase
ESA	erythropoiesis stimulating agent
ESD	esterase D
FCS	fetal calf serum
FDA	U.S. Food and Drug Administration
FN1	Fibronectin
FRET	fluorescence resonance energy transfer
GFP	green fluorescent protein
GO	gene ontology
GUSB	glucuronidase beta
h	hour(s)
HGF	hepatocyte growth factor
IAP	inhibitor of apoptosis proteins
IP	immunoprecipitation
I-SMAD	inhibitory SMADs
ITGB4	integrin beta 4
JAK2	Janus kinase 2
JNK	c-Jun N-terminal kinase
KRAS	Kirsten rat sarcoma
l	liter
MAPK	mitogen-activated protein kinase
MCIp	methyl-CpG immunoprecipitation
Mcl1	myeloid cell leukemia 1

Mdm2	mouse double minute 2 homolog
MEKi	MEK inhibitor
mg	milli gramm
min	minute(s)
miRNA	micro RNA
MMR	mismatch repair
mRNA	messenger RNA
NER	nuclear excision repair
NSCLC	non-small-cell lung carcinoma
ODE	ordinary differential equations
PBS	phosphate buffered saline
PCR	polymerase chain reaction
PI3K	phosphoinositide 3-kinase
PIAS	protein inhibitors of activated STATs
PIK3CA	phosphatidylinositol-4,5-bisphosphate 3-kinase
PLAU	plasminogen activator, urokinase
PS	polystyrene
PTEN	phosphatase and tensin homolog
PTP	protein tyrosin phosphatase
PUMA	p53 upregulated modulator of apoptosis
qRT-PCR	quantitative real time PCR
RAS	rat sarcoma
RFP	red fluorescent protein
RNA	ribonucleic acid
RNAseq	RNA sequencing
R-SMAD	receptor-regulated SMADs
SCLC	small-cell lung carcinoma
SDS-PAGE	sodium dodecyl sulfate polyacrylamide gel electrophoresis
SH2 domain	Src Homology 2 domain
SHP-1	Src homology region 2 domain-containing phosphatase-1
SMAD	mothers against decapentaplegic homolog

SMURF	SMAD ubiquitination regulatory factor-1
SNAI1	Snail
SNAI2	Slug
SOCS3	suppressor of cytokine signaling 3
SOP	standard operating procedures
STAT	signal transducers and activators of transcription
t	time
TCL	total cell lysate
TGFBR	TGF- β receptor
TGF- β	transforming growth factor beta
TKI	tyrosine kinase inhibitor
TP53	tumor protein p53
VIM	Vimentin
WGS	whole genome sequencing
XIAP	X-linked inhibitor of apoptosis protein
ZEB	zinc finger E-box-binding homeobox

9. References

1. Bender, E., *Epidemiology: The dominant malignancy*. Nature, 2014. **513**(7517): p. S2-3.
2. Desai, T.J., D.G. Brownfield, and M.A. Krasnow, *Alveolar progenitor and stem cells in lung development, renewal and cancer*. Nature, 2014. **507**(7491): p. 190-4.
3. Kim, C.F., et al., *Identification of bronchioalveolar stem cells in normal lung and lung cancer*. Cell, 2005. **121**(6): p. 823-35.
4. Xu, X., et al., *Evidence for type II cells as cells of origin of K-Ras-induced distal lung adenocarcinoma*. Proc Natl Acad Sci U S A, 2012. **109**(13): p. 4910-5.
5. Lin, C., et al., *Alveolar type II cells possess the capability of initiating lung tumor development*. PLoS One, 2012. **7**(12): p. e53817.
6. Cheng L, et al., *Molecular pathology of lung cancer: key to personalized medicine*. Mod Pathol, 2012. **25**(3): p. 347-69.
7. Ding L, et al., *Somatic mutations affect key pathways in lung adenocarcinoma*. Nature, 2008. **455**(7216): p. 1069-75.
8. Rodriguez, R. and M. Meuth, *Chk1 and p21 cooperate to prevent apoptosis during DNA replication fork stress*. Mol Biol Cell, 2006. **17**(1): p. 402-12.
9. Thaler, S., et al., *RASSF1A mediates p21Cip1/Waf1-dependent cell cycle arrest and senescence through modulation of the Raf-MEK-ERK pathway and inhibition of Akt*. Cancer Res, 2009. **69**(5): p. 1748-57.
10. Coqueret, O., *New roles for p21 and p27 cell-cycle inhibitors: a function for each cell compartment?* Trends Cell Biol, 2003. **13**(2): p. 65-70.
11. Chambard, J.C., et al., *ERK implication in cell cycle regulation*. Biochim Biophys Acta, 2007. **1773**(8): p. 1299-310.
12. Yamamoto, T., et al., *Continuous ERK activation downregulates antiproliferative genes throughout G1 phase to allow cell-cycle progression*. Curr Biol, 2006. **16**(12): p. 1171-82.
13. Jones, S.M. and A. Kazlauskas, *Growth-factor-dependent mitogenesis requires two distinct phases of signalling*. Nat Cell Biol, 2001. **3**(2): p. 165-72.
14. Squires, M.S., P.M. Nixon, and S.J. Cook, *Cell-cycle arrest by PD184352 requires inhibition of extracellular signal-regulated kinases (ERK) 1/2 but not ERK5/BMK1*. Biochem J, 2002. **366**(Pt 2): p. 673-80.
15. Zhao, Y. and A.A. Adjei, *The clinical development of MEK inhibitors*. Nat Rev Clin Oncol, 2014. **11**(7): p. 385-400.
16. Prior, I.A., P.D. Lewis, and C. Mattos, *A comprehensive survey of Ras mutations in cancer*. Cancer Res, 2012. **72**(10): p. 2457-67.
17. Akinleye, A., et al., *MEK and the inhibitors: from bench to bedside*. J Hematol Oncol, 2013. **6**: p. 27.
18. Flaherty, K.T., et al., *Improved survival with MEK inhibition in BRAF-mutated melanoma*. N Engl J Med, 2012. **367**(2): p. 107-14.
19. Jänne, P.A., et al., *Selumetinib plus docetaxel for KRAS-mutant advanced non-small-cell lung cancer: a randomised, multicentre, placebo-controlled, phase 2 study*. Lancet Oncol, 2013. **14**(1): p. 38-47.

20. Haura, E.B., et al., *A phase II study of PD-0325901, an oral MEK inhibitor, in previously treated patients with advanced non-small cell lung cancer*. Clin Cancer Res, 2010. **16**(8): p. 2450-7.
21. Ji, P., et al., *MALAT-1, a novel noncoding RNA, and thymosin beta4 predict metastasis and survival in early-stage non-small cell lung cancer*. Oncogene, 2003. **22**(39): p. 8031-41.
22. Oncology, A.S.o.C., *Clinical practice guidelines for the treatment of unresectable non-small-cell lung cancer. Adopted on May 16, 1997 by the American Society of Clinical Oncology*. J Clin Oncol, 1997. **15**(8): p. 2996-3018.
23. Kelland, L., *The resurgence of platinum-based cancer chemotherapy*. Nat Rev Cancer, 2007. **7**(8): p. 573-84.
24. Dasari, S. and P.B. Tchounwou, *Cisplatin in cancer therapy: Molecular mechanisms of action*. Eur J Pharmacol, 2014. **740C**: p. 364-378.
25. Yonezawa, A., et al., *Cisplatin and oxaliplatin, but not carboplatin and nedaplatin, are substrates for human organic cation transporters (SLC22A1-3 and multidrug and toxin extrusion family)*. J Pharmacol Exp Ther, 2006. **319**(2): p. 879-86.
26. medac. *Fachinformation - Cisplatin 0,5 mg/ml Lösung medac*. Feb. 2011.
27. Sparreboom, A. and J. Verweij, *Paclitaxel pharmacokinetics, threshold models, and dosing strategies*. J Clin Oncol, 2003. **21**(14): p. 2803-4; author reply 2805-6.
28. Himmelstein, K.J., et al., *Clinical kinetics on intact cisplatin and some related species*. Clin Pharmacol Ther, 1981. **29**(5): p. 658-64.
29. Go, R.S. and A.A. Adjei, *Review of the comparative pharmacology and clinical activity of cisplatin and carboplatin*. J Clin Oncol, 1999. **17**(1): p. 409-22.
30. Basu, A. and S. Krishnamurthy, *Cellular responses to Cisplatin-induced DNA damage*. J Nucleic Acids, 2010. **2010**.
31. Kuwana H, et al., *The phosphoinositide-3 kinase gamma-Akt pathway mediates renal tubular injury in cisplatin nephrotoxicity*. Kidney Int, 2008. **73**(4): p. 430-45.
32. Hayakawa, J., et al., *Inhibition of BAD phosphorylation either at serine 112 via extracellular signal-regulated protein kinase cascade or at serine 136 via Akt cascade sensitizes human ovarian cancer cells to cisplatin*. Cancer Res, 2000. **60**(21): p. 5988-94.
33. Belyanskaya, L.L., et al., *Cisplatin activates Akt in small cell lung cancer cells and attenuates apoptosis by survivin upregulation*. Int J Cancer, 2005. **117**(5): p. 755-63.
34. Lee, M.W., et al., *Akt1 inhibition by RNA interference sensitizes human non-small cell lung cancer cells to cisplatin*. Int J Cancer, 2008. **122**(10): p. 2380-4.
35. Dan, H.C., et al., *Akt phosphorylation and stabilization of X-linked inhibitor of apoptosis protein (XIAP)*. J Biol Chem, 2004. **279**(7): p. 5405-12.
36. Wang, X., J.L. Martindale, and N.J. Holbrook, *Requirement for ERK activation in cisplatin-induced apoptosis*. J Biol Chem, 2000. **275**(50): p. 39435-43.
37. DeHaan, R.D., E.M. Yazlovitskaya, and D.L. Persons, *Regulation of p53 target gene expression by cisplatin-induced extracellular signal-regulated kinase*. Cancer Chemother Pharmacol, 2001. **48**(5): p. 383-8.
38. Woessmann, W., X. Chen, and A. Borkhardt, *Ras-mediated activation of ERK by cisplatin induces cell death independently of p53 in osteosarcoma and*

- neuroblastoma cell lines*. *Cancer Chemother Pharmacol*, 2002. **50**(5): p. 397-404.
39. Schweyer, S., et al., *Cisplatin-induced apoptosis in human malignant testicular germ cell lines depends on MEK/ERK activation*. *Br J Cancer*, 2004. **91**(3): p. 589-98.
40. Choi, B.K., et al., *Role of ERK activation in cisplatin-induced apoptosis in A172 human glioma cells*. *Neurotoxicology*, 2004. **25**(6): p. 915-24.
41. Sanchez-Perez, I., J.R. Murguia, and R. Perona, *Cisplatin induces a persistent activation of JNK that is related to cell death*. *Oncogene*, 1998. **16**(4): p. 533-40.
42. Hernandez Losa, J., et al., *Role of the p38 MAPK pathway in cisplatin-based therapy*. *Oncogene*, 2003. **22**(26): p. 3998-4006.
43. Mansouri, A., et al., *Sustained activation of JNK/p38 MAPK pathways in response to cisplatin leads to Fas ligand induction and cell death in ovarian carcinoma cells*. *J Biol Chem*, 2003. **278**(21): p. 19245-56.
44. Wang, D. and S.J. Lippard, *Cellular processing of platinum anticancer drugs*. *Nat Rev Drug Discov*, 2005. **4**(4): p. 307-20.
45. Park, M.S., M. De Leon, and P. Devarajan, *Cisplatin induces apoptosis in LLC-PK1 cells via activation of mitochondrial pathways*. *J Am Soc Nephrol*, 2002. **13**(4): p. 858-65.
46. Kim, J.H., et al., *Role of antiapoptotic proteins in tumor necrosis factor-related apoptosis-inducing ligand and cisplatin-augmented apoptosis*. *Clin Cancer Res*, 2003. **9**(8): p. 3134-41.
47. Gao, J.J., et al., *DAP5 ameliorates cisplatin-induced apoptosis of renal tubular cells*. *Am J Nephrol*, 2012. **35**(5): p. 456-65.
48. Asselin, E., G.B. Mills, and B.K. Tsang, *XIAP regulates Akt activity and caspase-3-dependent cleavage during cisplatin-induced apoptosis in human ovarian epithelial cancer cells*. *Cancer Res*, 2001. **61**(5): p. 1862-8.
49. Miyashita, T., et al., *Tumor suppressor p53 is a regulator of bcl-2 and bax gene expression in vitro and in vivo*. *Oncogene*, 1994. **9**(6): p. 1799-805.
50. Selvakumaran, M., et al., *Immediate early up-regulation of bax expression by p53 but not TGF beta 1: a paradigm for distinct apoptotic pathways*. *Oncogene*, 1994. **9**(6): p. 1791-8.
51. Salvador, J.M., J.D. Brown-Clay, and A.J. Fornace, Jr., *Gadd45 in stress signaling, cell cycle control, and apoptosis*. *Adv Exp Med Biol*, 2013. **793**: p. 1-19.
52. Liu, W., et al., *Protective roles of Gadd45 and MDM2 in blueberry anthocyanins mediated DNA repair of fragmented and non-fragmented DNA damage in UV-irradiated HepG2 cells*. *Int J Mol Sci*, 2013. **14**(11): p. 21447-62.
53. Giaccone, G., et al., *Teniposide in the treatment of small-cell lung cancer: the influence of prior chemotherapy*. *J Clin Oncol*, 1988. **6**(8): p. 1264-70.
54. Zhang, Y. and X. Shen, *Heat shock protein 27 protects L929 cells from cisplatin-induced apoptosis by enhancing Akt activation and abating suppression of thioredoxin reductase activity*. *Clin Cancer Res*, 2007. **13**(10): p. 2855-64.
55. Liu, L.Z., et al., *AKT1 amplification regulates cisplatin resistance in human lung cancer cells through the mammalian target of rapamycin/p70S6K1 pathway*. *Cancer Res*, 2007. **67**(13): p. 6325-32.

56. Fraser, M., et al., *p53 is a determinant of X-linked inhibitor of apoptosis protein/Akt-mediated chemoresistance in human ovarian cancer cells*. *Cancer Res*, 2003. **63**(21): p. 7081-8.
57. Galluzzi, L., et al., *Molecular mechanisms of cisplatin resistance*. *Oncogene*, 2012. **31**(15): p. 1869-83.
58. Yang, H., et al., *MicroRNA expression profiling in human ovarian cancer: miR-214 induces cell survival and cisplatin resistance by targeting PTEN*. *Cancer Res*, 2008. **68**(2): p. 425-33.
59. Ahrendt SA, et al., *p53 mutations and survival in stage I non-small-cell lung cancer: results of a prospective study*. *J Natl Cancer Inst*, 2003. **95**(13): p. 961-70.
60. Takahashi T, et al., *p53: a frequent target for genetic abnormalities in lung cancer*. *Science*, 1989. **246**(4929): p. 491-4.
61. Malin, S., S. McManus, and M. Busslinger, *STAT5 in B cell development and leukemia*. *Curr Opin Immunol*, 2010. **22**(2): p. 168-76.
62. Bachmann J, et al., *Division of labor by dual feedback regulators controls JAK2/STAT5 signaling over broad ligand range*. *Mol Syst Biol*, 2011. **7**.
63. Pirker, R., et al., *Paclitaxel/cisplatin in advanced non-small-cell lung cancer (NSCLC)*. *Ann Oncol*, 1995. **6**(8): p. 833-5.
64. Zhu H, Jackson T, and B. HF, *Detecting and responding to hypoxia*. *Nephrol Dial Transplant.*, 2002. **17**: p. 3-7.
65. Becker V, et al., *Packing density of the erythropoietin receptor transmembrane domain correlates with amplification of biological responses*. *Biochemistry*, 2008. **47**(45): p. 11771-82.
66. Remy I, Wilson IA, and M. SW, *Erythropoietin receptor activation by a ligand-induced conformation change*. *Science*, 1999. **283**(5404): p. 990-3.
67. Richmond TD, Chohan M, and B. DL., *Turning cells red: signal transduction mediated by erythropoietin*. *Trends Cell Biol*, 2005. **15**(3): p. 146-55.
68. Hebenstreit D, Horejs-Hoeck J, and D. A., *JAK/STAT-dependent gene regulation by cytokines*. *Drug News Perspect*, 2005. **18**(4): p. 243-9.
69. Yasukawa, H., A. Sasaki, and A. Yoshimura, *Negative regulation of cytokine signaling pathways*. *Annu Rev Immunol*, 2000. **18**: p. 143-64.
70. Sasaki, A., et al., *CIS3/SOCS-3 suppresses erythropoietin (EPO) signaling by binding the EPO receptor and JAK2*. *J Biol Chem*, 2000. **275**(38): p. 29338-47.
71. Hilton, D., *Negative regulators of cytokine signal transduction*. *Cell Mol Life Sci*, 1999. **55**(12): p. 1568-77.
72. Chaves de Souza, J.A., et al., *SOCS3 expression correlates with severity of inflammation, expression of proinflammatory cytokines, and activation of STAT3 and p38 MAPK in LPS-induced inflammation in vivo*. *Mediators Inflamm*, 2013. **2013**: p. 650812.
73. Ehltling C, et al., *Regulation of suppressor of cytokine signaling 3 (SOCS3) mRNA stability by TNF-alpha involves activation of the MKK6/p38MAPK/MK2 cascade*. *J Immunol*, 2007. **178**(5): p. 2813-26.
74. Bode, J.G., et al., *The MKK6/p38 mitogen-activated protein kinase pathway is capable of inducing SOCS3 gene expression and inhibits IL-6-induced transcription*. *Biol Chem*, 2001. **382**(10): p. 1447-53.

75. Ru P, et al., *Anti-miR-203 Upregulates SOCS3 Expression in Breast Cancer Cells and Enhances Cisplatin Chemosensitivity*. *Genes Cancer*, 2011. **2**(7): p. 720-7.
76. da Silva, C.G., et al., *A20 promotes liver regeneration by decreasing SOCS3 expression to enhance IL-6/STAT3 proliferative signals*. *Hepatology*, 2013. **57**(5): p. 2014-25.
77. Sulahian R, Cleaver O, and H. L.J., *Ligand-induced EpoR internalization is mediated by JAK2 and p85 and is impaired by mutations responsible for primary familial and congenital polycythemia*. *Blood*, 2009. **113**(21): p. 5287-97.
78. Walrafen P, et al., *Both proteasomes and lysosomes degrade the activated erythropoietin receptor*. *Blood*, 2005. **105**(2): p. 600-8.
79. Becker V, et al., *Covering a broad dynamic range: information processing at the erythropoietin receptor*. *Science*, 2010. **328**(5984): p. 1404-1408.
80. Rangarajan, V. and S.E. Juul, *Erythropoietin: Emerging Role of Erythropoietin in Neonatal Neuroprotection*. *Pediatr Neurol*, 2014. **51**(4): p. 481-488.
81. Congote, L.F., et al., *Erythropoietin-dependent endothelial proteins: potential use against erythropoietin resistance*. *Cytokine*, 2010. **51**(2): p. 113-8.
82. Tsai, P.T., et al., *A critical role of erythropoietin receptor in neurogenesis and post-stroke recovery*. *J Neurosci*, 2006. **26**(4): p. 1269-74.
83. Haroon ZA, A.K., Jiang X, Arcasoy MO, *A novel role for erythropoietin during fibrin-induced wound-healing response*. *Am J Pathol*, 2003. **163**(3): p. 993-1000.
84. Mori M, et al., *Activation of extracellular signal-regulated kinases ERK1 and ERK2 induces Bcl-xL up-regulation via inhibition of caspase activities in erythropoietin signaling*. *J Cell Physiol*, 2003. **195**(2): p. 290-297.
85. Hedley, B.D., A.L. Allan, and A. Xenocostas, *The role of erythropoietin and erythropoiesis-stimulating agents in tumor progression*. *Clin Cancer Res*, 2011. **17**(20): p. 6373-80.
86. Baltaziak, M., et al., *Relationships of P53 and Bak with EPO and EPOR in human colorectal cancer*. *Anticancer Res*, 2009. **29**(10): p. 4151-6.
87. Todaro, M., et al., *Erythropoietin activates cell survival pathways in breast cancer stem-like cells to protect them from chemotherapy*. *Cancer Res*, 2013. **73**(21): p. 6393-400.
88. Sirén AL, et al., *Erythropoietin prevents neuronal apoptosis after cerebral ischemia and metabolic stress*. *Proc Natl Acad Sci U S A*, 2001. **98**(7): p. 4044-9.
89. Wright JR, et al., *Randomized, double-blind, placebo-controlled trial of erythropoietin in non-small-cell lung cancer with disease-related anemia*. *J Clin Oncol*, 2007. **25**(9): p. 27-32.
90. Saintigny P, et al., *Erythropoietin and erythropoietin receptor coexpression is associated with poor survival in stage I non-small cell lung cancer*. *Clin Cancer Res*, 2007. **13**(16): p. 4825-31.
91. Dunlop EA, et al., *Induction of signalling in non-erythroid cells by pharmacological levels of erythropoietin*. *Neurodegener Dis*, 2006. **3**(1-2): p. 94-100.
92. He B, et al., *SOCS-3 is frequently silenced by hypermethylation and suppresses cell growth in human lung cancer*. *Proc Natl Acad Sci U S A*, 2003. **100**(24): p. 14133-8.

93. Sos ML, et al., *Identifying genotype-dependent efficacy of single and combined PI3K- and MAPK-pathway inhibition in cancer*. PNAS, 2009.
94. Swift S, et al., *Absence of functional EpoR expression in human tumor cell lines*. Blood, 2010. **115**(21): p. 4254-4263.
95. Doleschel, D., et al., *Targeted near-infrared imaging of the erythropoietin receptor in human lung cancer xenografts*. J Nucl Med, 2012. **53**(2): p. 304-11.
96. Dagnon K, et al., *Expression of erythropoietin and erythropoietin receptor in non-small cell lung carcinomas*. Clin Cancer Res, 2005. **11**(3): p. 993-9.
97. Brown WM, et al., *Erythropoietin receptor expression in non-small cell lung carcinoma: a question of antibody specificity*. Stem Cells, 2007. **25**(3): p. 718-22.
98. Sinclair AM, et al., *Expression and function of erythropoietin receptors in tumors: implications for the use of erythropoiesis-stimulating agents in cancer patients*. Cancer, 2007. **110**(3): p. 477-88.
99. Jeon, H.S. and J. Jen, *TGF-beta signaling and the role of inhibitory Smads in non-small cell lung cancer*. J Thorac Oncol, 2010. **5**(4): p. 417-9.
100. Siegel, P.M. and J. Massague, *Cytostatic and apoptotic actions of TGF-beta in homeostasis and cancer*. Nat Rev Cancer, 2003. **3**(11): p. 807-21.
101. Derynck R and Z. YE, *Smad-dependent and Smad-independent pathways in TGF-beta family signalling*. Nature, 2003. **425**(6958): p. 577-84.
102. Wharton, K. and R. Derynck, *TGFbeta family signaling: novel insights in development and disease*. Development, 2009. **136**(22): p. 3691-7.
103. Lee, M.K., et al., *TGF-beta activates Erk MAP kinase signalling through direct phosphorylation of ShcA*. EMBO J, 2007. **26**(17): p. 3957-67.
104. Sorrentino, A., et al., *The type I TGF-beta receptor engages TRAF6 to activate TAK1 in a receptor kinase-independent manner*. Nat Cell Biol, 2008. **10**(10): p. 1199-207.
105. Yamashita, M., et al., *TRAF6 mediates Smad-independent activation of JNK and p38 by TGF-beta*. Mol Cell, 2008. **31**(6): p. 918-24.
106. Funaba, M., C.M. Zimmerman, and L.S. Mathews, *Modulation of Smad2-mediated signaling by extracellular signal-regulated kinase*. J Biol Chem, 2002. **277**(44): p. 41361-8.
107. Kretzschmar, M., et al., *A mechanism of repression of TGFbeta/ Smad signaling by oncogenic Ras*. Genes Dev, 1999. **13**(7): p. 804-16.
108. Bakin, A.V., et al., *Phosphatidylinositol 3-kinase function is required for transforming growth factor beta-mediated epithelial to mesenchymal transition and cell migration*. J Biol Chem, 2000. **275**(47): p. 36803-10.
109. Vinals, F. and J. Pouyssegur, *Transforming growth factor beta1 (TGF-beta1) promotes endothelial cell survival during in vitro angiogenesis via an autocrine mechanism implicating TGF-alpha signaling*. Mol Cell Biol, 2001. **21**(21): p. 7218-30.
110. Moustakas, A., et al., *Mechanisms of TGF-beta signaling in regulation of cell growth and differentiation*. Immunol Lett, 2002. **82**(1-2): p. 85-91.
111. Itoh, F., et al., *Promoting bone morphogenetic protein signaling through negative regulation of inhibitory Smads*. EMBO J, 2001. **20**(15): p. 4132-42.
112. Ten Dijke, P., et al., *Regulation of cell proliferation by Smad proteins*. J Cell Physiol, 2002. **191**(1): p. 1-16.

113. Onichtchouk, D., et al., *Silencing of TGF-beta signalling by the pseudoreceptor BAMBI*. *Nature*, 1999. **401**(6752): p. 480-5.
114. Pils, D., et al., *BAMBI is overexpressed in ovarian cancer and co-translocates with Smads into the nucleus upon TGF-beta treatment*. *Gynecol Oncol*, 2010. **117**(2): p. 189-97.
115. Khin, S.S., et al., *BAMBI gene is epigenetically silenced in subset of high-grade bladder cancer*. *Int J Cancer*, 2009. **125**(2): p. 328-38.
116. Lang, D.S., et al., *Transforming growth factor-beta signaling leads to uPA/PAI-1 activation and metastasis: a study on human breast cancer tissues*. *Pathol Oncol Res*, 2014. **20**(3): p. 727-32.
117. Jeon HS and J. J., *TGF-beta signaling and the role of inhibitory Smads in non-small cell lung cancer*. *J Thorac Oncol*, 2010. **5**(4): p. 417-9.
118. Lindley LE and B. KJ., *Molecular characterization of TGFbeta-induced epithelial-mesenchymal transition in normal finite lifespan human mammary epithelial cells*. *Biochem Biophys Res Commun* 2010. **399**(4): p. 659-64.
119. Roberts, A.B. and L.M. Wakefield, *The two faces of transforming growth factor beta in carcinogenesis*. *Proc Natl Acad Sci U S A*, 2003. **100**(15): p. 8621-3.
120. Kim, S.J., et al., *Molecular mechanisms of inactivation of TGF-beta receptors during carcinogenesis*. *Cytokine Growth Factor Rev*, 2000. **11**(1-2): p. 159-68.
121. Heldin, C.H., M. Vanlandewijck, and A. Moustakas, *Regulation of EMT by TGFbeta in cancer*. *FEBS Lett*, 2012. **586**(14): p. 1959-70.
122. Xiao, D. and J. He, *Epithelial mesenchymal transition and lung cancer*. *J Thorac Dis*, 2010. **2**(3): p. 154-9.
123. Perl, A.K., et al., *A causal role for E-cadherin in the transition from adenoma to carcinoma*. *Nature*, 1998. **392**(6672): p. 190-3.
124. Valcourt, U., et al., *TGF-beta and the Smad signaling pathway support transcriptomic reprogramming during epithelial-mesenchymal cell transition*. *Mol Biol Cell*, 2005. **16**(4): p. 1987-2002.
125. Imai K, et al., *Bronchioloalveolar invasion in non-small cell lung cancer is associated with expression of transforming growth factor- β 1*. *World J Surg Oncol*, 2013. **11**.
126. Giampieri S, Pinner S, and S. E., *Intravital imaging illuminates transforming growth factor beta signaling switches during metastasis*. *Cancer Res*, 2010. **70**(9): p. 3435-9.
127. Korpala M and K. Y., *Targeting the transforming growth factor-beta signalling pathway in metastatic cancer*. *Eur J Cancer*, 2010. **46**(7): p. 1232-40.
128. Levy L and H. CS, *Alterations in components of the TGF-beta superfamily signaling pathways in human cancer*. *Cytokine Growth Factor Rev*, 2006. **17**(1-2): p. 41-58.
129. Borczuk AC, et al., *Lung adenocarcinoma invasion in TGFbetaRII-deficient cells is mediated by CCL5/RANTES*. *Oncogene*, 2008. **27**(4): p. 557-64.
130. Christoffersen, N.R., et al., *miR-200b mediates post-transcriptional repression of ZFH1B*. *RNA*, 2007. **13**(8): p. 1172-8.
131. Gregory, P.A., et al., *The miR-200 family and miR-205 regulate epithelial to mesenchymal transition by targeting ZEB1 and SIP1*. *Nat Cell Biol*, 2008. **10**(5): p. 593-601.

132. Hurteau, G.J., et al., *Overexpression of the microRNA hsa-miR-200c leads to reduced expression of transcription factor 8 and increased expression of E-cadherin*. *Cancer Res*, 2007. **67**(17): p. 7972-6.
133. Korpala, M., et al., *The miR-200 family inhibits epithelial-mesenchymal transition and cancer cell migration by direct targeting of E-cadherin transcriptional repressors ZEB1 and ZEB2*. *J Biol Chem*, 2008. **283**(22): p. 14910-4.
134. Park, S.M., et al., *The miR-200 family determines the epithelial phenotype of cancer cells by targeting the E-cadherin repressors ZEB1 and ZEB2*. *Genes Dev*, 2008. **22**(7): p. 894-907.
135. Kajita, M., K.N. McClinic, and P.A. Wade, *Aberrant expression of the transcription factors snail and slug alters the response to genotoxic stress*. *Mol Cell Biol*, 2004. **24**(17): p. 7559-66.
136. Yang, A.D., et al., *Chronic oxaliplatin resistance induces epithelial-to-mesenchymal transition in colorectal cancer cell lines*. *Clin Cancer Res*, 2006. **12**(14 Pt 1): p. 4147-53.
137. Kurrey, N.K., et al., *Snail and slug mediate radioresistance and chemoresistance by antagonizing p53-mediated apoptosis and acquiring a stem-like phenotype in ovarian cancer cells*. *Stem Cells*, 2009. **27**(9): p. 2059-68.
138. Wolkenhauer, O. and M. Mesarovic, *Feedback dynamics and cell function: Why systems biology is called Systems Biology*. *Mol Biosyst*, 2005. **1**(1): p. 14-6.
139. Friboulet, A. and D. Thomas, *Systems Biology-an interdisciplinary approach*. *Biosens Bioelectron*, 2005. **20**(12): p. 2404-7.
140. Hood, L., *Systems biology: integrating technology, biology, and computation*. *Mech Ageing Dev*, 2003. **124**(1): p. 9-16.
141. Kitano, H., *Systems biology: a brief overview*. *Science*, 2002. **295**(5560): p. 1662-4.
142. Kitano, H., *Computational systems biology*. *Nature*, 2002. **420**(6912): p. 206-10.
143. Morris, M.K., et al., *Logic-based models for the analysis of cell signaling networks*. *Biochemistry*, 2010. **49**(15): p. 3216-24.
144. Fritz, B.R., et al., *Biology by design: from top to bottom and back*. *J Biomed Biotechnol*, 2010. **2010**: p. 232016.
145. Mack, G.S., *Can complexity be commercialized?* *Nat Biotechnol*, 2004. **22**(10): p. 1223-9.
146. Bruggeman FJ and W. HV, *The nature of systems biology*. *Trends Microbiol*, 2007. **15**(1): p. 45-50.
147. Bachmann, J., et al., *Predictive mathematical models of cancer signalling pathways*. *J Intern Med*, 2012. **271**(2): p. 155-65.
148. McClelland, M.L., et al., *Lactate dehydrogenase B is required for the growth of KRAS-dependent lung adenocarcinomas*. *Clin Cancer Res*, 2013. **19**(4): p. 773-84.
149. Xu, M., et al., *Perillyl alcohol-mediated inhibition of lung cancer cell line proliferation: potential mechanisms for its chemotherapeutic effects*. *Toxicol Appl Pharmacol*, 2004. **195**(2): p. 232-46.
150. ATCC, *ATCC Cell lines by gene mutations*. 2014: [http://www.atcc.org/~media/PDFs/Culture%20Guides/Cell Lines by Gene Mutation.ashx](http://www.atcc.org/~media/PDFs/Culture%20Guides/Cell%20Lines%20by%20Gene%20Mutations.pdf).

151. Tang, Z., et al., *Dual MET-EGFR combinatorial inhibition against T790M-EGFR-mediated erlotinib-resistant lung cancer*. Br J Cancer, 2008. **99**(6): p. 911-22.
152. La Monica, S., et al., *Gefitinib inhibits invasive phenotype and epithelial-mesenchymal transition in drug-resistant NSCLC cells with MET amplification*. PLoS One, 2013. **8**(10): p. e78656.
153. Mathur, A., *Quantitative analysis and mathematical modelling of HGF induced signalling and migration in lung cancer cells*, in Faculty of Biosciences. 2011, Ruprecht-Karls-Universität Heidelberg.
154. Velten, L., *Dynamics of HGF induced responses in lung cancer cells*, in Faculty of Biosciences. 2012, Ruprecht-Karls-Universität Heidelberg.
155. Gysin, S., et al., *Pharmacologic inhibition of RAF-->MEK-->ERK signaling elicits pancreatic cancer cell cycle arrest through induced expression of p27Kip1*. Cancer Res, 2005. **65**(11): p. 4870-80.
156. Chang, F., et al., *Signal transduction mediated by the Ras/Raf/MEK/ERK pathway from cytokine receptors to transcription factors: potential targeting for therapeutic intervention*. Leukemia, 2003. **17**(7): p. 1263-93.
157. Salahudeen AK, et al., *Antiapoptotic properties of erythropoiesis-stimulating proteins in models of cisplatin-induced acute kidney injury*. Am J Physiol Renal Physiol, 2008. **294**(6): p. 1354-65.
158. Shcherbo, D., et al., *Practical and reliable FRET/FLIM pair of fluorescent proteins*. BMC Biotechnol, 2009. **9**: p. 24.
159. Tibshirani, R., *Regression shrinkage and selection via the lasso*. J. R. Statist. Soc., 1996. **58**(1): p. 267-288.
160. Kukreja, S.L., J. Lofberg, and M.J. Brenner. *A least absolute shrinkage and selection operator (LASSO) for nonlinear system identification*. 2006.
161. Goeman, J.J., *L1 penalized estimation in the Cox proportional hazards model*. Biom J, 2010. **52**(1): p. 70-84.
162. Schmidt, M., G. Fung, and R. Rosales, *Fast optimization methods for L1 regularization: A comparative study and two new approaches*. Springer-Verlag Berlin, 2007. **4701**: p. 286-297.
163. Luwor, R.B., et al., *Targeting Stat3 and Smad7 to restore TGF-beta cytosolic regulation of tumor cells in vitro and in vivo*. Oncogene, 2013. **32**(19): p. 2433-41.
164. Li, J., et al., *Gene expression response to cisplatin treatment in drug-sensitive and drug-resistant ovarian cancer cells*. Oncogene, 2007. **26**(20): p. 2860-72.
165. Matsunoshita, Y., et al., *Suppression of osteosarcoma cell invasion by chemotherapy is mediated by urokinase plasminogen activator activity via up-regulation of EGR1*. PLoS One, 2011. **6**(1): p. e16234.
166. Tsai, C.M., et al., *Interrelationships between cellular nucleotide excision repair, cisplatin cytotoxicity, HER-2/neu gene expression, and epidermal growth factor receptor level in non-small cell lung cancer cells*. Jpn J Cancer Res, 2000. **91**(2): p. 213-22.
167. Arany, I., et al., *Cisplatin-induced cell death is EGFR/src/ERK signaling dependent in mouse proximal tubule cells*. Am J Physiol Renal Physiol, 2004. **287**(3): p. F543-9.
168. Jo, S.K., et al., *MEK inhibitor, U0126, attenuates cisplatin-induced renal injury by decreasing inflammation and apoptosis*. Kidney Int, 2005. **67**(2): p. 458-66.

169. Guégan, J.P., et al., *MAPK signaling in cisplatin-induced death: predominant role of ERK1 over ERK2 in human hepatocellular carcinoma cells*. *Carcinogenesis*, 2013. **34**(1): p. 38-47.
170. Wang, J., J.Y. Zhou, and G.S. Wu, *ERK-dependent MKP-1-mediated cisplatin resistance in human ovarian cancer cells*. *Cancer Res*, 2007. **67**(24): p. 11933-41.
171. Mandic, A., et al., *The MEK1 inhibitor PD98059 sensitizes C8161 melanoma cells to cisplatin-induced apoptosis*. *Melanoma Res*, 2001. **11**(1): p. 11-9.
172. Persons, D.L., et al., *Cisplatin-induced activation of mitogen-activated protein kinases in ovarian carcinoma cells: inhibition of extracellular signal-regulated kinase activity increases sensitivity to cisplatin*. *Clin Cancer Res*, 1999. **5**(5): p. 1007-14.
173. Hayakawa, J., et al., *Inhibition of extracellular signal-regulated protein kinase or c-Jun N-terminal protein kinase cascade, differentially activated by cisplatin, sensitizes human ovarian cancer cell line*. *J Biol Chem*, 1999. **274**(44): p. 31648-54.
174. Boucher, M.J., et al., *MEK/ERK signaling pathway regulates the expression of Bcl-2, Bcl-X(L), and Mcl-1 and promotes survival of human pancreatic cancer cells*. *J Cell Biochem*, 2000. **79**(3): p. 355-69.
175. Yeh, P.Y., et al., *Increase of the resistance of human cervical carcinoma cells to cisplatin by inhibition of the MEK to ERK signaling pathway partly via enhancement of anticancer drug-induced NF kappa B activation*. *Biochem Pharmacol*, 2002. **63**(8): p. 1423-30.
176. Tamura, Y., S. Simizu, and H. Osada, *The phosphorylation status and anti-apoptotic activity of Bcl-2 are regulated by ERK and protein phosphatase 2A on the mitochondria*. *FEBS Lett*, 2004. **569**(1-3): p. 249-55.
177. Wood, P.A. and W.J. Hrushesky, *Cisplatin-associated anemia: an erythropoietin deficiency syndrome*. *J Clin Invest*, 1995. **95**(4): p. 1650-9.
178. Groopman, J.E. and L.M. Itri, *Chemotherapy-induced anemia in adults: incidence and treatment*. *J Natl Cancer Inst*, 1999. **91**(19): p. 1616-34.
179. Schreiber, G.B., et al., *The risk of transfusion-transmitted viral infections. The Retrovirus Epidemiology Donor Study*. *N Engl J Med*, 1996. **334**(26): p. 1685-90.
180. Sazama, K., *Reports of 355 transfusion-associated deaths: 1976 through 1985*. *Transfusion*, 1990. **30**(7): p. 583-90.
181. Shulman, I.A., *The risk of an overt hemolytic transfusion reaction following the use of an immediate spin crossmatch*. *Arch Pathol Lab Med*, 1990. **114**(4): p. 412-4.
182. Popovsky, M.A. and S.B. Moore, *Diagnostic and pathogenetic considerations in transfusion-related acute lung injury*. *Transfusion*, 1985. **25**(6): p. 573-7.
183. Oberhoff, C., et al., *Recombinant human erythropoietin in the treatment of chemotherapy-induced anemia and prevention of transfusion requirement associated with solid tumors: a randomized, controlled study*. *Ann Oncol*, 1998. **9**(3): p. 255-60.
184. Dunphy, F.R., et al., *Erythropoietin reduces anemia and transfusions after chemotherapy with paclitaxel and carboplatin*. *Cancer*, 1997. **79**(8): p. 1623-8.

185. Del Mastro, L., et al., *Randomized phase III trial evaluating the role of erythropoietin in the prevention of chemotherapy-induced anemia*. J Clin Oncol, 1997. **15**(7): p. 2715-21.
186. Plataniias, L.C., et al., *Treatment of chemotherapy-induced anemia with recombinant human erythropoietin in cancer patients*. J Clin Oncol, 1991. **9**(11): p. 2021-6.
187. Ponchio, L., et al., *Evaluation of erythroid marrow response to recombinant human erythropoietin in patients with cancer anaemia*. Haematologica, 1992. **77**(6): p. 494-501.
188. Hardee, M.E., et al., *Erythropoietin biology in cancer*. Clin Cancer Res, 2006. **12**(2): p. 332-9.
189. Elliott, S., et al., *Anti-Epo receptor antibodies do not predict Epo receptor expression*. Blood, 2006. **107**(5): p. 1892-5.
190. Szenajch, J., et al., *The role of erythropoietin and its receptor in growth, survival and therapeutic response of human tumor cells From clinic to bench - a critical review*. Biochim Biophys Acta, 2010. **1806**(1): p. 82-95.
191. Li, J., et al., *Erythropoietin reduces cisplatin-induced apoptosis in renal carcinoma cells via a PKC dependent pathway*. Cancer Biol Ther, 2007. **6**(12): p. 1944-50.
192. Mirmohammadsadegh, A., et al., *Role of erythropoietin receptor expression in malignant melanoma*. J Invest Dermatol, 2010. **130**(1): p. 201-10.
193. Belenkov, A.I., et al., *Erythropoietin induces cancer cell resistance to ionizing radiation and to cisplatin*. Mol Cancer Ther, 2004. **3**(12): p. 1525-32.
194. McBroom, J.W., et al., *Erythropoietin receptor function and expression in epithelial ovarian carcinoma*. Gynecol Oncol, 2005. **99**(3): p. 571-7.
195. Bittorf, T., et al., *Activation of STAT5 during EPO-directed suppression of apoptosis*. Cell Signal, 2000. **12**(1): p. 23-30.
196. Silva, M., et al., *Erythropoietin can promote erythroid progenitor survival by repressing apoptosis through Bcl-XL and Bcl-2*. Blood, 1996. **88**(5): p. 1576-82.
197. Tsushima, H., et al., *Human erythropoietin receptor increases GATA-2 and Bcl-xL by a protein kinase C-dependent pathway in human erythropoietin-dependent cell line AS-E2*. Cell Growth Differ, 1997. **8**(12): p. 1317-28.
198. Kapur, R. and L. Zhang, *A novel mechanism of cooperation between c-Kit and erythropoietin receptor. Stem cell factor induces the expression of Stat5 and erythropoietin receptor, resulting in efficient proliferation and survival by erythropoietin*. J Biol Chem, 2001. **276**(2): p. 1099-106.
199. Li, G., et al., *Effective targeting of STAT5-mediated survival in myeloproliferative neoplasms using ABT-737 combined with rapamycin*. Leukemia, 2010. **24**(8): p. 1397-405.
200. Yoshimura, A., A.D. D'Andrea, and H.F. Lodish, *Friend spleen focus-forming virus glycoprotein gp55 interacts with the erythropoietin receptor in the endoplasmic reticulum and affects receptor metabolism*. Proc Natl Acad Sci U S A, 1990. **87**(11): p. 4139-43.
201. Evren, S., et al., *Characterization of SHP-1 protein tyrosine phosphatase transcripts, protein isoforms and phosphatase activity in epithelial cancer cells*. Genomics, 2013. **102**(5-6): p. 491-9.

202. Mok, S.C., et al., *Overexpression of the protein tyrosine phosphatase, nonreceptor type 6 (PTPN6), in human epithelial ovarian cancer*. *Gynecol Oncol*, 1995. **57**(3): p. 299-303.
203. Cao, R., et al., *SHP1-mediated cell cycle redistribution inhibits radiosensitivity of non-small cell lung cancer*. *Radiat Oncol*, 2013. **8**: p. 178.
204. Maiwald, T., et al., *Dynamic pathway modeling: feasibility analysis and optimal experimental design*. *Ann N Y Acad Sci*, 2007. **1115**: p. 212-20.
205. Raue, A., et al., *Addressing parameter identifiability by model-based experimentation*. *IET Syst Biol*, 2011. **5**(2): p. 120-30.
206. Sonkoly, E., et al., *MicroRNAs: novel regulators involved in the pathogenesis of psoriasis?* *PLoS One*, 2007. **2**(7): p. e610.
207. Wei, T., et al., *The expression of microRNA-203 during human skin morphogenesis*. *Exp Dermatol*, 2010. **19**(9): p. 854-6.
208. Frevel, M.A., et al., *p38 Mitogen-activated protein kinase-dependent and -independent signaling of mRNA stability of AU-rich element-containing transcripts*. *Mol Cell Biol*, 2003. **23**(2): p. 425-36.
209. Massagué, J., *TGFbeta in Cancer*. *Cell*, 2008. **134**(2): p. 215-30.
210. Ranganathan, P., et al., *Expression profiling of genes regulated by TGF-beta: differential regulation in normal and tumour cells*. *BMC Genomics*, 2007. **8**: p. 98.
211. Renzoni, E.A., et al., *Gene expression profiling reveals novel TGFbeta targets in adult lung fibroblasts*. *Respir Res*, 2004. **5**: p. 24.
212. Vega, S., et al., *Snail blocks the cell cycle and confers resistance to cell death*. *Genes Dev*, 2004. **18**(10): p. 1131-43.
213. Niimi, H., et al., *Notch signaling is necessary for epithelial growth arrest by TGF-beta*. *J Cell Biol*, 2007. **176**(5): p. 695-707.
214. Ryu, B. and S.E. Kern, *The essential similarity of TGFbeta and activin receptor transcriptional responses in cancer cells*. *Cancer Biol Ther*, 2003. **2**(2): p. 164-70.
215. Peinado, H., et al., *Snail mediates E-cadherin repression by the recruitment of the Sin3A/histone deacetylase 1 (HDAC1)/HDAC2 complex*. *Mol Cell Biol*, 2004. **24**(1): p. 306-19.
216. Carver, E.A., et al., *The mouse snail gene encodes a key regulator of the epithelial-mesenchymal transition*. *Mol Cell Biol*, 2001. **21**(23): p. 8184-8.
217. Ozdamar, B., et al., *Regulation of the polarity protein Par6 by TGFbeta receptors controls epithelial cell plasticity*. *Science*, 2005. **307**(5715): p. 1603-9.
218. Derynck, R. and R.J. Akhurst, *Differentiation plasticity regulated by TGF-beta family proteins in development and disease*. *Nat Cell Biol*, 2007. **9**(9): p. 1000-4.
219. Hartsough, M.T. and K.M. Mulder, *Transforming growth factor beta activation of p44mapk in proliferating cultures of epithelial cells*. *J Biol Chem*, 1995. **270**(13): p. 7117-24.
220. Xie, L., et al., *Activation of the Erk pathway is required for TGF-beta1-induced EMT in vitro*. *Neoplasia*, 2004. **6**(5): p. 603-10.
221. Ellenrieder, V., et al., *Transforming growth factor beta1 treatment leads to an epithelial-mesenchymal transdifferentiation of pancreatic cancer cells requiring extracellular signal-regulated kinase 2 activation*. *Cancer Res*, 2001. **61**(10): p. 4222-8.

222. Sapkota, G.P., *The TGFbeta-induced phosphorylation and activation of p38 mitogen-activated protein kinase is mediated by MAP3K4 and MAP3K10 but not TAK1*. Open Biol, 2013. **3**(6): p. 130067.
223. Drömann, D., et al., *The TGF-beta-pseudoreceptor BAMBI is strongly expressed in COPD lungs and regulated by nontypeable Haemophilus influenzae*. Respir Res, 2010. **11**: p. 67.
224. Fritzmann, J., et al., *A colorectal cancer expression profile that includes transforming growth factor beta inhibitor BAMBI predicts metastatic potential*. Gastroenterology, 2009. **137**(1): p. 165-75.
225. Togo, N., et al., *Prognostic significance of BMP and activin membrane-bound inhibitor in colorectal cancer*. World J Gastroenterol, 2008. **14**(31): p. 4880-8.
226. Malkoski, S.P., et al., *Loss of transforming growth factor beta type II receptor increases aggressive tumor behavior and reduces survival in lung adenocarcinoma and squamous cell carcinoma*. Clin Cancer Res, 2012. **18**(8): p. 2173-83.

10. Erklärung

Ich erkläre hiermit, dass ich die vorgelegte Dissertation selbst verfasst und mich dabei keiner anderen als der von mir ausdrücklich bezeichneten Quellen und Hilfen bedient habe.

Weiterhin erkläre ich hiermit, dass ich an keiner anderen Stelle ein Prüfungsverfahren beantragt bzw. die Dissertation in dieser oder anderer Form bereits anderweitig als Prüfungsarbeit verwendet oder einer anderen Fakultät als Dissertation vorgelegt habe.

Heidelberg, den 29.01.2015

Ruth Merkle